Coherent Optical Interactions in Graphene Multilayers

by
SHRADDHA M S RAO

A thesis submitted in fulfilment of the requirements
for the degree of Doctor of Philosophy

Heriot-Watt University

School of Engineering and Physical Sciences
October 2016

Abstract

The work discussed in this thesis deals with the generation, control and modulation of optical interactions in two-dimensional materials, specifically in unpatterned, subwavelength graphene multilayers, using the process of Coherent Perfect Absorption (CPA). It aims to address the problem of inefficient light-matter coupling at the nanoscale by studying new geometries for enabling total absorption in 50% absorbing graphene films. Total optical absorption is demonstrated and a $\sim 80\%$ modulation of the absorption and scattering is achieved by controlling the relative phases of the interacting optical beams.

Degenerate four-wave mixing (DFWM) in graphene multilayers leads to the generation of optical phase conjugation and negative refraction. These nonlinear responses are generated with a conversion efficiency of 5 x 10^{-5}, and using the CPA arrangement their amplitudes are modulated with a modulation contrast of $\sim 100\%$. It is shown that the two-dimensionality of graphene gives rise to a 'phase-dependent' nonlinearity, which differs significantly from that in bulk materials. The optical nonlinearity in graphene is seen to be controlled by the relative phases of the interacting optical fields in a manner such that the nonlinear polarisation itself can be switched on or off. The phase-dependent nonlinearity of the two-dimensional medium is then explored in three alternative geometries. The first one uses only two input beams, and a light-with-light modulation of the nonlinear signals is observed with a contrast of 90%. The second geometry involves a single beam interacting with the sample, wherein, nonlinear signals are generated in a self-pumping mode, due to reflection from a mirror placed very close to the graphene sample. The last configuration also uses a mirror in order to require only a single light beam and leads to the observation of a 'negative reflection' signal.

Finally, a nonlinear imaging technique 'phase-contrast imaging' is performed using a traditional DFWM configuration with three input optical fields. A phase-object applied on one of the pump beams is transformed into an intensity object in the resulting negative refraction. A few basic phase objects are imaged on the negatively refracted beam and are reported in this work, offering a possible application for the advantages offered by two-dimensional optical nonlinearities.

I dedicate this thesis to my parents and my sister.

Acknowledgements

First and foremost I would like to thank my supervisor, Prof. Daniele Faccio for his invaluable guidance and unending motivation that kept me going through my PhD. Many thanks for all the hill-walks, the chats and the group meeting treats.

Secondly, I would like to thank Dr. Thomas Roger, Dr. Matteo Clerici, Dr Constantine Aniculaesi and Dr. Chunyong Li for their support and guidance - inside and outside the lab. A special shout-out to Tom for being an incredible office-mate, a friend and my first-stop in the case of every question/problem, and to Matteo for his energy and enthusiasm which helped me understand and decipher many experimental observations.

I am extremely grateful to my fellow 'Extreme Light'ers - Rishad, Julius, Nic, Mike, Hatef, Ashley, David, Genevieve, Calum, Lucia, Pier and Kali - for making life and science more enjoyable and interesting. To all the other Heriot-Watt friends - Rose, Anusha, Cristtel, Lisa, Gillian, Magda, Aurora, Nitin, Hari, Vikram, Megan, Eliot and many more - I am ever thankful for your camaraderie, food, stories and adventures. The biggest cheer goes to AnushamoL for being my best buddy through thick and thin; through laughter and tears.

A big thanks to Linda Bruce, who has been more like a mother than a landlady. I have thoroughly enjoyed my time spent in the 'Bonaly Curry House' - cooking, laughing, bird-watching, learning about Scotland and Scotch, and having a splendid time in general.

I would like to send out a huge cheer to Alessandro Boccolini for being my thesis-printing champion! Let's all 'be more human.'

Most importantly, I wish to thank my parents, my sister Medha, my big family, and friends from India for extending their support and, most importantly, their ears and wits from the other side of the world.

Contents

List of Figures

List of Abbreviations

CPA	**C**oherent **P**erfect **A**bsorption
FWM	**F**our **W**ave **M**ixing
DFWM	**D**egenerate **F**our **W**ave **M**ixing
2D	**Two D**imensional
OPC	**O**ptical **P**hase **C**onjugate (/conjugation)
EM field	**E**lectro**m**agnetic field
IR	**I**nf**r**ared
TEM	**T**ransmission **E**lectron **M**icroscope
SLM	**S**patial **L**ight **M**odulator

List of Symbols

r	reflection coefficient
t	transmission coefficient
α	total absorption
$\chi^{(3)}$	third order nonlinear susceptibility
k	wave vector
n	refractive index
n_2	imaginary part of the refractive index

List of Publications

0.1 Peer reviewed journals

1) **S. M. Rao**, J. J. F. Heitz, T. Roger, N. Westerberg, and D. Faccio, *Coherent control of light interaction with graphene*, Opt. Lett. **39**, 5345–5347 (2014).

2) **S. M. Rao**, A. Lyons, T. Roger, M. Clerici, N. I. Zheludev, and D. Faccio, *Geometries for the coherent control of four-wave mixing in graphene multilayers*, Sci. Rep. **5**, 15399 (2015).

0.2 Conference papers

1) **S. M. Rao**, A. Lyons, T. Roger, M. Clerici, and D. Faccio, *Coherent control of optical negative refraction in graphene*, Frontiers in Optics, FTh2A. 4 (2014).

2) D. Christodoulides, S. Wengerowsky, and **S. M. Rao**, *Accelerating beams and light pulses*, International School of Physics “Enrico Fermi" - Course 190: Frontiers of Modern Optics (2014).

0.3 Posters

S. M. Rao and D. Faccio, *Controlling laser-induced cavitation dynamics in water with pulse shaping*, National Laser Symposium-22, Manipal, India (2014).

S. M. Rao, J. J. F. Heitz, T. Roger and D. Faccio, *Light-with-light modulation in graphene*, International School of Physics “Enrico Fermi" - Course 190: Frontiers of Modern Optics, Como, Italy (2014).

Chapter 1

Introduction and background

1.1 Introduction

Light has proven to be one of the most powerful and resourceful tools in the study of the nature and behaviour of matter. Light which is organized, controlled and disciplined, namely a LASER, has greatly enhanced the functionality of light as a tool. As our understanding of light has evolved through ages, so have the different technologies based on how we treat light and its interactions with matter. For example, the semiconductor technologies can be attributed to the hypothesis of quantum electrodynamics. Most new technologies are based on enabling, controlling and modulating interaction of electromagnetic radiation with matter. And there is a constant competition towards development of improved - efficient and faster - phenomena/technologies. One way of probing into inventing improved technologies is to actively look into new materials and their properties.

The work discussed in this thesis deals with the generation, control and modulation of light interactions in two-dimensional (2D) materials, specifically graphene multilayers. This is as strongly motivated by the need for compact, miniaturised, all-optical components in optics-based technologies such as telecommunication and data networks as it is in exploring new physics and curious relationships between laser characteristics and dimensionality of an optical medium. Most optoelectronic components are limited by electronics and this has been a driving factor for several fields of research in optics and material-science to develop compact, all-optical systems. A major challenge in the use of 2D materials for optical applications is the highly inefficient light–matter coupling at the nanoscale and the universal limit of absorption in an ultrathin film (50%). This thesis aims to address this very problem by studying new geometries for efficient linear and

nonlinear light interactions using graphene films. In our experiments, an optical modulation of linear absorption and linear scattering, with modulation contrast close to 80% is achieved using the technique of Coherent Perfect Absorption (CPA). Following the coherent generation of linear optical effects, a 'phase-dependent' approach for realising optical nonlinearity in a graphene sample through the process of degenerate four-wave mixing (DFWM) is demonstrated. Additionally, the CPA arrangement allows for a coherent modulation of the nonlinear signals with a modulation contrast of $\sim 100\%$, thus providing a method for effectively generating and also optically modulating nonlinear excitations in graphene multilayers. Three alternative geometries for enabling nonlinear interactions in the two-dimensional graphene sample are explored and reported in this thesis. A brief background of the evolution of the ideas and techniques reported here is discussed in this chapter.

The experimental separation of a single layer of carbon atoms arranged in a honeycomb-lattice pattern was performed in 2004, although graphene was theoretically being studied since 1947. The isolation of graphene by Andre Geim and Konstantin Novoselov [1] and the subsequent discovery of its unusual properties led to a huge surge in the research in 2D materials. Graphene, considered the forefather of 2D materials, opened up a playing-field for the development and investigation of materials like the monolayer Transition Metal Dichalcogenides (TMD)s: MoS_2, $MoTe_2$, WS_2 and patterned metamaterials. Along with unusual mechanical and electronic properties, these subwavelength materials also exhibit fascinating optical properties. It has been demostrated that metamaterials, graphene, and heterostructure layered media [2, 3, 4] showcase great potential for enhancing the functionality of photonic and optomechanical devices. In general, the class of sub-wavelength media has become a powerful addition to the list of optical materials. A summary of the unique optical properties of graphene and its potential uses are discussed further in this chapter.

1.2 Methods Adopted

The main motivation of the work reported here is to optimise a methodology for efficiently generating and controlling both linear and nonlinear optical interactions in two-dimensional media. Specifically, unpatterned graphene multilayers are used to study the

generation and modulation of **absorption and scattering** in the linear regime, and optical phase conjugation (OPC) and negative refraction through **Degenerate Four-Wave Mixing (DFWM)** in the nonlinear regime. The process that enables the control of these phenomena is called *coherent perfect absorption*. Coherent perfect absorption is a process by which two coherent monochromatic optical fields are perfectly absorbed by a partially absorbing medium, in the presence of a standing-wave environment. It is also considered a time-reversed process of a laser [5, 6], more of which is discussed in the following chapter. The phenomenon of CPA was first proposed in bulk absorbing media, i.e., thicker than the optical wavelength [7, 8], wherein the medium acts as an etalon and traps all the optical energy inside the medium leading to total absorption. The principle of CPA has been further demonstrated in alternative geometries involving composite films and graphene [9, 10] and also in other optical regimes: with single photons [11] and in nonlinear media [12].

The most important feature of CPA is that it allows 'light-with-light' manipulation without the use of nonlinearity [13, 14, 15]. This is possible due to the interplay between the absorption of the medium and optical interference. CPA and the subsequent light-with-light modulation in partially absorbing sub-wavelength films would arise in the presence of two counter-propagating light beams that form a standing wave (within the coherence length of the laser). A sub-wavelength film that is placed in the position of the resulting standing wave experiences a very different electric field amplitude depending on its position. If the medium is positioned at a node of the standing wave, the field amplitude is constant in time and equal to zero, which causes the light beams to pass through the film without loss. However at an antinode, the position of maximum amplitude of the field, the light beams undergo strong, ideally 100% absorption. This nature of light-matter interaction at nanoscale provides a method to modulate, i.e., enhance or suppress, the absorption of light with a thin absorbing film by simply changing the relative phases of the interacting beams.

The demonstration of CPA in 2D materials was first reported in optical metamaterial structures with properties designed so as to provide a single-pass absorption close to the ideal 50% limit that is required for perfect 100% coherent absorption [13, 16]. The precise conditions required for coherent perfect absorption are discussed in the course of this thesis. Similar absorption properties have been demonstrated in patterened single layer graphene [16, 17] and metallic metamaterial structures [18, 19, 20, 21]. Alternatively, 2D materials can be used in conjunction with other optical geometries for increased light

interaction [22], thus providing the conditions for perfect absorption. It is to be noted that since structured graphene and optical metamaterials rely on a resonance between the light field and the medium itself for efficient optical interactions, they can only function over a specific wavelength range [16, 23].

In our experiments, un-patterned, undoped graphene multilayers are used for performing CPA measurements. Graphene exhibits uniform linear absorption [24, 25] over a wide wavelength-range and hence offers an advantage over using wavelength specific metamaterials or structured films. Absorption experiments are performed with both continuous-wave and pulsed laser sources attenuated to operate within the linear optics regime. CPA deals with complete absorption of optical energy, and it also offers the advantage to tune the degree of absorption by controlling the relative phase of the interacting optical fields. Additionally, a coherent modulation of linear scattering from the graphene film is also detected and studied in our experiments using the same CPA configuration. In addition to these linear effects two-dimensional films can also exhibit extraordinarily strong nonlinear effects. The optical mixing process of degenerate four wave mixing (DFWM) under the conditions of coherent perfect absorption not only demonstrates the generation of optical nonlinearities, but also a method for coherently modulating these nonlinear responses.

This work features 2D films exhibiting a phase-controllable nonlinearity, i.e., the amplitude of the nonlinear polarisation wave in the medium is controlled via the relative phases of the interacting optical fields. Controlling the phase of one beam, say pump 1, determines whether a 'probe' beam will encounter the nonlinearity or not. This configuration provides a remarkable advantage over bulk nonlinearities where propagation in the medium averages out any such phase dependence, i.e., in a bulk medium four-wave mixing will ensue regardless of the relative phases between the input pump beam (say, with phase ϕ_p) and signal beam (with phase ϕ_s) and the resultant beam from FWM will be generated with a relative phase difference $\phi_i = 2\phi_p - \phi_s$. When the medium is illuminated simultaneously with four input waves, nonlinear polarisation is still generated and will ensure energy flow between the beams, wherein the relative pump/signal/idler phases only determine the direction in which the energy flows. In this sense of the direction of energy flow, a specific nonlinear process is phase-dependent but the presence of the nonlinearity itself is not. This is the main difference in the nonlinearity that is observed in the two-dimensional graphene sample in our work. Here, the DFWM effect is enabled in graphene multilayers in the presence of a CPA environment set up by two coherent counterpropagating pump beams, and one probe beam incident at an angle with respect

to the normal to the sample surface. The optical nonlinearities manifest as time-reversal: optical phase conjugation and negative refraction [26].

The series of experiments on optical nonlinear effects performed in multilayer graphene samples is a study to find new and alternative geometries for inducing and possibly, controlling the nonlinearity. The thesis highlights some of the important consequences of the phase-dependent optical nonlinearity, such as the coherent control of nonlinearly diffracted beams (phase conjugation and negative refraction), a simpler DFWM setup with only two beams: pump-probe induced phase-conjugation and the demonstration of a nonlinear mirror characterised by 'negative reflection'. The observed phase sensitivity is a result of the dimensionality of the graphene sample, rather than being specific to graphene's properties, and is therefore expected to be observed in other 2D nonlinear materials. Also, since negatively refracted beams have been used to perform perfect imaging [27], we also explore the possibility of developing a new nonlinear imaging tool using one of the DFWM geometries. The phase-sensitivity of the nonlinearity (particularly negative refraction, in our experiments) offers the prospect for imaging phase objects in a pump beam into intensity objects in the nonlinear signal, viz., the negative refraction. Some basic results from this study are reported in this thesis.

A general overview of the concepts and experiments investigated in each chapter of the thesis is given at the end of this chapter. The following section provides a concise background on the experimental materials and methods.

Two-dimensional Materials: The 'two-dimensional material' referred to in this thesis is optically two-dimensional, in the sense that the material is two dimensional with respect to the wavelength of light. Optical 2D materials are deeply sub-wavelength or have mono-atomic thickness. This relatively new class of optical materials includes photonic metamaterials, plasmonic, heterostructure layered materials, and structured or few-layer graphene and exhibit new physics owing to their dimensionality and the flexibility with which they can be fabricated. Their functionality in the field of photonics-application is well established in terms of cloaking [28], ultrafast modulators [15] and optical magnetism [29, 30].

Graphene: The unique optoelectronic properties of graphene is mainly attributed to its Dirac conical and gap-less electronic band structure. The electronic transport and optical

properties of a material are largely determined by the electronic band structure. Hence, its gap-less condition provides graphene the advantage of having constant absorption for a broad spectral range, making it optically active between near-infrared region to the ultra-violet region of the electromagnetic spectrum. This makes graphene a feasible candidate for broadband applications.

Optical interactions in graphene have opened up a whole new universe of applications, as listed below:

1) Bilayer graphene has shown the potential to be used for infrared light sources and sensors for measuring biological molecules as many have unique signatures in the infrared region [31]. This is due to the fact that in an graphene bilayer, the bandgap can be tuned by introducing an electromagnetic filed perpendicular to the layer.
2) Light or heat-induced activation of graphene sheet behaves as an origami-robot, which can perform self-folding, walking and turning a corner. This material holds potential for applications such as sensing, artificial muscles and robotics [32].
3) Direct light manipulation of matter on a bulk scale was recently demonstrated using graphene integrated material. Light-induced propulsion (in horizontal and vertical direction) and rotation of a bulk graphene sponge material with dimensions on the scale of a centimetre and milligram weight was achieved with lasers, and also using xenon lamp illumination [33]. This phenomenon has been attributed to the electronic band-structure

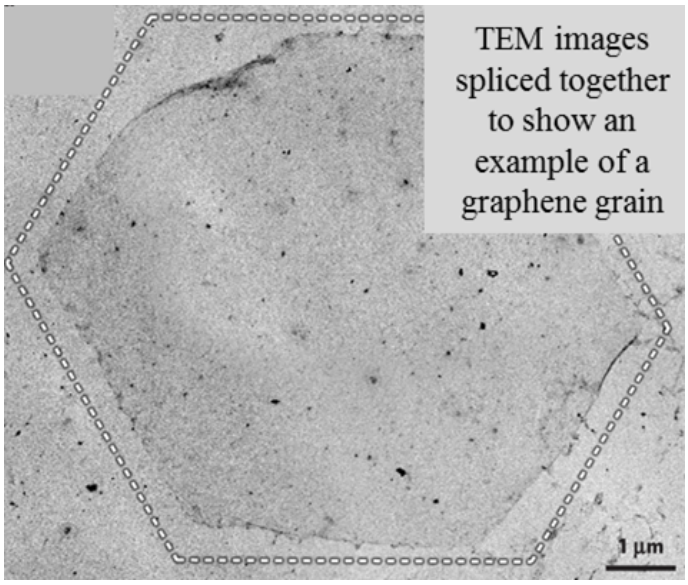

FIGURE 1.1: A TEM image of graphene - a single atomic layer of hexagonally arranged Carbon atoms. This image is originally from [38].

of graphene and its unique absorption-relaxation dynamics.

Graphene has proved to be a resourceful optical material with its unique properties related mostly to the linear dispersion of the material in vicinity of the Dirac points, e.g., high yet constant absorption over a huge bandwidth [25], electrically controllable optical properties [34] and high electron mobility. Graphene - pure or in a heterogeneous form - is also being explored for its nonlinear optical properties, with it being studied as a saturable optical absorber [35] and also for its third order nonlinear properties [36]. Graphene exhibits 8-order of magnitude enhancement of the value of $\chi^{(3)}$ with respect to typical dielectric materials [37], which is of particular interest to our study. It is also a 'self-conjugate' medium. A medium can be called *self-conjugate* [26] if it can support both positively and negatively refracting states of an electromagnetic wave. Such materials have been proposed as ideal for studying time-reversal and negative refraction of electromagnetic radiation and the link between them. These processes are discussed in detail in Chapters (3 and 5), in the context of four-wave mixing (FWM). Graphene, along with certain chiral media [26], belongs to this rare class of self-conjugate media. This unique optical trait of graphene is attributed to its Fermi electrons, which control the phase evolution of the incident wave [39], thus making it capable of supporting negatively refracting states, as discussed in more detail in Chapter (3). This allows the use of graphene for investigating the generation of negative refraction as a consequence of FWM processes in novel configurations. In addition to that, the availability of high-quality graphene as a stable material with all its extraordinary optoelectronic properties makes a convincing case for exploring its ability to harness light for potential applications. However, a single sheet of homogeneous graphene has very low optical absorbance, about 2.3$\%$ absorption. This poses a big challenge of transforming it into a perfect absorber, which is addressed in the Chapter on CPA, Chapter 2.

Coherent Perfect Absorption: A well-crafted interplay between optical absorption and wave interference gives rise to coherent perfect absorption (CPA). In this effect, a material with precise amount of absorption (a 'loss medium') when illuminated by coherent monochromatic light, becomes a perfect absorber [7]. This concept was first published in 2010 by a team of Yale theorists led by Douglas Stone, and since been explored for achieving total absorption in optical systems. The coherent perfect absorbers can be described as absorptive interferometers and the phenomenon was first demonstrated in a Silicon slab geometry which is discussed in detail in the Chapter 2. The evolution of the idea of CPA as a tool for enabling efficient light coupling into ultrathin media is discussed

in the next chapter of the thesis. Coherent perfect absorbers have the potential to be used in detectors, transducers, and optical switches. In this work CPA is used as a tool for enabling and controlling linear and nonlinear optical interactions.

Overview of the Thesis: This thesis summarizes a series of studies performed to probe into many conditions and possibilities of optical interactions in graphene and the ways to coherently control these interactions. The optical interactions investigated are absorption, linear-scattering and the nonlinear process of Four-Wave Mixing (FWM). A brief idea of each chapter is given below:

Chapter 2: *Coherent Perfect Absorption*: The theory of Coherent Perfect Absorption (CPA), which is the basis of all the experiments reported in this thesis is discussed in this chapter. It gives an overview of the course of evolution of the concept from being first demonstrated in a cavity to a method for the excitation of light interactions in two-dimensional materials.

Chapter 3: *Nonlinear Optics: Four-Wave Mixing*: In this chapter a theoretical background of the phenomenon of Four-Wave Mixing (FWM) process and the resulting Optical Phase Conjugation effect is discussed. FWM is a nonlinear interaction of (typically) three optical fields in a medium which results in a time-reversed or phase-conjugated field.

Chapter 4: *Coherent Control of Absorption and Scattering in Graphene*: This chapter reports the experimental methods of performing coherent perfect absorption with graphene multilayers. It demonstrates the 'light-with-light' modulation concept, in which light at very low level, in a coherent perfect absorption configuration, is perfectly absorbed or transmitted, turning the graphene sample into an all-optical modulator.

Chapter 5: *Coherent Control of Nonlinear Optical Interactions in Graphene*: The concept of FWM and CPA are harmoniously brought together in this chapter, as a graphene multilayer demonstrates coherent control of generation and modulation of four-wave mixing. The products of this nonlinear process are observed in the form of a time-reversed field, the typical phase-conjugated field, accompanied by an additional nonlinear signal - the negatively refracted field. The negative refraction is a product of performing the FWM in graphene, which is a result of its two-dimensionality and its unusual optical properties.

Chapter 6: *Negative Refraction in 2D materials and Phase-Contrast Imaging*: This chapter discusses the different optical geometries that can be used to realise nonlinear optical interactions in graphene multilayers. Due to the advantages of the reduced dimensionality of graphene, simpler FWM configurations are possible and this chapter reports three

new geometries for observing phase-conjugation and negative refraction. This chapter also discusses a possible application of realising FWM in graphene: a 'phase-contrast imaging' concept. Here, phase-objects imprinted on an input beam is translated into an intensity-object in the negatively refracted beam. This is performed by using the typical FWM geometry using three pump beams and the imaging is done using the resulting negative refraction.

Chapter 7: *Conclusions*: This chapter offers a summary of all the methods and results reported in the thesis. It also offers new possibilities for using the concepts explored here to apply in new optical situations, thus concluding the thesis.

Chapter 2

Coherent Perfect Absorption

2.1 Introduction

Optical systems like photo-detectors, optical transducers and sensors rely on efficient absorption of light, the ideal case being complete absorption. Achieving total absorption in optical systems follows two approaches: (1) using highly disordered (dissipating) medium, such that all the energy is trapped in the medium and eventually absorbed [40], or (2) by the method of ***critical-coupling*** [41, 42]. The 'critical coupling' method is based on matching the rate of coupling (of light into the medium) with its dissipative rate, so that no energy is reflected or transmitted, thus leading to perfect absorption. The method of critical coupling has been mostly used in efficiently coupling optical fibre with nano-structured arrays of optical materials [42]. *Coherent Perfect Absorption* (CPA) is based on the critical coupling effect, wherein a medium absorbs all the optical energy incident on it, under precise coupling conditions.

The process of coherent perfect absorption is the basic phenomenon behind most of the experiments reported in this thesis. This chapter aims at providing a background and an explanation of the working principle of CPA and its evolution as an idea. It was first demonstrated in bulk materials and has lately been proved to be a prominent and efficient way of generating optical interactions in two-dimensional materials. The phenomenon involves total absorption of coherent, monochromatic radiation by a lossy medium. The following sections detail the conditions needed for CPA to occur and how two-dimensional (2D) materials feature in the realization of this phenomenon. CPA in 2D materials opens up new avenues for the efficient use of these increasingly popular type of materials in optical manipulation and also in realising new ways of controlling nonlinear interactions. To comprehensively understand the exact physical processes that lead to coherent perfect

absorption, the process realised in bulk medium is discussed first, followed by a discussion of the modified conditions required for it to occur in a 2D medium. The chapter also considers the optical properties of graphene multilayers that make it an ideal candidate to use for coherent perfect absorption.

2.2 Coherent Perfect Absorption (CPA)

The theory of coherent perfect absorption was proposed by Y. D. Chong et al. [7] in 2010 and experimentally demonstrated in a silicon slab by W. Wan et al. [8] in 2011. The letter [7] describes a 'coherent perfect absorber' as a linear, absorptive interferometer and coherent perfect absorption as a process where a medium can be made perfectly absorbing at discrete frequencies in the presence of a precise amount of loss, when illuminated by coherent and monochromatic optical fields, viz., a laser. This effect is a cumulative effect of optical absorption and wave interference. A schematic representation of coherent perfect absorption is shown in Fig. (2.1). It shows an illustration of CPA in an absorbing medium (grey box) when two equal-intensity beams are incident on opposite sides of the medium. (A) and (B) show the complete absorption and complete transmission of the incident light energy, respectively. The first depiction (A) shows light being completely absorbed, as the output field (in red) is zero. The two different images (top and bottom) show the oscillation of the interacting fields inside the medium. Figure (B) shows zero absorption of the input fields and hence the output field (in red) remains unchanged. The total field (in blue) is shown to be changing due to constructive interference at the edges of the medium, resulting in total transmission of the input energy. Therefore, the process of CPA occurs as a combination of interference and absorption in the medium. The interference of input fields at the boundaries of the medium causes the field to be trapped in the medium, leading to perfect absorption of the energy. By changing the relative phase of the input fields, the condition of constructive interference can be achieved, which results in zero loss of the input energy in the medium, leading to a full transmission scenario. The detailed theory of CPA is discussed in the following part, in the form of a review of work reported by Y.D. Chong et al [7] and W. Wan et al [8], followed by a discussion on CPA in 2D materials.

Y. D. Chong, et al in their article [7], offered a comprehensive explanation of the conditions required for CPA and later the same team along with H. Cao et al. demonstrated the physical realisation of the process in 2011 [8]. The summary of the theoretical and experimental exploration of the phenomenon of coherent perfect absorption as a time-reversed

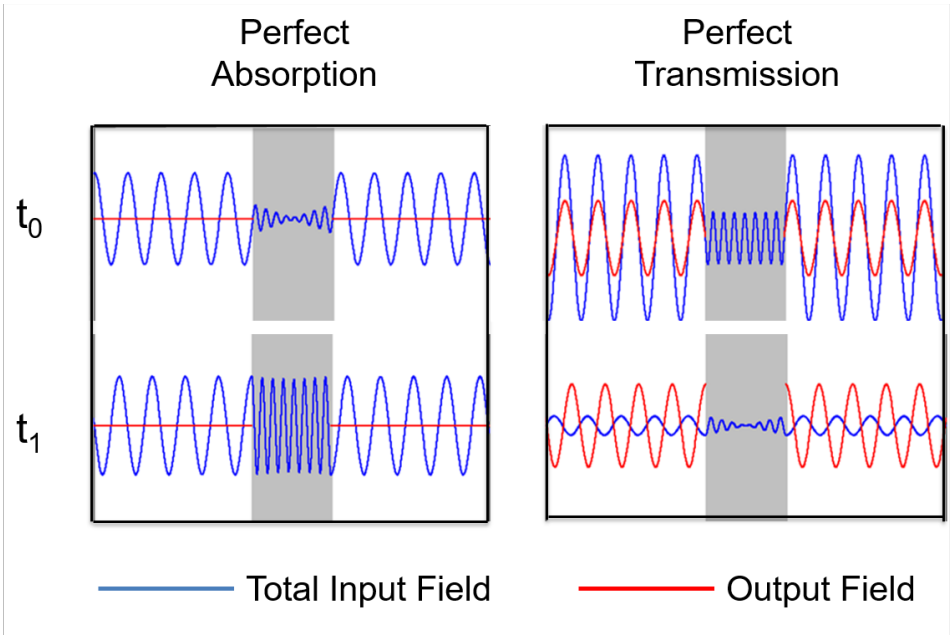

FIGURE 2.1: The figure schematically represents the phenomenon of coherent perfect absorption. Two light beams of equal intensity, travelling in opposite directions, are incident on the opposite sides of an absorbing medium (shown as the gray slab). The total input electric field is shown in blue, and the outgoing component in red. By choosing the appropriate relative phase of the input beams, the slab can either absorb the incident light completely (A), or it can become strongly scattering such that most of the input light re-emerge without being absorbed, as shown in (B). The figure is adapted from an animation demonstrating the working of a coherent perfect absorber as found on the website http://www.eng.yale.edu/stonegroup/cpa/cpa.html.

laser at threshold is presented here. Conventionally, a laser is a nonlinear optical system above the lasing threshold. The population inversion generated by the pump gives rise to a negative (amplifying) imaginary part of the refractive index. Hence, at the first threshold, lasers satisfy a linear wave equation with a refractive index that includes a negative imaginary part. In traditional lasers where the gain medium is confined in high Q-factor resonators, the lasing modes are closely related to passive-cavity modes (Q-factor is defined in terms of energy storage as: the ratio of the stored energy to the energy dissipated per oscillation cycle). However, as demonstrated in new laser systems, such as 'random lasers', lasing threshold can be reached and coherent lasing obtained in resonators with no high-Q passive-cavity modes [43]. This can be explained in terms of semiclassical laser theory, for which we have to consider the S-matrix, which relates the initial state and the final state of a physical system undergoing a scattering process. The S-matrix is closely related to the transition probability amplitude of various interactions and the elements in

the S-matrix are known as scattering amplitudes. Poles of the S-matrix in the complex-energy plane are identified with resonances of the system.

According to the laser theory the first lasing mode in any cavity is an eigenvector of the electromagnetic scattering matrix (S-matrix) with an infinite eigenvalue, i.e., lasing occurs when a pole of the S matrix is moved to the real axis by including gain as a negative imaginary part of the refractive index.

This suggests the possibility of the time-reversed process of lasing at threshold, if instead of a gain medium (negative imaginary part of refractive index) there is a loss medium (positive imaginary part of refractive index). Therefore, if a specific degree of dissipation (loss) corresponding to a positive imaginary refractive index equivalent to that at the lasing threshold is added to the resonator, a time-reversal of laser is achieved. Simplifying, a system with an absorbing medium being illuminated by coherent, monochromatic fields, i.e., the time reverse of the output of a lasing mode, leads to the incident radiation being perfectly absorbed. Such an optical system is referred to as a coherent perfect absorber (CPA).

The precise explanation of the principles of CPA is as follows. Consider a laser cavity and at threshold, a simple scalar wave equation is given by:

$$[\,\nabla^2 + n^2(r)k^2\,]\phi_k = 0 \tag{2.1}$$

Here $k = \omega/c$, ω is the frequency, c is the speed of light, ϕ_k is the electric field, and $n = n_1 + in_2$ is the refractive index. The imaginary part of the refractive index: $n_2 < 0$ for gain and $n_2 > 0$ for absorption. Steady-state solutions of this equation are obtained by the S-matrix which provides the relationship between the input and output states in terms of complex vectors α and β, which obey

$$S[n(r)k] \cdot \alpha = \beta \tag{2.2}$$

For a loss-less medium, $n_2 = 0$ and the S-matrix is unitary. Under time-reversal, it satisfies the general condition:

$$S[n^*(r)k] \cdot \beta^* = \alpha^* \tag{2.3}$$

The two equations, (2.2) and (2.3) imply that every scattering solution of the amplifying problem with $n = n_1 - in_2$ ($n_2 > 0$) and outgoing amplitudes β, is accompanied by a solution to the absorbing problem with $n = n_1 + in_2$ and incoming amplitudes β^*. Or, in simpler terms, when a field β^* is incident on a cavity with loss it is completely absorbed. This lossy cavity forms the time-reversed version of the laser considered, which is the 'coherent perfect absorber'.

In the Science article [8] by W. Wan et al., a simple two-channel CPA is demonstrated in a silicon slab. Two collimated counterpropagating laser fields are directed onto opposite surfaces of a silicon wafer which functions as a Fabry-Perot etalon. CPA occurs when, at one interface of the wafer, the multiply transmitted components from one of the beams interferes destructively with the multiply reflected components from the other beam. The same conditions are met on the remaining face of the Si wafer. This condition acts as a 'trap' for the incident fields and the total energy is absorbed due to silicon's interband absorption processes. On the other hand, if the two fields incoherently illuminate the medium, it causes the reflected components to constructively interfere with the transmitted components, leading to the escape of the radiation from the Si slab. This offers the advantage of coherent control of absorption by the medium: either a near 100% absorption or near 100% transmission.

It is noted here that only a certain range of absorption coefficients would yield strong CPA resonances, because of the conditions on the reflection and transmission coefficients of the medium. For efficient constructive and destructive interference to occur on either interface of the lossy medium (which in turn enables perfect absorption and perfect transparency, respectively), the reflectance (R) and (T) have to be equal. i.e., for CPA resonances to arise, the condition of R = T ($|r|^2 = |t|^2$) is to be satisfied (where $randt$ are reflection and transmission coefficients of the medium, respectively). Also, not only must the two interacting fields have equal intensities, they have to have the correct relative phase. Using these conditions, the operating wavelength for a system is determined and λ within this interval is fine-tuned such as to yield strong CPA resonances.

Several other demonstrations of CPA have been reported in metal-dielectric composites [9], in nonlinear medium [12, 44] and proposed in PT symmetric materials [45] and corrugated metal films [46]. Coherent Perfect Absorption with its many advantages such as its non-dependence on atomic/molecular resonances of material leading to a flexibility

in the material-wavelength compatibility and also the ability to switch between perfect absorption and super-scattering, have paved a new path for exploring this phenomenon in different optical situations - in 2D, plasmonic and metamaterial contexts.

2.3 CPA in Two Dimensional Materials

Coherent perfect absorption in a 2D material is also a consequence of the interplay between absorption and interference, but in a *standing-wave* scenario. The biggest obstacle

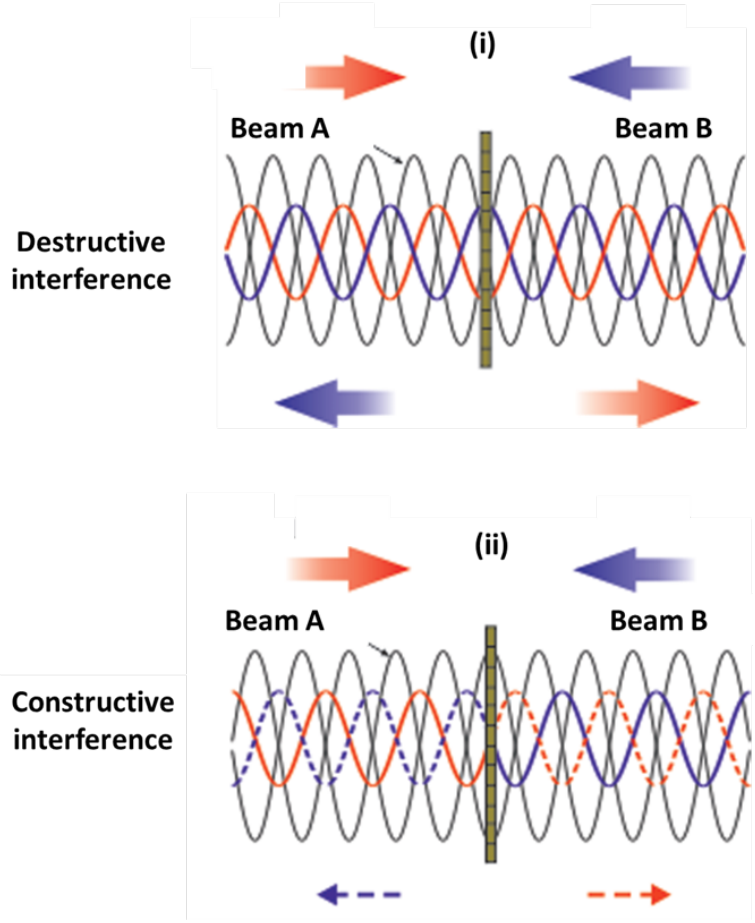

FIGURE 2.2: A schematic representation of two limiting cases of CPA using a two-dimensional material is shown here. The two interacting beams - A and B - are shown in red and blue, respectively. The resulting standing wave is shown in grey. (i) shows the 2D film at a node of the standing wave formed by Beams A and B, and they are hence transmitted with no loss. In (ii) the medium is at the antinode of the standing wave, enabling absorption of the incident beams. This figure is adapted from [14]

in using 2D materials for optical interactions is the inefficient light-mater coupling. However, in the CPA geometry this exact weakness of the material, i.e., its two-dimensionality, becomes its biggest advantage. This is because an optically 2D material can be scanned through a standing-wave formed by two counterpropagating beams (a premise similar to that of CPA in bulk materials) such that the material encounters each node and subsequent antinode individually. Under certain conditions, like the precise amount of dissipation and symmetric illumination, a two-dimensional medium can exhibit full-absorption or full-transmission.

Consider a standing wave formed by two counterpropagating beams and an optical medium of sub-wavelength thickness placed in the area of interference of the two beams. The optical medium is partially absorbing at the operating wavelength of the incident light. Fig. (2.2) illustrates two counterpropagating optical signals, Beams A and B incident on a two-dimensional material. It shows the two limiting cases possible in the interaction of the 2D material with the resulting standing wave: (i) shows the absorbing medium at a node, position of zero-field, of the standing wave. Since the film is much thinner than the wavelength of the incident light, its interaction with the field at this minimum is negligible and the film will appear to be transparent for both incident waves. On the other hand, as shown in (ii), if a standing wave field maximum, i.e., an antinode, is formed at the absorbing film, the interaction is strongest and absorption becomes very efficient. The main advantage of this arrangement is that altering either the phase or intensity of one beam will disturb the interference pattern and change the absorption (and thereby transmission) of the other.

Elaborating, when the film is placed at a node of the standing wave, blocking beam A will lead to an increase in loss for beam B, decreasing its transmitted intensity. On the other hand, if the film is located at an antinode of the standing wave, a position of maximum absorption, blocking beam A will lead to a decrease of losses for beam B, increasing its transmitted intensity. So effectively, the relative-phase or intensity of the two interfering fields dictate the condition for absorption, similar to the case of bulk medium. But the geometry involving a 2D material provides a simpler CPA model as it involves no etalon. Hence this phenomenon is also called “light-with-light" manipulation [13], since it is a demonstration of light manipulating light at linear regime.

Although the above arrangement allows for a modulation between maximum and no absorption (or transmission), it is the material property that factors critically in establishing

complete absorption. For observing 100% modulation, the optical absorption of the sample needs to be considered. It is found that if the 2D medium absorbs half of the energy of a single beam passing through it, it leads to complete absorption of all the optical energy incident on it, providing the optimum modulation contrast. The maximum absorption that can be achieved in an ultrathin film is 50%, due to the *thin film limit*. In the following subsections, the universal thin-film limit of absorption in 2D materials is discussed. It is followed by the equations governing the phase-control of beams interacting at a beam-splitter which enable the coherent perfect absorption in a 2D medium.

2.3.1 Thin Film Limit

There exists a fundamental limit for absorption in a free standing thin film. This is explained in [16] in terms of the relationship between the reflection and transmission coefficients of a ultrathin film illuminated by an electromagnetic wave. Say, if r is the reflection coefficient, then the transmission coefficient, t will be equal to $1 \pm r$. The upper and lower limits for the value of t are for s- and p-polarised light, respectively, and the reasons for

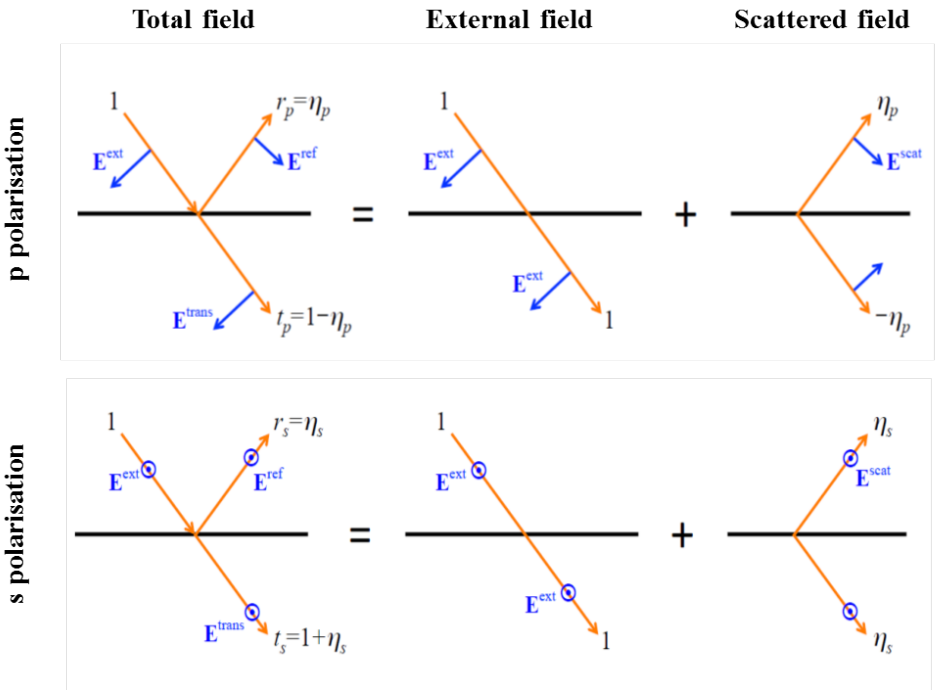

FIGURE 2.3: A pictorial representation of reflection and transmission components of EM fields with respect to their polarisation when scattered by an optical thin film. This figure is adapted from [16].

this condition are explained using the scenario represented in Fig. (2.3).

When an ultrathin medium (shown in Fig. (2.3) as the black line) is illuminated by a light wave, shown as E^{ext}, the *p*- and *s*-polarisation components are reflected differently. Let η_p and η_s be the scattered amplitudes, respectively. The phase change over the thickness of the thin layer is insignificant (unless the material is a high refractive-index dielectric) and hence the scattered fields are symmetric, as shown under the 'Scattered field' representation in the Fig. (2.3). For *p*-polarisation, the scattered amplitudes on either side of the film have opposite signs, following the convention for reflection of fields at an interface (owing to the boundary conditions for continuity in electrodynamics). Consequentially, the reflection and transmission coefficients, r_p and t_p can be expressed as $r_p = \eta_p$ and $t_p = 1 - \eta_p$. In the case of *s*-polarisation, the external field and scattered fields have the same direction, which leads to $r_s = \eta_s$ and $t_s = 1 + \eta_s$. Summarising, the relation between the transmission and reflection coefficients of a thin layer can be written as

$$t = 1 \pm r. \tag{2.4}$$

Under these conditions, the absorption of a thin film is expressed as

$$\alpha = 1 - |r|^2 - |1 \pm r|^2. \tag{2.5}$$

And based on this relation, the maximum absorption is limited to 50% by values of *r* (± 0.5). This is the universal limit of absorption of a thin film in a symmetric environment. Hence there is a need for a geometry which can be used for achieving 100% absorption in thin films and this is where the relation between the beams interacting at a lossy beamsplitter comes into play. The basic behaviour of two optical beams interacting at a beamsplitter is discussed in the following subsection.

2.3.2 Perfect absorption in an absorbing thin film

Consider two optical signals incident on two ports of a beamsplitter. Two cases are considered under this arrangement: *Case 1* involves a loss-less beam-splitter and *Case 2* involves a lossy beam-splitter. The conditions in Case 1 were studied by Vittorio Degiorgio [47] in 1979. He considered two optical fields interacting at a Michelson interferometer. Taking into account the phase shift experienced by either beam at each reflection (at the mirror and the beamsplitter) he concluded that the reflected and transmitted components at the output would have a phase difference of $\pi/2$. This is only true if the beamsplitter is

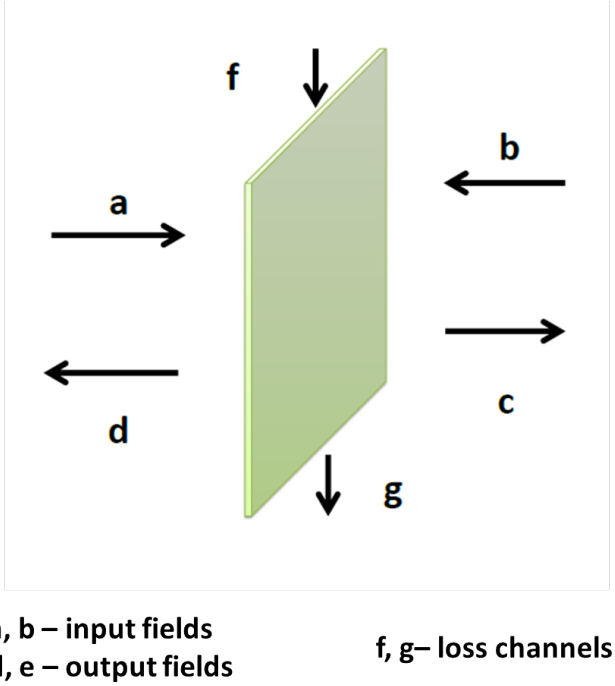

FIGURE 2.4: A schematic representation of a three-port model of light interaction at a two-dimensional medium, where a and b are the input fields, c and d - the output fields, and f and g are the loss modes.

completely lossless.

We consider Case 2, by looking at the scattering matrix (S) of a partly lossy beamsplitter, which is equivalent to an absorbing thin optical medium as discussed by S. M. Barnett et. al., in [48] where they investigate lossy beamsplitters in the quantum optics scenario. Fig. (2.4) shows a three-port model of an absorbing two-dimensional medium, with two counterpropagating input beams, a and b; with two output fields c and d, and loss modes f and g (plasmon modes). The relationship between the input, output and the loss fields in this system can be expressed in terms of the scattering matrix, **S**, can be written as follows:

$$\begin{pmatrix} c \\ d \\ g \end{pmatrix} = \begin{pmatrix} t & r & A \\ r & t & B \\ C & D & E \end{pmatrix} \begin{pmatrix} a \\ b \\ f \end{pmatrix} \tag{2.6}$$

Based on the assumption that the absorber is ultrathin (2D), loss modes are considered in only one direction. Applying the principle of conservation of energy on the above relation, we arrive at:

$$|A|^2 = |B|^2 = 1 - |t|^2 - |r|^2 = \alpha, \tag{2.7}$$

where α represents the absorption of the system. Also, another relation that holds for complex *t* and *r* is:

$$\begin{aligned} 2Re(tr^*) \pm |A|^2 &= 0 \\ 2Re(tr^*) &= \mp\alpha \\ 2|t||r|cos(\phi_s) &= \mp L\alpha \end{aligned} \tag{2.8}$$

where, ϕ_s is the relative phase between *r* and *t*.
Equation (2.7) yields a circle of constant absorption, α and equation (2.8) gives an ellipse of constant phase, ϕ_s. Plotting them together gives an area of intersection defining the relation between the transmission and reflection coefficients, i.e., combining (2.7) and (2.8), we get the condition:

$$t \pm r|^2 = 1 \tag{2.9}$$

which implies,

$$t = 1 \pm r. \tag{2.10}$$

This agrees with the Equation (2.4), which was deducted in the previous section.

Now for a case of complete absorption, we consider the scattering matrix scenario as described in Equation (2.6). In reference to Fig. (2.4), we only consider the input modes a and b, and the two output modes c and d, which can be related to each other linearly.

From Equation (2.6), we can write

$$\begin{pmatrix} c \\ d \end{pmatrix} = \begin{pmatrix} t & r \\ r & t \end{pmatrix} \begin{pmatrix} a \\ b \end{pmatrix} \tag{2.11}$$

The output modes are a linear composition of the input modes where S defines their relation. We suppose a case where a linear superposition of a and b in the system yields no output, i.e., it leads to total absorption. This corresponds to the particular eigenmode of the scattering matrix, where the eigenvalue is 0. Likewise, for total transmission the corresponding eigenvalue is 1. Therefore, for total absorption, the determinant of the sub matrix

$$S^* = \begin{pmatrix} t & r \\ r & t \end{pmatrix} \tag{2.12}$$

is 0. Thus we arrive at

$$t = \pm r. \tag{2.13}$$

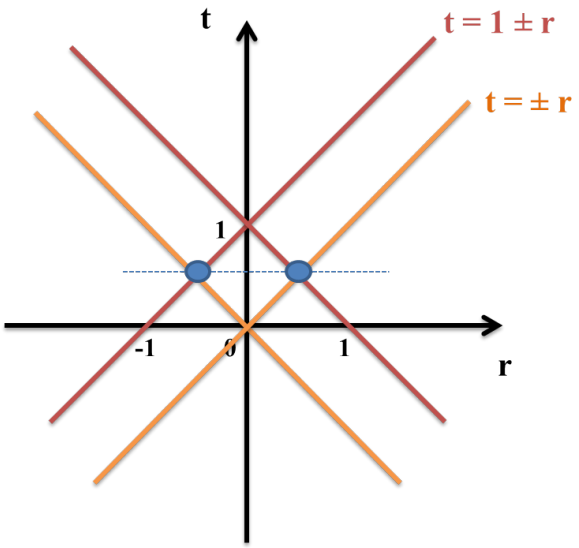

FIGURE 2.5: A graphical representation of relationship between the transmission and reflection coefficients for complete absorption in an absorbing thin film. The two blue dots corresponding to the values $t = \pm r = \pm 0.5$ represent the critical condition for enabling CPA.

This relation and the relation between transmission and reflection coefficients of a thin film, devised in the previous subsection, $t = 1 \pm r$, together lead to a unique pair of *t* and *r* values as depicted in Fig. (2.5), i.e., $t = \pm r = \pm 0.5$. The figure is a representation of the two values of *t* and *r* (shown as blue dots) that are possible while satisfying the two conditions mentioned above.

Next, the phase relation between the two input beams that allows for the switch between total absorption and total transmission at a thin film is considered. For an easier representation, we consider a beamsplitter scenario, where the input beams are at $90°$, instead of at $180°$. A normal 50:50 beamsplitter is equivalent to a thin film surface with no loss. For our experiments, we consider a lossy beamsplitter and its four ports, schematically shown in Fig. (2.6) - two input and two output ports. The expression $r = e^{i\phi_s}t$, where ϕ_s is the phase-shift, expresses the relation between the reflected and transmitted component at the beamsplitter. However, as derived previously, for total absorption we need $t = \pm r$, and this is only possible for $\phi_s = 0, \pi, 2\pi, etc.$ In the first case, we consider the two input beams having zero phase difference. This results in both the output ports with reflected and transmitted components which are phase-shifted by π and this leads to destructive interference at either outputs, trapping the energy in the lossy beamsplitter. This arrangement corresponds to the *total absorption* condition. In the second case, the input

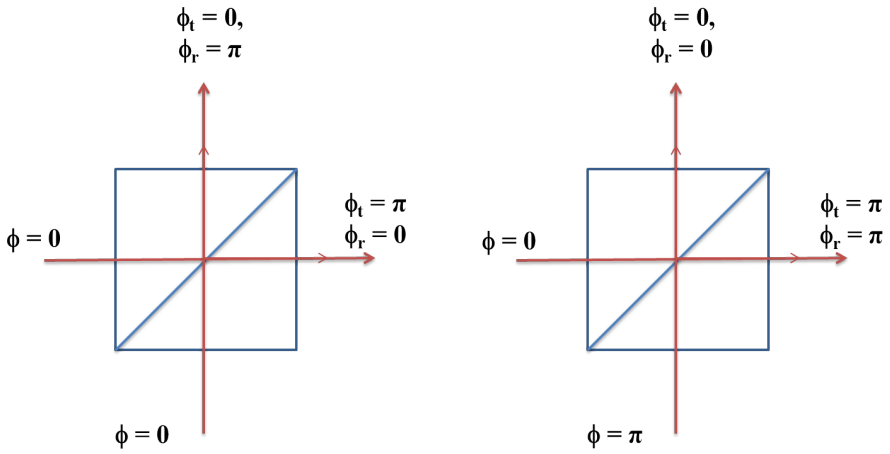

FIGURE 2.6: A schematic representation of the four port lossy beamsplitter depicting conditions for total absorption (left) and total transmission (right).

beams have a relative phase of 0, which means they undergo constructive interference at the output ports and all the energy passes through the beamsplitter giving rise to *total transmission*.

In conclusion, taking into account the universal limit of thin film absorption (50 %) in a symmetrical environment, the critical condition for coherent perfect absorption to occur in an ultrathin film is in a standing wave environment which is created by two coherent counterpropagating beams of equal energy, with a suitable phase-difference between the interacting fields. Figures (2.7 and 2.8) present a series of images (at different time intervals) extracted from a video showcasing the behaviour of two counter-propagating waves at a thin film, in the presence of two beamsplitters. Fig. (2.7) shows the setting up of a standing wave between the beamsplitters such that the thin film (shown in black) is at a position of an antinode. In the last frame we see that there are no beams coming out of the beamsplitter pair and all of the input energy is trapped inside the cavity, leading to total absorption.

In Fig. (2.8) on the other hand, we see the standing wave is formed such that the thin film is at a node, i.e., at position of zero intensity, leading to total transmission (seen in the bottom frame).

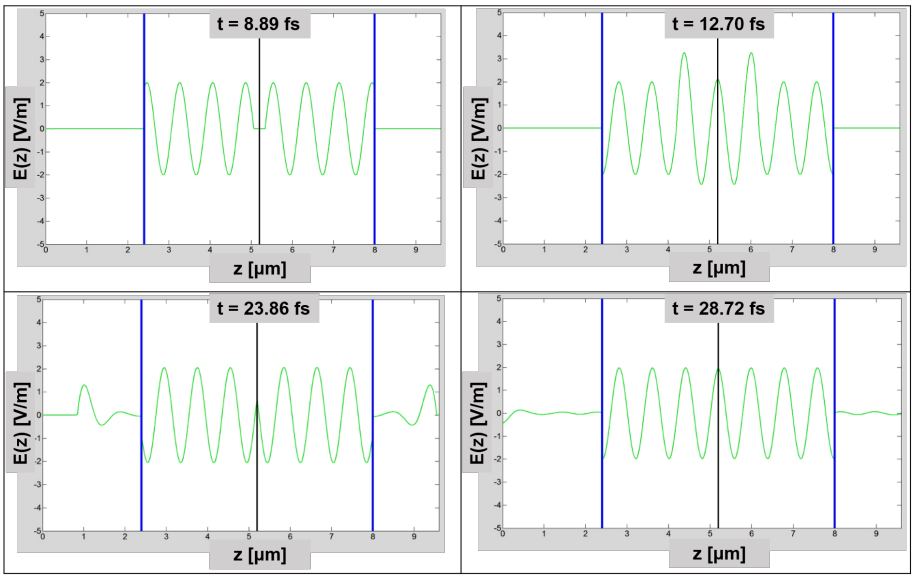

FIGURE 2.7: The figures show the propagation evolution (z-t plot) of the two counter-propagating fields evaluated with a numerical finite-difference time-domain (FDTD) simulation. Two continuous wave sources (positions indicated with solid blue lines) emit 785 nm light in opposite directions. The graphene sheet (whose position is indicated with a black line) is tuned to transmit and reflect equal amounts (R = T = 0.25, such that α 50%). The wavefronts, switched on at t=0, approach the graphene sheet from either side and start to form a standing wave at around t = 10 - 15 fs. The series of illustrations shows the setting up of 'coherent perfect absorber'. In these illustrations, the counterpropagating beams form an antinode (highest intensity position) at the 2D film. (c) and (d) show that the optical energy is trapped inside the beamsplitter pair and the 2D material perfectly absorbs all the energy incident on it. These simulations were carried out by N. Westerberg.

2.3.3 Graphene for Coherent Perfect Absorption

Carbon, in its allotropic forms like graphite and Carbon Nano-Tubes (CNT), has proved to be a great candidate for strong light absorption [40]. Graphene is the most basic two-dimensional allotrope of Carbon and it exhibits almost uniform linear absorption [24, 25] over a wide wavelength-range and hence may offer an advantage over using metamaterials or structured films which are fabricated for a certain frequency. Graphene in conjunction with other optical systems such as micro-cavity [49], photonic crystals [50, 51] metamaterials [52] etc., has been used for demonstrating perfect absorption. Graphene, in different physical forms, has also been used for total light absorption (TLA). Thongrattanasiri, S. et al., used doped graphene in the form of a single patterned sheet of nano-disks to demonstrate full absorption under total internal reflection conditions [16]. Their results provided

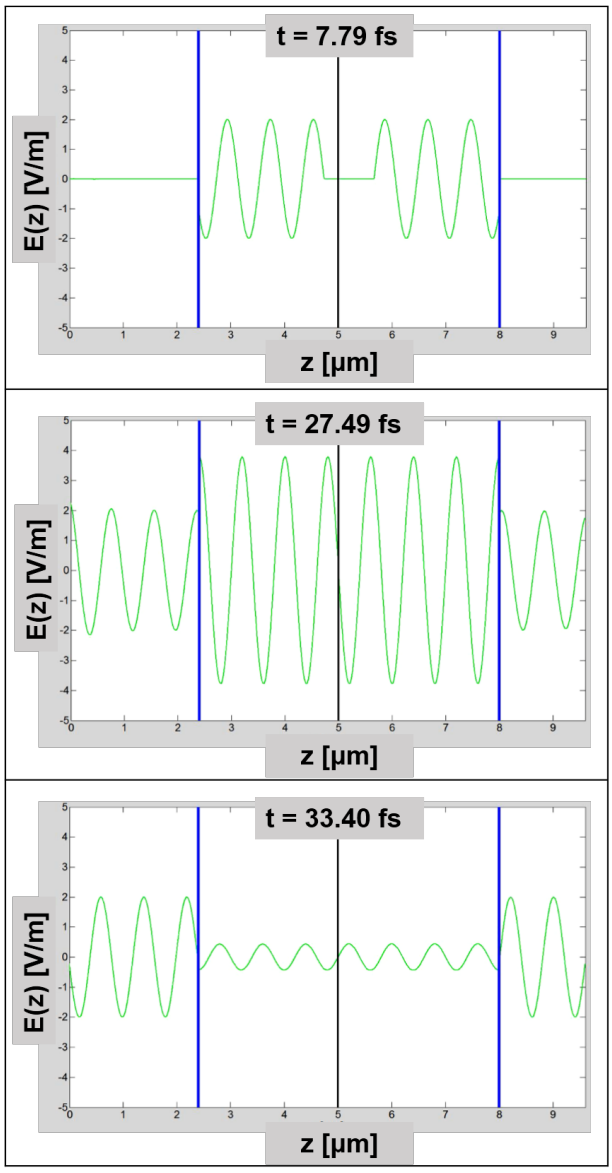

FIGURE 2.8: The figures show the propagation evolution (z-t plot) of the two counter-propagating fields evaluated with a numerical finite-difference time-domain (FDTD) simulation. Two continuous wave sources (positions indicated with solid blue lines) emit 785 nm light in opposite directions. The position of the graphene sheet is indicated with a black line. The stills (a) to (c) showcase the case where the incident beams form a node (zero-field position) at the 2D film, which leads to zero absorption/perfect transmission. (c) shows that the optical energy is completely transmitted outside beamsplitter pair and the 2D material absorbs no energy incident on it, i.e., it exhibits total transparency. These simulations were carried out by N. Westerberg.

a method to overcome the universal limit to absorption in a thin film by considering an asymmetric environment (patterned graphene sheet above a metallic substrate). Following this method, J. Zhang, et.al., applied the theory of Coherent Perfect Absorption [7] to patterned monolayer of graphene to realise a modulation of absorption from 99.93% to 0.01%, utilising the plasmonic resonance of graphene [53].

As discussed previously, a thin film needs to be 50% absorbing for it to exhibit total absorption in the coherent perfect absorption arrangement. Pristine, unbiased graphene absorbs 2.3% of the incident visible light. Absorbance of graphene is given by $\alpha = a_0\pi$, where

$$a_0 = \frac{e^2}{4\pi\epsilon_0\hbar c} \tag{2.14}$$

which is the fine structure constant. Therefore, the value of α for a single atomic layer graphene is 0.0229.

The transmittance of graphene multilayers, with N being the number of atomic layers, is defined by the formula

$$T = (1 - 0.023)^N \tag{2.15}$$

Therefore a graphene sample with 30 layers, i.e., N = 30 gives a transmittance of 0.497, which means its absorption is $\sim$50 %. The question at this point is whether a graphene sample with 30 atomic layers ceases to be graphene and becomes graphite, which possesses very different optical properties compared to that of graphene. This is addressed by examining the Raman spectrum of the graphene sample, peaks in which give the indication of whether the sample exhibits the properties of graphene or not. The characteristic *G* and *D* peaks in the Raman spectrum are the deciding factors while categorising multilayered graphene samples [54].

The thickness of graphene sample with 30 atomic layers is $\sim$ 10 nm (theoretically, a monolayer graphene is of thickness 0.335 nm) which makes it two-dimensional with respect to the optical wavelengths. The optical two-dimensionality and the fact that it also exhibits 50% absorption in the same wavelength range, makes 30 atomic layered graphene sample a good candidate for performing CPA experiments.

2.4 Summary

Coherent perfect absorption is an all-optical process which offers a flexibility in terms of tunability of absorption by modulating the relative phase of the interacting optical fields. This chapter summarised the conditions required for realising CPA in bulk and 2D materials. The conditions to achieve maximum absorption in an optical thin film were deduced and discussed. The properties of graphene multilayers that make them the ideal candidate for the CPA purposes were also discussed. A combination of all these factors could potentially allow for a light-with-light control of optical effects, which can be used in many applications such as data processing (optical modulator [14, 15]) and light manipulation at nanoscale [55].

Chapter 3

Nonlinear Optics: Four-Wave Mixing

3.1 Introduction

Nonlinear optics is a branch of optics which came to light in 1961, closely following the invention of LASER by Theodore Maiman in 1960. Peter Franken and co-workers at the University of Michigan observed second-harmonic generation in a quartz crystal using light from the Ruby laser [56]. This can be attributed to the fact that the essential ingredient for the observation of nonlinear optical phenomena, that were probed in the initial days (frequency conversions), was high intensity (10^9 W/cm^2) of coherent light. When high intensity light field encounters certain optical medium, the interaction is no longer linear: the light modifies the material response to the field, which in turn alters the optical field itself. This light-modification-by-light opens up many possibilities for new optical interactions. Such nonlinear optical interactions include frequency conversion, optical mixing, propagation effects like self-focusing and self-phase modulation, and optical parametric oscillation. As the field of nonlinear optics has grown, the pool of optical nonlinear materials has also considerably expanded - crystals [57], optical fibres, liquids made of asymmetric molecules [58], two-dimensional media like metamaterials, heterostructured layers and also graphene (patterned, doped or in a multilayer form).

In this chapter we discuss optical phase conjugation (OPC), a nonlinear phenomenon which breaks the limitation of conventional linear optics by making possible reversible optical imaging systems. In a conventional imaging system, owing to aberration caused by optical elements and the medium, a wavefront cannot be retrieved perfectly [59]. The phenomenon of optical phase conjugation provides a way to overcome this limitation. In the sections that follow, the process of Degenerate Four-Wave Mixing (DFWM) is discussed. DFWM is one of the methods for generating OPC and it is the method used in

the experiments reported in this thesis. Another nonlinear effect that changed the face of imaging is negative refraction, which allows for sub-wavelength resolution and perfect imaging [60]. The following sections discuss the theory behind the time-reversal and negative refraction effects and also include comments on a curious symmetry they share.

3.2 Optical Phase Conjugation

Optical phase conjugation (OPC) is also called the 'time-reversal' effect. Consider a coherent optical wave passing through an inhomogeneous, but transparent medium. At the output its amplitude wavefront and the phase-front are distorted due to the inhomogeneity of the propagating medium. Optical phase conjugation is a process by which a time-reversed replica of the original wave is retrieved by passing the deformed wavefront through the same inhomogeneous medium a second time, but after passing via a phase-conjugating reflector. A pair of beams are phase conjugated when they are phase reversed with respect to each another, but possess the same transverse amplitude profile. If the frequency of the phase conjugate wave is same as that of the original beam, this process is called frequency-degenerate phase conjugation. We focus only on the degenerate case as it is relevant to the experimental observations reported in this thesis.

The concept is schematically represented in Fig. (3.1 (ii)) shows the phase conjugation operation, where the original amplitude profile of the *Input Wave* is restored in the *Output Wave* after being reflected by the *Phase Conjugated Reflector* and passing through the distorting medium a second time, in comparison to (i), where a normal mirror is used and the *Output Wave* is distorted after emerging from the optical medium a second time. The *Output Wave* in Fig. (3.1 (ii)) is the time-reversed form of the *Input Wave*, as shown.

Now, the plane *Input Wave* as shown in Fig. (3.1) can be represented as:

$$E(x, y, \omega) = A_0(x, y)e^{ikz}e^{-\omega t} \tag{3.1}$$

Passing through the *Inhomogeneous Medium* introduces random phase distortions, such that the beam becomes:

$$E'(x, y, \omega) = A_0(x, y)e^{i[kz+\phi(x,y)]}e^{-\omega t} \tag{3.2}$$

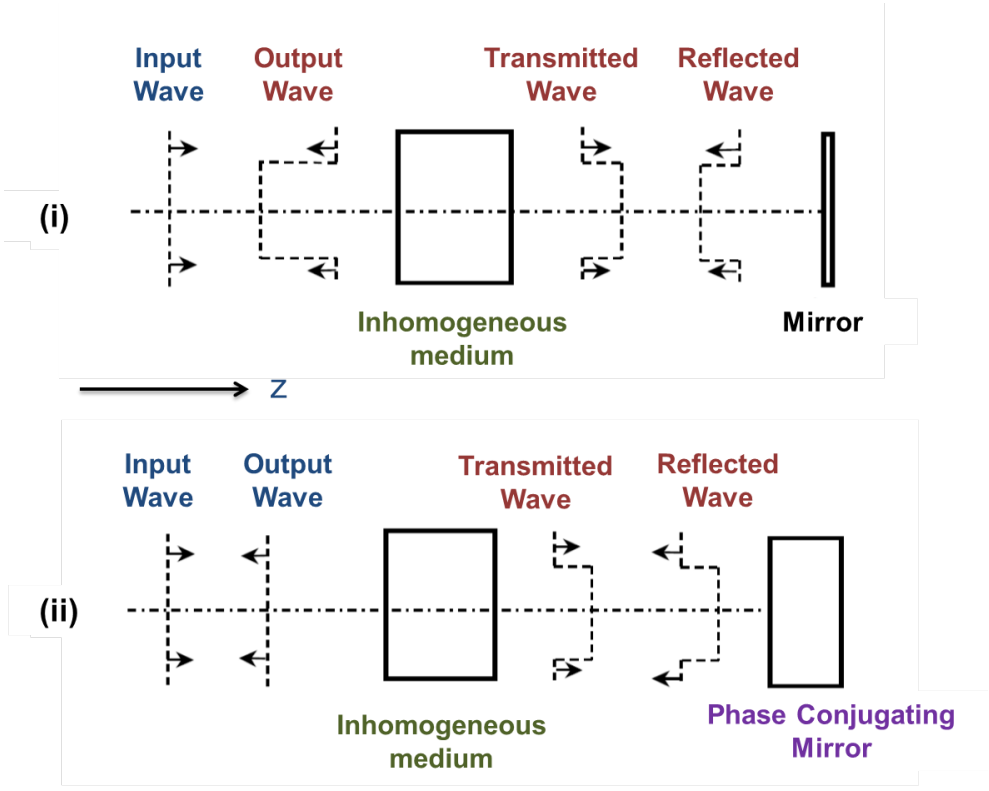

FIGURE 3.1: The two illustrations are a schematic representation of an input plane wave which travels through an inhomogeneous medium and is reflected back through it by two different mirrors. (i) and (ii) show the difference between the effect of a normal mirror and a phase-conjugating reflector. In (i) we see the *Input Wave* passing through a distorting medium, which introduces a certain phase-front to the beam (*Transmitted Wave*), which is then reflected by the mirror, so that the phase profile is preserved. This Reflected Wave goes through the *Inhomogeneous medium* again, experiencing an additional phase-distortion as seen in *Output Wave*. Whereas, in (ii) the mirror is replaced by a *Phase Conjugating Mirror*, and the *Reflected Wave* is time-reversed and hence another passage through the medium restores its original phase-front. This figure is adapted from [59].

where ϕ describes resultant phase distortion due to the aberration influence on the plane wavefront. If this beam then undergoes a reflection at a mirror, with reflectivity $\bar{R}$, as shown in Fig. (3.1 (i)), the *Reflected Wave* is written as:

$$E''(x,y,\omega) = \bar{R} \cdot A_0(x,y) e^{i[-kz+\phi(x,y)]} e^{-\omega t} \tag{3.3}$$

This *Reflected Wave* undergoes an additional ϕ phase shift on its second passage through the medium, leading to:

$$E'''(x, y, \omega) = \bar{R}' \cdot A_0(x, y) e^{i[-kz+2\phi(x,y)]} e^{-\omega t}.$$

Now we consider the second case, as shown in Fig. (3.1 (ii)), where the transmitted wave is reflected by phase conjugating mirror, such that the *Reflected Wave* is of the form:

$$E''(x, y, \omega) = \bar{R} \cdot A_0(x, y) e^{i[-kz-\phi(x,y)]} e^{-\omega t} \tag{3.4}$$

As this beam passes through the distorting medium a second time, the resulting *Output Wave* takes the form:

$$E'''(x, y, \omega) = \bar{R}' \cdot A_0(x, y) e^{i[-kz-\phi(x,y)]} e^{i\phi(x,y)} e^{-\omega t} = \bar{R}' \cdot A_0(x, y) e^{-ikz} e^{-\omega t} \tag{3.5}$$

This phase-conjugate wave is an ideal plane wave, with no effect of the aberration influence from the medium.

Optical Phase Conjugation can be achieved through three approaches: (i) stimulated backward scattering (for eg., Brillouin, Raman scattering) [61], (ii) four-wave mixing [62], and (iii) stimulated backward emission from a laser [63]. The first nearly 'time-reversed' signal was experimentally demonstrated by Zel'dovich et al., [61] using the stimulated Brillouin scattering method. Since then, numerous ways of achieving OPC have been explored. Also, OPC can be differentiated into four categories: backward degenerate, backward non-degenerate, forward degenerate and forward non-degenerate. In practice, backward degenerate optical phase conjugation has proved to be the easiest and most efficient to realise. The most popular method to generate a backward phase conjugate wave is the backward degenerate four-wave mixing (FWM), proposed first by Hellwarth in 1977 [62]. The optical phase conjugation experiments reported in this thesis are generated by backward degenerate FWM of optical fields at graphene multilayers. The following section explains in detail the Four-Wave Mixing (FWM) approach to generating phase-conjugated waves.

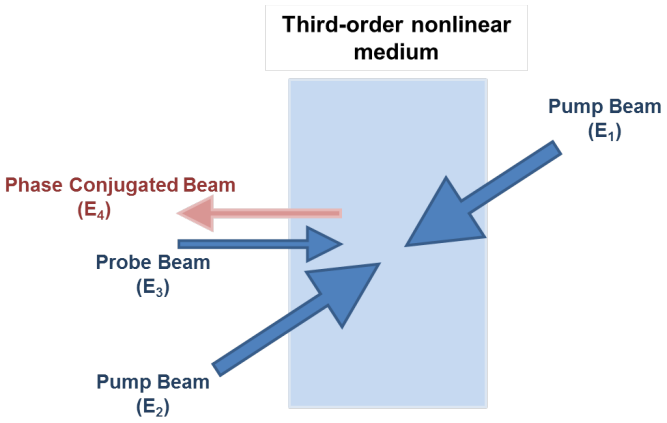

FIGURE 3.2: A pictorial representation of Four-Wave Mixing in a third-order nonlinear medium. Here the Pump Beams E_1 and E_2 interact at the medium to produce a holographic grating with which the Probe beam, E_3, interacts to produce its Phase Conjugated Beam E_4. The phase conjugated beam travels in the direction opposite to the probe beam.

3.2.1 Four-Wave Mixing

Four-Wave Mixing (FWM) is a third-order nonlinear phenomenon. It can be generated through various processes depending on the type of nonlinear medium. It is generated by the photorefractive effect in most isotropic, dielectric media. However, the process of FWM greatly varies in two-dimensional materials as discussed later in this section. The general scenario of FWM is shown in Fig. (3.2), where a medium with high third-order nonlinearity is illuminated by two counter-propagating monochromatic plane waves E_1 and E_2, both with the same frequency ω. A third beam, $E_3(\omega)$ - the *Probe Beam*, is incident on the medium at an angle other than the angles of incidence of the two pumps. Under the conditions of simultaneous illumination by all three beams, the medium stands a chance at generating a fourth wave (E_4 in Fig. (3.2)), with the same frequency ω which travels in a direction exactly opposite to that of the Probe. This effect is called backward degenerate four-wave mixing and the resulting optical wave can be proved to be the phase-conjugate wave of $E_3(\omega)$. The physical manifestation of this process in a photorefractive medium is explained in the following part.

From a purely photorefractive effect point-of-view, the interference fringes produced in the nonlinear medium induce a spatially modulated intensity distribution, *I(x)* as shown in Fig. (3.3). This, in turn, produces a spatial re-distribution of charge carriers, ρ(x), and an induced static field amplitude distribution, *E(x)*, in the medium [64]. Due to linear

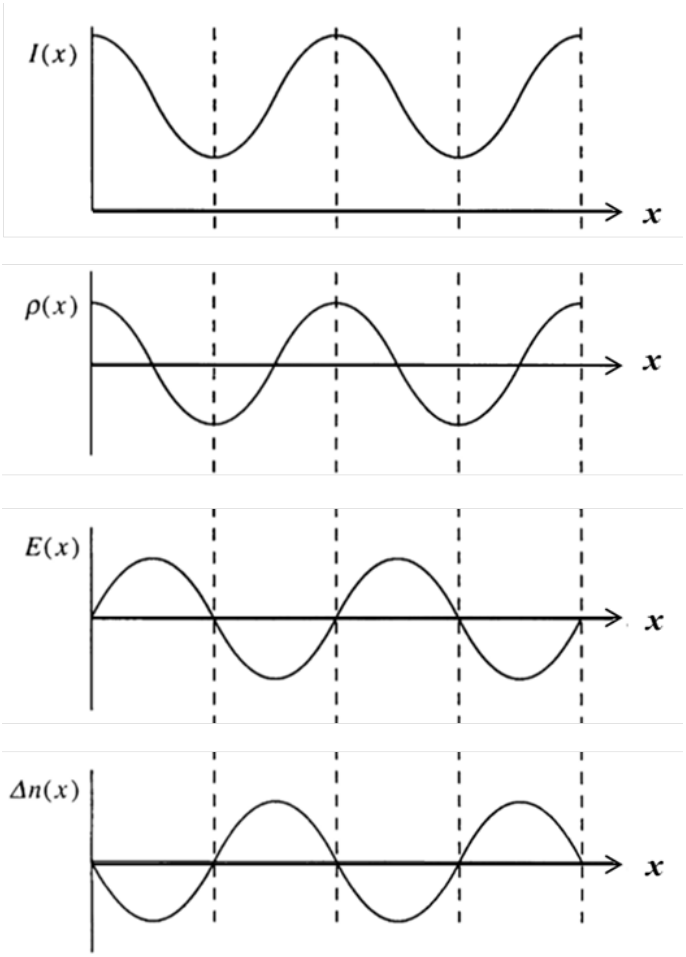

FIGURE 3.3: Photorefractive effect in a nonlinear optical medium, representing induced spatial distributions of intensity I(x), charge density ρ(x), induced static field amplitude *E(x)* and induced refractive index change Δn(x) as a function of spatial coordinate x.

electro-optic effect the induced static field produces a refractive index variation, Δn(x), as shown in the figure. A look at the spatial distribution of the various quantities shows a 90° shift in the maxima of the electric field and the charge distribution, which is attributed to Maxwell's equation $\nabla \cdot D = \rho$. Since the refractive index variation is a consequence of the induced static electric field, it is observed that Δn(x) too is shifted by 90 degrees with respect to the intensity distribution, *I(x)*. This phase shift leads to transfer of energy between optical fields interacting with the medium, giving rise to optical mixing processes. New beams are generated or chosen input beams can be amplified using the displacement between the induced refraction grating in the medium and the intensity distribution that caused it. Under this condition, the pump beam(s) interferes destructively with the scattered light from the input beams and the signal wave interferes constructively

with the scattered light, leading to its amplification. These effects can be mathematically described using the concept of coupled-amplitude wave equations which represents the transient behaviour of beam coupling [64]. In four-wave mixing process, the material response gives rise to four distinct gratings but by carefully controlling the experimental situations (input angles, propagation directions and coherence properties) only one of the gratings can be made accountable for generating the nonlinear mixing.

The model of induced holographic grating is generally considered to explain the theory of generating optical phase conjugation using FWM. Here, two of the three interacting beams interfere to produce volume grating in the medium and subsequently the third beam is reflected back in the same direction (travels in the opposite direction) as a consequence of wavefront reconstruction, thus giving rise to a phase-conjugated beam. Fig. (3.4) shows the conditions for induced holographic gratings to be set up in a nonlinear medium by incident beams. The two plane pump waves, E_1 and E_2, are incident on the medium such that they are counter-propagating and the third, 'signal wave,' E_3 is incident at an angle θ with respect to the pump wave E_1. This arrangement provides the opportunity for FWM through two possible induced gratings, to produce the backward propagating wave E_4. The first possibility is shown in Fig. (3.4) (i), where the interference between the two waves E_1 and E_3 leads to fringes along the bisector direction of the crossing angle θ, represented as dashed lines in Fig. (3.4 (i)).

The interference fringes produced in the nonlinear medium induce a refractive-index change as a function of the local light intensity. This can be interpreted as an induced holographic grating within the nonlinear medium. The pump wave E_2, considered the reading beam, encounters the induced grating produced by the interference of E_1 and E_3 and is diffracted (or reflected) into the wave E_4, as depicted in the figure. The principle of holography implies that this diffracted wave E_4 will restore the spatial information carried by the incident signal wave E_3. Alternatively, it can be said that the waves E_3 and E_4 are a pair of phase conjugate waves.

As further explanation, if the nonlinear medium is treated like a holographic medium its transmission function determined by the interference-induced refractive-index modulation can be written as:

$$T \propto (E_1 + E_3)(E_1 + E_3)^* = |E_1|^2 + |E_3|^2 + E_1^* E_3 + E_1 E_3^* \tag{3.6}$$

As E_1 and E_2 are counterpropagating plane waves, $E_2 = E_1^*$, and hence the transmitted field of E_2 can be expressed as:

$$E_2' \propto TE_2 = TE_1^* = [|E_1|^2 + |E_3|^2]E_2 + E_3(E_1^*)^2 + E_1E_2E_3^* \tag{3.7}$$

A look at the right hand side of the final expression shows that the third term represents a diffracted component, $E_1E_2E*_3$, which contains the spatial information carried by the wave E_3 and can be written as:

$$E_4 \propto E_1E_2E_3^*, \tag{3.8}$$

which is essentially the phase-conjugate of E_3. Another possibility under these illumination conditions is that E_1 is the reading beam, while E_2 and E_3 form the induced holographic grating, as shown in Fig. (3.4 (ii)). This case too leads to the generation of a phase conjugate wave, travelling in the direction opposite to that of the signal wave. Similarly, it can be shown that non-degenerate backward four-wave mixing can generate non-degenerate optical conjugation. But as per the scope of the experiments reported in this thesis, only physics behind the frequency-degenerate case is discussed.

This section assumes the medium to be bulk nonlinear and the experiments performed

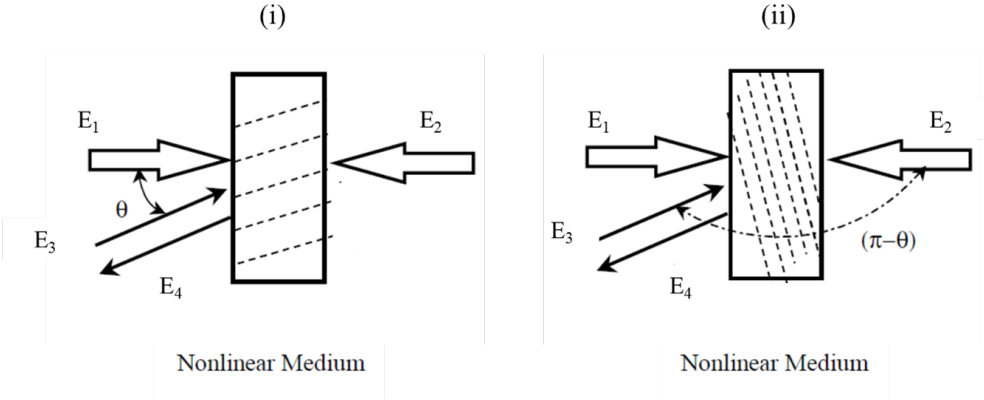

FIGURE 3.4: A schematic representation of possibilities for the generation of FWM in a third-order nonlinear medium with three input beams, E_1, E_2 and E_3. (i) the beams E_1 and E_3 interfere in the medium to produce a holographic grating (shown as dashed parallel lines) with which the probe beam, E_2, interacts to produce its Phase Conjugated Beam E_4, and (ii) shows a possibility of the holographic gratings formed as a result of interaction between E_2 and E_3.

(and reported here) are in 2D graphene multilayers, the basic principle of generation is still applicable. Phase conjugation at an interface, similar to OPC in the two-dimensional scenario, was theoretically proposed by Zel'dovich et al. [65] in 1980. Phase conjugation using surface nonlinearity induced by DFWM was demonstrated in 1992 by Maki, et al.[66] They examined the nonlinear response from the surface of an atomic potassium vapour, which was induced by a spatially varying reflectivity pattern resulting from the interference of two optical fields. This surface reflectivity varies as a function of the intensity of the total optical energy incident across the surface thus scattering the pump energy into a phase-conjugated wave. The surface nonlinearity is excited by the electric field distribution across the boundary between the vapour and the flat window of the vapour cell. This model provided a valid theoretical model for generating surface phase conjugation for any homogeneous optical nonlinear medium with a high third-order susceptibility.

In 2013, H. Harutyunyan et al. demonstrated optical phase conjugation in a few layered (20 atomic layers) graphene sample utilising its high third-order nonlinear susceptibility [36], bringing focus to the third order optical nonlinearity of graphene. Photorefractive effect usually implies generation and migration of charges which is a slow effect. We note that the nonlinearity observed in our experiments is due a modulation of the third order nonlinear conductivity, $\sigma^{(3)}$ which is related to the third-order nonlinear susceptibility through the equation

$$\chi^{(3)} = \frac{\sigma^{(3)}}{\omega d} \tag{3.9}$$

where ω is the frequency of the optical signal and d is the thickness of the graphene sample as explained in [37]. The third order nonlinear conductivity changes the refractive index and the material properties on an ultrafast time scale and gives rise to FWM effects as explained in the photorefractive case. The experiments performed as part of this thesis follow a varied geometrical configuration to excite optical nonlinearities in graphene multilayers, the specifics of which are discussed more in detail in the experimental results chapter, Chapter (5). The following section discusses another nonlinear optical process: negative refraction, which manifests in graphene multilayers in partnership with the phase conjugation.

3.3 Negative refraction

Victor Veselago, in 1964, conjectured the existence of a type of material which has negative values for both its electric permittivity ϵ and magnetic permeability μ [67] . Such a material would exhibit a negative index of refraction which is not a natural optical phenomenon. This idea opens up a whole new arena of optical effects and experiments. In 2000, Smith et al., showed a composite material exhibiting a negative refractive index for radiation in the microwave region [68]. Pendry, also in 2000 [60] , proposed a method for realising this process using a thin slab (40 nm) of silver and also showed how it could potentially be used for a new class of lenses which would resolve objects of a few nanometers in dimension. Since then, a new class of engineered materials, called metamaterials, has been designed and used to demonstrate negative refraction in various regions of the electromagnetic spectrum [69]. Chen and Alù [27] reported the demonstration of perfect imaging using negatively refracted beams. Intensive research is being performed to realise this phenomenon and a lot of focus also lies on the kind of material that can support these effects. In 2006, Kobayashi [39] proposed the idea of using two-dimensional graphite lattices as a medium to perform negative refraction (briefly discussed further in this section), following which Pendry proposed the idea of using graphene for simultaneous generation of negative refraction and phase conjugation [26]. In 2013, Harutyunyan et al., reported an experimental demonstration of negative refraction in graphite thin films (20 atomic layered graphene) [36] and this concept is used in one of the experiments reported in this thesis (Chapter 5).

The basic behaviour of light interacting with a material with negative refractive index is shown in the Fig. (3.5). The schematic representation shows the medium converging a diverging beam at both its interfaces, indicating a phase reconstruction in the forward direction. A possible connection between the phase conjugation and negative refraction processes is handled briefly in the following part of this section.

3.3.1 Time reversal and negative refraction: A symmetry

In 2008, J. B. Pendry proposed an intimate link between two nonlinear processes: time reversal, also called phase-conjugation, and negative refraction [26]. During the process of phase conjugation, a wave is reflected into a state where its phase evolves backwards in time and in the process of negative refraction, a wave is transmitted into the medium while its phase evolves backward in space. However, for negative refraction to occur, the

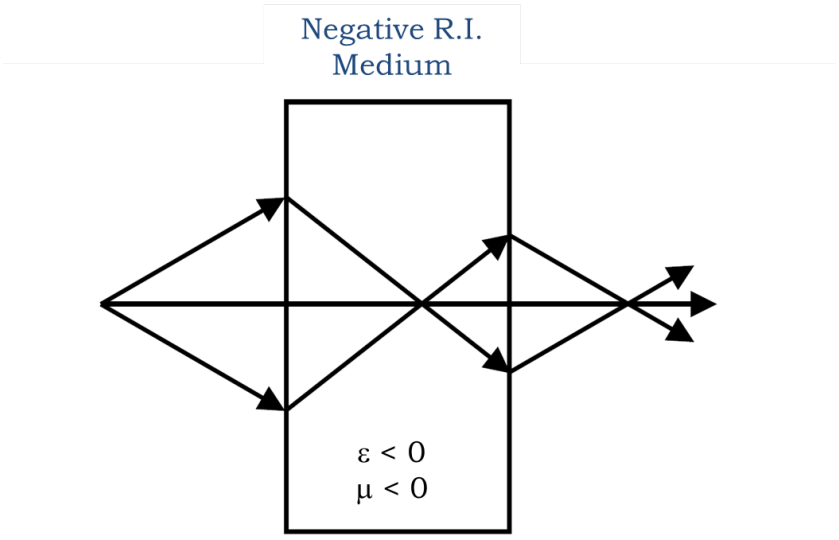

FIGURE 3.5: A negative refractive index medium is shown converging light waves to a point, which were formerly diverging from a point source. A diverging beam emerging from this medium converges again outside the medium. This figure is adopted from [60] .

refractive index of the material has to be negative as discussed in the previous section. With the expansion of the class of optical materials, it has been found that some materials called the 'self-conjugate' materials which include chiral media and graphene, exhibit a property where the medium supports both positively and negatively refracting states, i.e., it allows for the realisation of negative refraction. This scenario treats negative refraction as a phase conjugated field that is transmitted, rather than reflected as in the standard situation (backward OPC) and moreover, at negative angles. The property of graphene to support negative refraction was theoretically explored by K. Kobayashi [39] by considering a complementary medium (negatively refracting medium) of electrons. Interfaces of the graphitic lattice forming complementary systems was investigated by the transfer matrix approach. Graphene's electronic band structure (massless dispersion [70]) gives rise to the condition necessary to form a complementary system.

3.4 Summary

This chapter was an overview of some of the concepts of nonlinear optics which are relevant in the context of this thesis. It covered the basic theory behind the degenerate four wave mixing process (DFWM) and the generation of optical phase conjugation (OPC)

using DFWM. It also introduced the concept of negative refraction and included a brief review of the evolution of the concept from a purely theoretical point to being realised in 2D materials. These concepts cover the physics behind the experiments performed and observations discussed in the experimental-results chapter, Chapter 5. The fine connection between the phase conjugation and negative refraction processes was briefly mentioned and more of it is discussed in the said experimental chapter.

Chapter 4

Coherent Control of Absorption and Scattering in Graphene

4.1 Introduction

The method of light-with-light modulation in a thin film based on the process of 'coherent perfect absorption' is discussed in detail in Chapter 2. This chapter elaborates the experimental methods of putting the theory of CPA to action using a Sagnac interferometer and graphene multilayers. The experimental configuration and the procedure for generating efficient light-matter interactions in graphene are discussed in the following sections of this chapter. The first experiment performed in this regard is the coherent control of perfect absorption/transparency and linear scattering of light using graphene multilayers. This chapter is a detailed discussion of the experiments demonstrating, for the first time, the use of unstructured multilayer graphene films for coherent absorption. A summarized version is reported in [71].

The phenomenon of CPA was previosuly demonstrated in metamaterials [15] and structured graphene [16]. In addition to control of absorption, the work discussed in this chapter also shows that this geometry can be used to control, i.e., enhance or suppress, other optical interactions such as linear scattering. These effects are observed in linear optics regime as the experiments are performed with laser sources attenuated to operate at low light intensities. Hence the light-with-light control is attributed to two factors: the coherent-perfect-absorption geometry and the dimensionality of graphene. It is also to be noted that because of graphene's mostly linear band structure for all of visible and NIR region of the electromagnetic spectrum, the CPA process not only works for monochromatic continuous wave laser beam, but also for a 100 femtosecond laser pulse with a

bandwidth of 10 nm. Detailed discussions are presented in the following sections of the chapter.

4.2 Experimental Methods

The experimental configuration for observing CPA in graphene multilayers, as discussed in Chapter 2, is to place it in a standing-wave environment. The geometry involves a three-armed Sagnac interferometer, which is a type of ring interferometer. The advantage of using a Sagnac interferometer is that it is easier to align and it provides excellent contrast and fringe visibility. Here, it allows for an arrangement where two coherent counter-propagating laser beams form a standing wave so that a graphene multilayer can be placed in the position of this standing-wave envelope. The sample is mounted in a manner such that it can be scanned through the different nodes and antinodes of the standing wave.

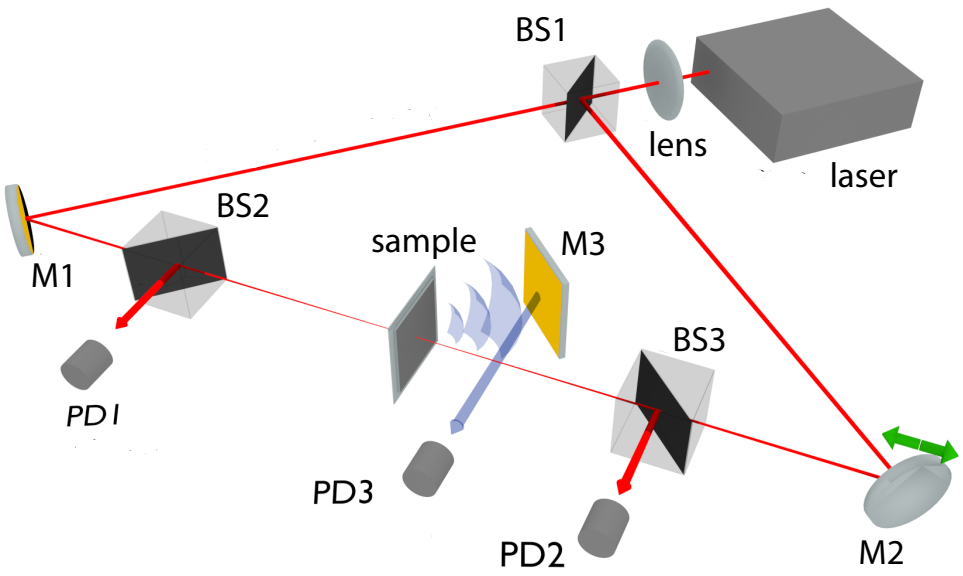

FIGURE 4.1: A schematic representation of the experimental layout showing the Sagnac interferometer with the graphene sample at the region of interaction of the counter-propagating beams. The photodiodes PD1 and PD2 record the on-axis light energy. A Mirror, M3, collects the off-axis scattered light and redirects it to photodiode PD3. Mirror M2, which directs one of the beams to the sample is mounted on a piezoelectric stage. This figure has been adapted from [71].

The main condition for such a geometry to exhibit CPA is that the absorbing medium needs to be much thinner than the laser wavelength and it should exhibit 50% absorption. In one of the experimental cases, the laser pulse width is 100 fs (length of the laser pulse is 30 μm) and the central wavelength is 800 nm. In the CW case of the experiment, the wavelength used is 532 nm. The thickness of the graphene multilayer is $\sim$9 nm, which is significantly less than the wavelength of the interacting optical beams, which enables the graphene sample to be scanned through the nodes and antinodes individually. As a result, the graphene sample experiences an absence or a presence of the optical field, respectively. This is not possible in a bulk medium because the intensity distribution between nodes and antinodes is averaged out. In this respect, the two-dimensionality of the graphene sample becomes an advantage. The standing-wave environment allows for maximum light-matter interaction, but the working principle of CPA requires the 2D material to possess 50% absorption to satisfy the condition for perfect absorption or perfect transparency of the sample.

In our experiments, we manipulate the relative phase of the two counter-propagating laser beams to produce successive nodes and antinodes at the sample position, instead of spatially scanning the graphene sample through the standing-wave pattern. This method essentially produces the same effect. The experimental setup and the relevant parameters are detailed in the following section of this chapter. The experiments are conducted using both CW and pulsed laser beams. Accordingly, the optical components of the experimental layout are changed.

4.2.1 Experimental configuration

Fig. (4.1) shows the general experimental layout. The output from a laser source [(i) Nd:YAG CW laser and (ii) Ti:Sapphire, mode-locked laser] is split into two coherent beams of equal energies by a beamsplitter, BS1. The angle of the beam-splitter is carefully chosen so as to achieve 50:50 splitting of the original laser beam, and also so that the two resulting beams travel at angles suitable to form a triangular laser ring, with the help of two mirrors M1 and M2. The mirror M2 is mounted on a piezoelectrically actuated 1-D translation stage that can be automated (using a LABVIEW program) or controlled manually. The piezoelectric stage has a working range of 0-75 V, which corresponds to a range of 0-25 μm, with 0.1 V as the resolution. This corresponds to a resolution of $\sim$30 nm and is suitable for the measurements we intend to perform. The beamsplitter along

with the two mirrors form the **Sagnac interferometer**. The graphene sample is placed at the midpoint of this interferometer arrangement, such that it is at equal distance from the beamsplitter on each of its arms. A long focal length (f=1 m) lens is used to loosely focus the two counterpropagating beams at the center of the interferometer, where the sample is to be positioned. Experimentally, each of the arms of the interferometer (beamsplitter to center of the interferometer) is of the length 60 cm. It is designed in this particular way for convenience of incorporating other optical components in the interferometer (for analysis purposes) and also so the focusing lens can be placed outside the interferometer.

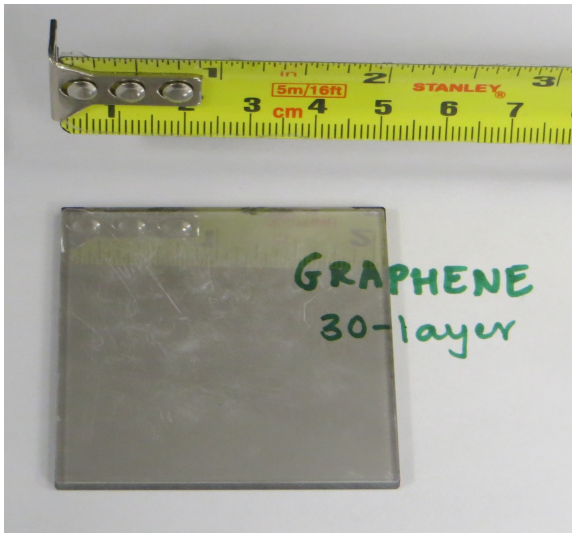

FIGURE 4.2: A photograph of the 30-layer graphene sample on a fused silica substrate obtained from *Graphene Platform*.

The optical thin film needs to possess an absorption of $\sim 50\%$ for the purposes of the experiment. We commercially obtain unstructured and 30-atomic layered graphene samples deposited on fused silica substrates from *Graphene Platform*, which is shown in Fig. (4.2). As discussed earlier, 30 layers of graphene has an absorption of $\sim 50\%$, which is experimentally confirmed by measuring the single beam transmission of the sample. This graphene multilayer is sandwiched between two fused silica substrates to provide uniform conditions for both the interacting laser beams. The sample is mounted on a 3-D translational stage for effective alignment. The sample is then placed close to the focal plane of the lens, inside the interferometer. To assist with the precise sample positioning and also to ensure that the sample is perpendicular to the counterpropagating beams, a pellicle beamsplitter is placed on one of the arms of the interferometer which directs the transmitted and reflected beams from the sample to a camera. The occurrence of interference between the transmitted and reflected beams on either side of the graphene sample

ensures the presence of the graphene film in the standing-wave position. The sample angle and the position is finely tuned until the camera shows a central interference fringe. By trial-error method we distinguish the reflection from the glass-air interfaces from that produced by the graphene layer.

After the conditions for observing CPA are set, the actual process of modulation of absorption is seen (by scanning one laser beam over another at the sample position along the propagation direction (z or -z axis). This is done by scanning the piezoelectric stage enabled mirror, M2, over a distance covering several nodes and antinodes. As the mirror is scanned, the relative phase of the interfering beams at the sample position changes, thus exposing graphene to a series of maximum and minimum energy distribution, i.e., this effectively scans the nodes and the antinodes of the standing wave through the graphene sample. The reflected and transmitted beams on either side of the sample are monitored via silicon photodiodes PD1 and PD2. The piezoelectric stage and the photodiodes are automated to record the modulation of absorption and scattering of the optical energy as a function of the relative phase between the two beams. The photodiodes record the light energies in terms of voltage and are hence calibrated beforehand.

The first experiment is carried out using a CW laser source, an Nd:YAG laser operating at 1064 nm, the SHG of which (532 nm) is used for the experiments. The fused-silica substrates include an anti-reflection coating at 532 nm, so that all the light-matter interaction occurs at the graphene layers. The second set of experiments is performed using a pulsed laser source : a Titanium:Sapphire laser (Amplitude Technologies) working at 785 nm, producing 100 fs pulses with a repetition rate of 100 Hz. The observations and inferences are discussed in the following sections of this chapter.

4.3 Results and Discussions

(1) For the measurement with a continuous wave (CW), 532 nm laser source we use an output power of 500 μW measured at BS1. The coherent modulation of the transmittance, *hence absorption*, of light at the graphene sample is shown in Fig. (4.3). As the relative phase between the two interacting beams is changed, the graphene layer experiences a sequence of nodes and antinodes in the field pattern and consequently the transmitted energy undergoes a periodic modulation, which is recorded by PD1 and PD2. The modulation in

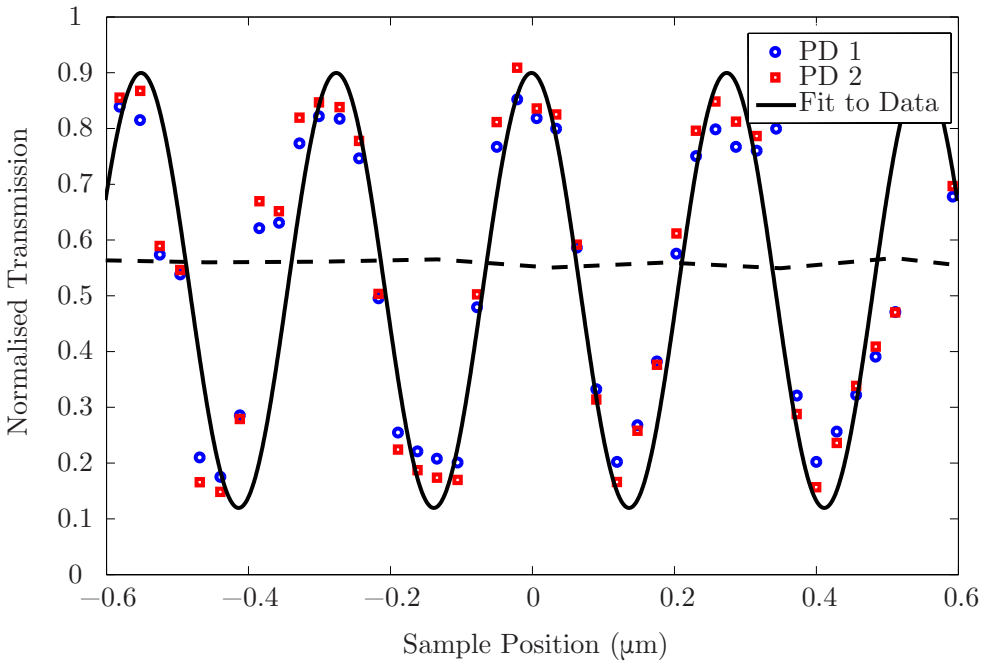

FIGURE 4.3: Experimental data: Coherent absorption with CW, 532 nm illumination, from a multilayer graphene film, as a function of the sample position within the standing wave. The dashed line between represents the travelling-wave absorption of the graphene sample. This figure has been adapted from [71].

the two arms of the transmitted light is shown by the red squares and blue circles. The measured transmission is normalised to the total energy input to each arm of the interferometer. We see that the absorption is modulated between 90% to 10% - the curves are sinusoidal fits to the data. This indicates the occurrence of CPA at the graphene sample. Since the sample is not perfectly 50% absorbing, a perfect absorption (0% transmission) or a perfect transparency (100% transmission) is not observed. Instead, a modulation contrast of 80% is recorded. The horizontal dashed line shows the single beam absorption of graphene at 532 nm, in the absence of a standing wave, i.e. with one arm of the interferometer blocked. The transmitted energy plotted in Fig. (4.3) is normalised to the total energy incident on the sample.

(2) When the experiment is performed with femtosecond laser pulses, similar results are observed. In this case, the laser beam consisting of 100 fs optical pulses obtained from a Ti:Sapphire laser and centered at 785 nm is heavily attenuated so that the energy in each arm of the interferometer is measured to be less than 10 μJ. The counterpropagating beams are focused at the mid-point of the interferometer with a long focal length lens

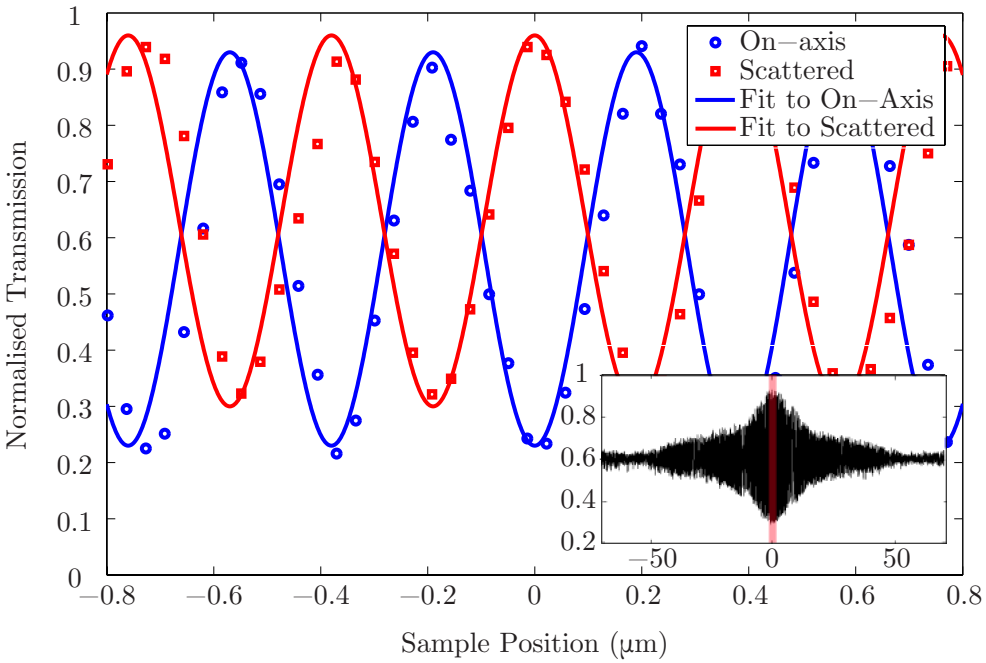

FIGURE 4.4: Experimental data: Modulation of the transmitted light energy at 785 nm, using a pulsed laser source. On-axis transmission modulation (blue circles) and scattered energy (red squares) as a function of the sample position within the standing wave. Both data are fit with sine functions oscillating at twice the laser frequency. The on-axis transmission and the scattering energies are normalised different values. The inset shows the full autocorrelation trace. This figure has been adapted from [71]

(1 m) because the light intensities at the focus need to be low enough to not damage the graphene sample. The intensity of each focused beam at the sample position is measured to be $\sim$ 1.4 x 10^{10} W/cm^2. The damage threshold of the graphene sample used in the experiments is estimated to be $\sim$ 10^{11} W/cm^2, at which the sample is observed to undergo ablation. In this case the active region for the sample to encounter coherent laser pulses is defined by the length of the pulse, which is 30 μm. The graphene sample is aligned with high precision to encounter the standing-wave envelope formed by the pulses and the energy on either side of the sample is monitored with the photodiode PD2. The mirror, M3, placed off-axis at an angle of $\sim$ 10° with respect to the counter-propagating beams, collects the scattered light and redirects it to another photodiode, PD3.

Fig. (4.4) shows the modulation of the transmitted energy as the two counter-propagating pulses are scanned through each other (along the propagation direction). The blue curve shows the modulation in the transmitted energy measured at photodiode PD2. The absorption is greatly enhanced or suppressed, with a modulation contrast that is almost 80%. The

modulation visibility observed here is slightly less when compared to the CW case. We attribute this difference to a small chirp in the laser pulse due to propagation through the dispersive optics in the system and also to a slight imbalance in the reflection and transmission coefficients related to the anti-reflection coatings that were not optimised for this wavelength. The off-axis mirror M3, placed at an angle of $\sim 10^{\circ}$ in order to collect the largest portion of scattered light without blocking the on-axis beam, directs some of the scattered energy from graphene to photodiode, PD3. The photodiode records the linear scattering simultaneously with the transmitted light. The measured scattered energy is plotted as the red solid curve in Fig. (4.4). A modulation in the scattered energy is observed as one pulse is scanned over the other. It was also seen that if one pulse is scanned over the other over a distance of a full pulse length, we can trace the pulse envelope. The inset to Fig. 4.4 shows the full pulse autocorrelation trace obtained by monitoring the scattered energy for a scan over the full pulse length.

It is clear from the figure that the on-axis transmitted energy and the scattered energy are perfectly out-of-phase. In agreement with the measurements, at an antinode it is expected that the sample experiences maximum field strength so that both absorption and scattering are maximized. At a node of the standing wave since there is no net field, the on-axis transmission (as discussed above) is maximum. For the same reason, scattering from the film and absorption by the film are minimised. These observations lead to the belief that an effective control and manipulate absorption and scattering of light is possible using a graphene film placed within a standing wave by controlling the relative phase between two optical beams, i.e., it is a demonstration of light-with-light modulation of optical interactions. This proposes a geometry to not only exploit graphene, but also other thin films for a range of applications such as optical switching, sensing, etc. [13, 72].

The creation of a signal amplitude modulator is possible with the setup described here and integrated versions of such a modulator have also been proposed [72, 15]. Similar studies with different geometries [73, 74] have been used to achieve high speed modulation by directly modifying the thin film properties. Fig. (4.5) shows the propagation evolution ($z-t$ plot) of the two counter-propagating fields evaluated with a numerical finite-difference time-domain (FDTD) simulation. Two continuous wave sources (positions indicated with solid white lines) emit 785 nm light in opposite directions. The graphene sheet (whose position is indicated with dashed red line) is modelled as a Lorentzian medium [75] tuned to transmit and reflect equal amounts ($R = T = 0.25$, such that $\alpha = 50\%$ [16]). These simulations were performed by N. Westerberg as a part of the article [71]. The mesh size of the simulations performed was 1.25 nm. The different regions marked “a”, “b” and

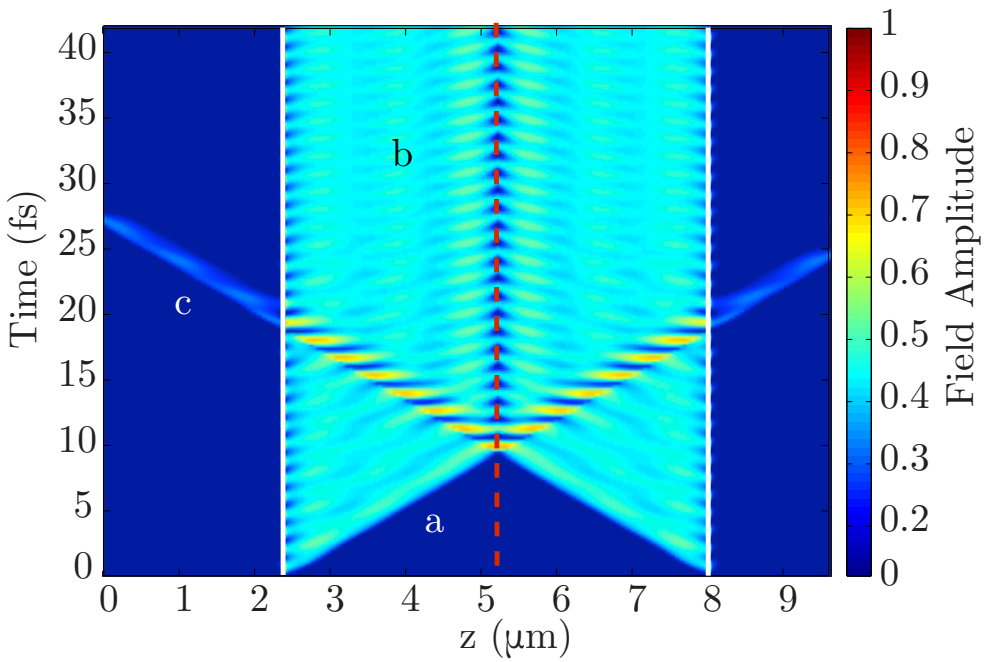

FIGURE 4.5: A z-t plot of the evolution of the electromagnetic fields evaluated numerically with an FDTD simulation. Two continuous wave sources (solid white lines) emit 785 nm light in opposite directions which meet a 2D absorbing medium, shown as a red dotted line. "a", "b" and "c" indicate regions of initial build up of the standing wave, transmitted single cycle signal and stationary regime with CPA, respectively. This figure has been adapted from [71] and the simulation was carried out by N. Westerberg.

"c" represent the different stages of evolution of the CPA phenomenon. In region "a" the wavefronts, switched on at $t = 0$, approach the graphene sheet from either side and start to form a standing wave at around $t \sim 10 \rightarrow 15$ fs. Region "b" ($t > 20$ fs) represents the steady state solution, where all the light emitted from the sources is absorbed. However, there is a build up time for the standing wave to form during which ~ 1 optical cycle of light is seen leaving the set-up, as seen in region "c". This indicates that the ultimate limitation on the bandwidth of an optical switch based on CPA in thin films is equal to the frequency of the light pulse itself.

4.4 Summary

The coherent modulation of absorption in sub-wavelength graphene multilayers is demonstrated using the coherent perfect absorption method, resulting in a 80% modulation between optical absorption and transmission. Additionally, linear scattering of light by the graphene film is also coherently modulated by changing the relative phase of the two input optical fields. These results and observations lead to the conclusion that along with absorption, other light-matter interactions can also be controlled by the light-with-light manipulation technique. So the obvious next step is to look into the possibility of generating and controlling nonlinear optical interactions using the same geometry. The following chapter deals with implementing the CPA geometry with graphene multilayers to observe nonlinear optical interactions and modulate the nonlinear signals by accessing phase-dependent nonlinearity.

Chapter 5

Coherent Control of Nonlinear Optical Interactions in Graphene

5.1 Introduction

The continuously growing need to miniaturize optical elements for the development of integrated optical assemblies makes it imperative that 2D materials and their optical nonlinearity be considered. Nonlinear optical interactions in two-dimensional materials are especially challenging to achieve due to the fact that there is very little medium available for interaction. Therefore for 2D materials to be used as nonlinear media, two aspects need to be addressed: (i) the material itself needs to exhibit a high optical nonlinearity, and (ii) a configuration to enable effective light-matter interaction. The observations discussed in the previous chapter (4), wherein $\sim 100\%$ absorption of light was demonstrated in graphene multilayers, prove that by the method of coherent perfect absorption (CPA), efficient optical interactions can be performed in two-dimensional materials. In additon to that, CPA provides a method for a light-with-light manipulation of the optical interactions. We thus have a promising method to address the second aspect of the nonlinearity-in-2D-material problem. Hence an extension of this method into investigating nonlinear optical interactions begs to be considered. The results discussed in this chapter were published in Scientific Reports in 2015 [76].

Graphene exhibits unique optical nonlinear properties which are discussed in detail in Chapter (1). In addition to having unique linear properties, it is also being widely considered for its nonlinear properties, for example, it being used as a saturable optical absorber [35]. With a third order nonlinear susceptibility ($\chi^{(3)}$) value 8-orders of magnitude higher than that of typical dielectric materials [37], it is also being used for FWM processes [36].

This particular property is of interest for the purpose of the experiments explored in this thesis. Another unique property of graphene is that it is a “self-conjugate" material [26], which enables it to host both positively and negatively refracting states. These properties of graphene make it an ideal material to realize coherent nonlinear processes as shown in [36, 26]. Optical two-dimensionality of graphene, once a disadvantage, now poses as its greatest strength for realising self-conjugation phenomenon, i.e., for generating time-reversal and negative refracting signals. The following section contains a brief discussion of the studies reported in [36] and [26] which form the basis of the experiments reported here.

5.1.1 Background

In [26], Pendry discusses the intricate connection between time-reversal and negative refraction. He demonstrates that a two-dimensional self-conjugate material, a material which supports both positive and negative refraction, like graphene and certain chiral media, could be used to generate a phase-conjugate and a negatively refracted beam simultaneously by the process of *four-wave mixing*. A brief discussion of the premise of the paper is as follows. At an optical interface, when a wave is reflected into a state in a

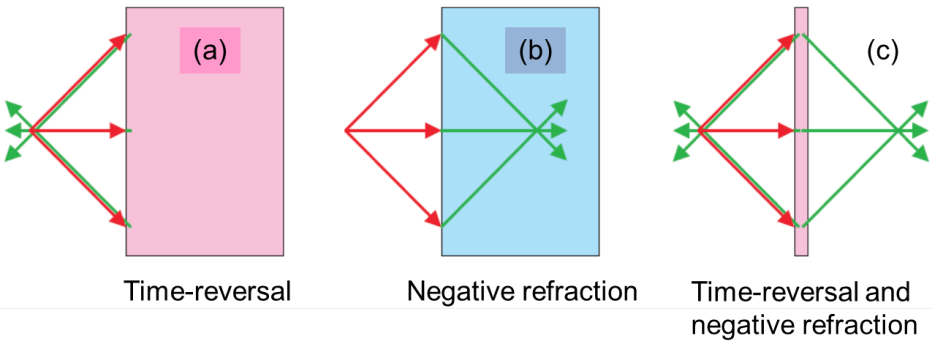

FIGURE 5.1: The behaviour of a defocusing beam incident on different material is schematically represented in this figure. Medium **(a)** time-reverses a wave winding the phase backward in time to refocus on the source. Medium **(b)** is negatively refracting and reverses the spatial evolution of the phase refocusing at some point inside the medium. A thin sheet, **(c)**, of time-reversing (/phase-conjugating) material produces negative frequency waves on both sides of the sheet: it both time-reverses and negatively refracts. The figure is adapted from [26].

way that its phase evolves backward in time, it is referred to as 'time-reversal' or 'phase conjugation'. On the other hand, 'negative refraction' is said to occur when a wave incident on a negatively refracting medium is transmitted through the medium such that its phase evolves backwards in space. Here, the refraction is at a negative angle with respect to the normal refraction. The negative refraction phenomenon was first predicted theoretically (unlike many optical phenomena, which are first experimentally observed followed by theoretical explanations). As shown in Fig. (5.1), the two processes seem to share a symmetry with phases evolving back in time and space for the phase conjugate and negatively refracted beams, respectively. The article discusses the physical realization of this link using a phase-conjugating surface which is time-dependent. If a wave of the form

$$E = E_0 exp(ik \cdot r - i\omega t) \tag{5.1}$$

undergoes a frequency shift of $\delta\omega = 2\omega$, the resulting field would be

$$E' = E_0 exp(ik \cdot r + i\omega t) \tag{5.2}$$

This shows that reversing the frequency has the same effect as reversing time, a schematic representation of which is shown in the dispersion relation figure 5.2. It also indicates that any linearly dispersing medium can be regarded as a self-conjugate material when negative frequencies are included. This is not possible at an interface between two ordinary positively refracting materials. However, a phase-conjugating medium of sub-wavelength thickness with a uniformly pulsating permittivity could be used for the realization of both phase-conjugation and negative refraction. The condition for this to occur is that the frequency of the oscillating permittivity needs to be 2ω, as discussed before. The article suggests that this parametric oscillation would lead to transitions between positive and negative frequencies.

The experimental demonstration of negative refraction in graphene by FWM was first reported by Harutyunyan *et al.* [36]. This realization is based on the fact that for ultathin films all propagation effects and in particular, all phase-matching constraints are very different compared to that for bulk materials. Two coherent counterpropagating optical beams interacting at the subwavelength thickness graphene form a pulsating permittivity at frequency 2ω. A probe beam which is coherent and meets this 'oscillating' interface sets up the condition for four-wave mixing. The wave-vector components along the propagation direction, z, that dominate the nonlinear beam evolution in bulk media, become irrelevant in a two-dimensional medium. Only the parallel components of the wave-vectors

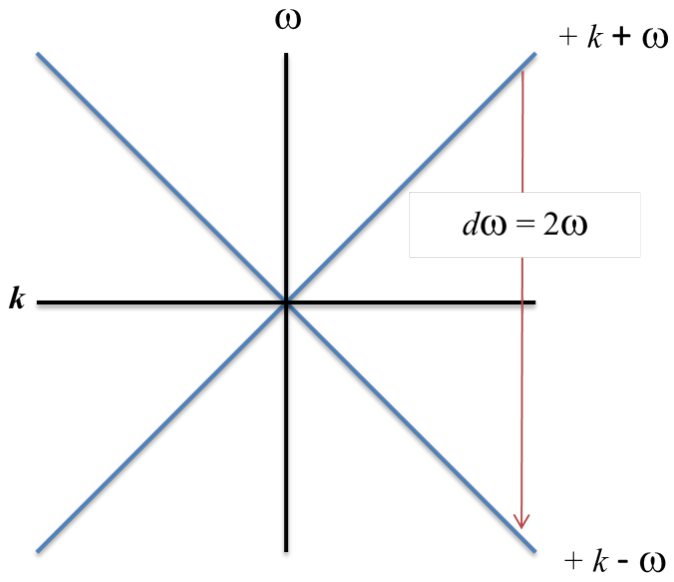

FIGURE 5.2: Dispersion of a wave in a medium with constant velocity $\omega = ck$ (where c is the velocity of light). Both positive and negative frequencies are displayed. Time reversal can be understood as a vertical transition between positive and negative frequencies. The figure is adapted from [26].

are conserved. Or, it can be said that the scattering of an input probe beam into an output beam arising from the nonlinear polarisation wave depends only on the transverse components of the wave-vector components, $k_{\perp}^{in}$ and $k_{\perp}^{out}$.

This condition also rules the nonlinear interactions at surfaces, where the onset of a quadratic nonlinearity leads to the generation of transmitted and reflected nonlinear signals [77, 78]. If the two counter-propagating pump beams are at normal incidence on the film, then momentum conservation implies

$$k_{\perp}^{out} = -k_{\perp}^{in}, \tag{5.3}$$

i.e. the output beam appears as if it is propagating in a medium with an *effective* refractive index $n = -1$. Along with the generation of the conventional time reversed (phase conjugated) signal, which travels in the direction opposite to that of the probe, another signal with the opposite momentum travelling through the sample is generated, transmitted at a negatively refracting angle. It is noted that the four-wave mixing process responsible for the negatively diffracted beam has been referred to in the past as *forward degenerate four-wave mixing* or *forward phase conjugation* [79]. It has also been employed for the characterization of resonant nonlinearities in multiple quantum wells [80]. However, in recent literature this same effect is often referred to as "*optical* negative refraction" [81, 36] in relation to the fact that the medium behind the nonlinear 2D surface behaves to all effects as if it where a negative index medium [26].

The theory of four-wave mixing in a dielectric bulk medium is discussed in Chapter (3). The nonlinearity of an optical two-dimensional material, though, is found to be very different. Bulk 3D nonlinear interactions are treated as a "phase independent" effect, in the sense that they are not affected by the relative phases between the interacting input beams. For example, four-wave mixing will ensue regardless of the relative phases between the input pump beam (with phase ϕ_p) and input probe or signal beam (with phase ϕ_s) so that an "idler" wave will always be generated and will acquire the relative phase difference $\phi_i = 2\phi_p - \phi_s$. Even in the case in which a phase-dependence is known to arise, i.e. when all four beams (two pumps, a signal and an idler) are simultaneously incident on the nonlinear medium, a nonlinear polarisation is still generated and will ensure photon-photon interactions, i.e. energy flow between the beams where the relative pump/signal/idler phases only determine the direction in which the energy flows. In this sense, the specific nonlinear process (characterized by the direction of energy flow) is phase-dependent but

the (presence of the) nonlinearity itself is not. This is true also for other optical processes that are phase sensitive, for example, the optical poling induced by the sum of a fundamental and a second harmonic field [82] .

However, this is not the case when we consider two-dimensional materials. We infer that graphene allows us to investigate the 'phase-dependent' Four-Wave Mixing (FWM) process. In the phase-dependent case, a nonlinear polarisation wave in the medium is physically excited (or not excited) only for certain relative phases of the input beams. Access to such a phase-control of the nonlinearity would extend the applications and control currently available in nonlinear optics: some ideas in this sense are demonstrated in the following sections. The two-dimensionality of graphene multilayer not only provides the perfect conditions for coherent control of optical interactions, but also sets the premise for the investigation of the phase-dependent nonlinearity. This chapter is a study of the typical geometry and configuration in which light can be used with graphene to generate nonlinear signals. The following chapter deals with the alternative geometries which fully utilise the phase-dependent nature of the 2D optical nonlinearity.

5.2 Experimental Layout

The experimental setup is similar to the one used for coherent control of linear optical interactions experiments discussed in the previous chapter. The nonlinear geometry has one additional laser beam - the probe. The setup is composed of a Sagnac-interferometer that enables coherent interaction between the two counterpropagating pump laser pulses (100 fs) at a multilayer graphene sample, as shown in Fig. (5.3). The probe beam, of the same wavelength and spatial width, is spatially and temporally overlapped onto the pump beams at the sample position (see Fig. (5.4)). The phase of one of the pump beams on the sample is then finely controlled by a piezoelectric stage mounted on the last mirror that directs the pump beam onto the sample.

The laser source is a Titanium Sapphire system with 100 fs pulse duration, 100 Hz repetition rate, $\lambda = 780$ nm wavelength. In the Sagnac-interferometer the typical energy of each pump beam on the graphene sample is of the order of 1 μJ and the beams are focused down to diameters of $\sim$50 μm, i.e. the laser intensity on the graphene film are of the order of 100 GW/cm^2. The nonlinear sample is constructed by sandwiching a multilayer

(30 layers) film of graphene, of thickness ~ 9 nm, between two fused-silica substrates. The optical absorption of the multilayered graphene is $\sim 50\%$ as per the requirements for coherent perfect absorption. The sample is mounted on a 3D translational stage for fine alignment of the angle and the positioning of the sample. The temporal overlap of the probe beam at the sample is optimised with a tunable optical delay line on the probe beam-path. This layout is essentially the same as that used to demonstrate the coherent modulation of the linear properties of deeply subwavelength films, e.g. absorption as demonstrated by Zhang et al. [13] using metamaterials and more recently also using graphene [71].

5.2.1 Three-beam interaction

The first experimental configuration follows the traditional four-wave mixing geometry. The measurements are performed with the graphene sample being coherently illuminated

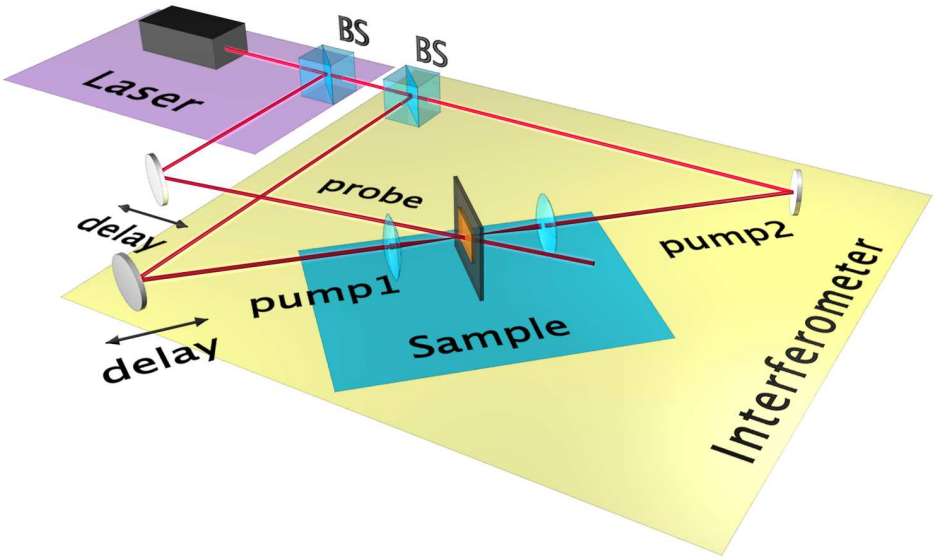

FIGURE 5.3: A schematic representation of the experimental layout: the counter-propagating pump beams (pump 1 and pump 2) and a probe beam, generated from a Ti:Sapphire laser (100 fs pulses centred at 780 nm), overlap on a 30-layer graphene sample. The two pump beams counter-propagate in a Sagnac interferometer loop and the arrangement allows to finely tune the relative phase of pump 1 with respect to pump 2 with a piezoelectric stage-controlled mirror. A piezoelectric actuator is placed also on the probe arm. This figure is adapted from [76].

by three laser beams. Two counterpropagating pump beams and a probe beam, all having the same frequency ω, as shown in Fig. 5.4, are incident on the graphene sample.

All three beams are maintained at the same input energy (5 μJ) and intensity (100 GW/cm^2). For descriptive purposes we indicate any beams that are orthogonal to the graphene film as "pump" and any beams that are incident at an angle with respect to the surface normal as "probe". The counterpropagating pump beams therefore form a standing wave across the graphene sample, creating a holographic grating whenever they form an antinode at the sample. The probe beam, at the presence of the holographic grating sets up the four-wave mixing process.

Precise alignment of the three input laser beams on the graphene sample leads to Degenerate Four-Wave Mixing (DFWM) between them. This creates a phase conjugated signal that is reflected and propagates exactly along the input probe, but in the backward direction, and is separated from the latter by a partially reflecting beam-splitter. In addition to this signal, we also observe a beam that is transmitted through the sample and, with respect to the input probe beam, is negatively refracted. The perfect optical path lengths for this to occur are achieved by tweaking the Sagnac interferometer with respect to the sample position and by manipulating the optical delay-line in the path of the probe beam. Once we visualize the presence of these signals using a Sony digital camera, we add mirrors to their paths to steer these signals into Silicon photodetectors. These photodetectors

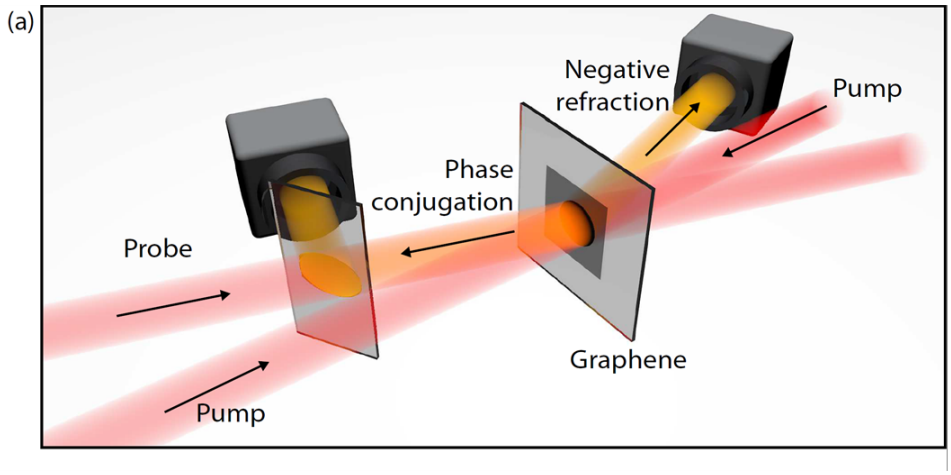

FIGURE 5.4: A schematic representation of the generation of the phase conjugated and the negatively diffracted signals (shown in orange) when the two counter-propagating pump beams and the probe beam are in phase. This figure is adapted from [76].

and the piezoelectric-stage which controls one of the pump beams are programmed to be controlled synchronously through a Labview program. This arrangement enables us to scan the standing-wave pattern across the graphene sample, while monitoring the signal strength of the phase-conjugated and negatively refracted signals as a function of the relative phase of the two pumps.

The raw data acquired from the photodetectors is plotted in Fig. (5.5). The modulations seen here are not the perfect modulation that we expect. This is mainly due to the fact that the interferometer is highly sensitive to the environment and in addition to this, the resultant nonlinear beams too are quite sensitive to the portion of graphene sample the beams are incident on, the laser stability, the speed with which we scan one pulse over the other, i.e., the speed with which we subject the graphene to alternating nodes and antinodes of the standing-wave and also the angle of the probe beam with respect to the graphene layer and the pump beams. After several combinations of these parameters, we

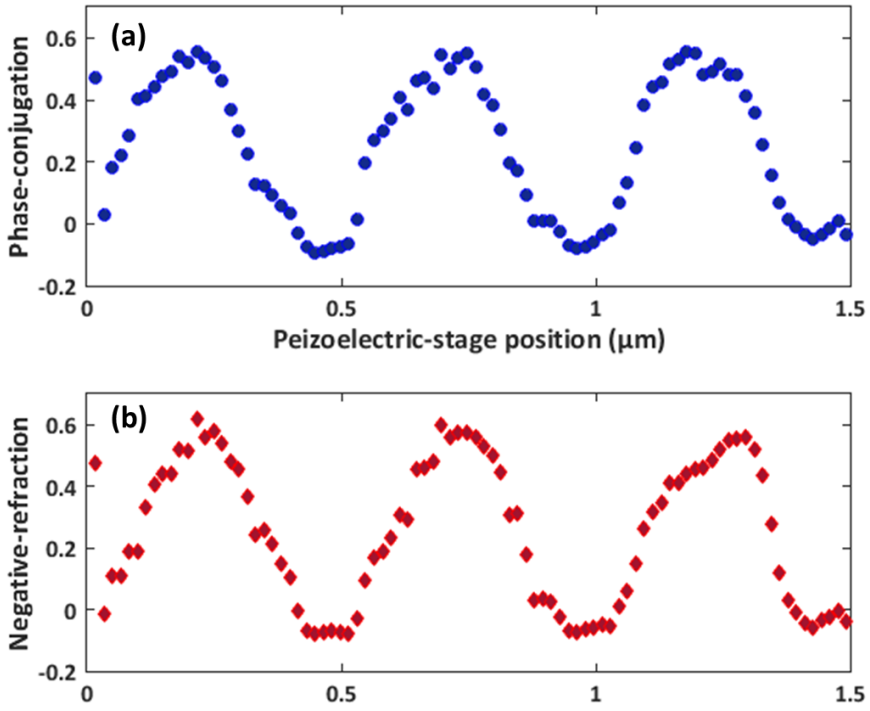

FIGURE 5.5: The raw data recorded by the photodetectors showing the phase-conjugated and negatively refracted beam amplitudes as a function of the relative delay between pump 1 and pump 2.

observe efficient modulation of the nonlinear signals.

Energy conservation dictates that both of these beams also have the same frequency ω as the input beams. A marked difference with respect to previous measurements is the phase-dependence of the nonlinearity. This becomes evident by controlling the relative phase of the two pump beams. The amplitude of the nonlinear polarisation wave that is responsible for emission of the phase conjugated and negatively refracted signals is given by:

$$P_{nl}^2 \propto \chi^{(3)}(\mathcal{E}_{\text{pump 1}} + \mathcal{E}_{\text{pump 2}} + \mathcal{E}_{\text{probe}})^3 \tag{5.4}$$

where $\mathcal{E}$ is the real electric field. It is hence clear that at a given propagation coordinate selected by the sub-wavelength film, for a fixed phase of two of the beams, the nonlinear polarisation depends on the phase of the third one.

In Fig. (5.6) we plot the time-averaged P_{nl}^2, calculated for a chosen film position that shows the phase-dependence in the form of clear oscillations, with respect to the relative phase between $\mathcal{E}_{\text{pump 1}}$ and $\mathcal{E}_{\text{pump 2}}$, which determines whether DFWM will occur (with the

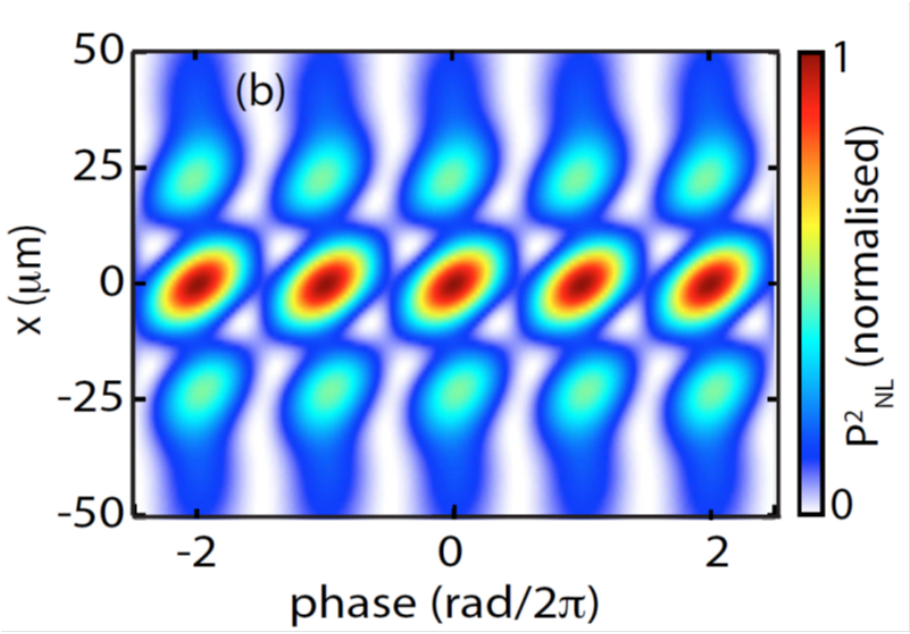

FIGURE 5.6: The full spatial distribution on the graphene film of the time-averaged nonlinear polarisation P_{nl}^2, as a function of the relative phase delay between pump 1 and pump 2 is shown in this simulated figure. This figure is adapted from [76].

generation of a phase conjugated and negatively refracted beam) or not. Another way of viewing this is to write the polarisation component that is responsible for the generation of the optical negative refraction and the phase conjugation as

$$P = \varepsilon_0[\chi^{(1)} + 2\chi^{(3)}(\mathcal{E}_{\text{pump 1}} + \mathcal{E}_{\text{pump 2}})^2]\mathcal{E}_{\text{probe}} \tag{5.5}$$

where we have isolated the polarisation term that is linear in $\mathcal{E}_{\text{probe}}$ and neglected all third harmonic and nonlinear mixing terms that involve only the two other (pump) beams. This formula shows that the two pump beams create, at a fixed propagation coordinate, an effective film susceptibility

$$\chi_{\text{eff}} = \chi^{(1)} + 2\chi^{(3)}(\mathcal{E}_{\text{pump 1}} + \mathcal{E}_{\text{pump 2}})^2 \tag{5.6}$$

which oscillates at twice the pump frequency and whose amplitude is determined by the relative pump beam phases.

This viewpoint highlights the phase dependence of the material susceptibility, which in turn determines whether the incoming probe beam encounters a "linear" or a "nonlinear" medium. In Fig. (5.6) we plot the time-averaged nonlinear polarisation, P_{nl}^2 calculated at the film position, which is clearly oscillating as a result of the χ_{eff} phase-sensitivity.

5.2.2 Experimental observations

In the experiments, both the nonlinear signals have a conversion efficiency (ratio of energies of the probe field and the resultant nonlinear signal) of $\simeq 3 \times 10^{-5}$, which is calculated by calibrating the photodetectors with a known optical energy of the laser. This is lesser than the value previously reported in [36], where a 20 layered graphene sample generated the phase conjugation and negative refraction. The decline in the conversion efficiency is attributed to the increased number of graphene layers, which causes the properties of the sample to divert from its truly 2D nature. With respect to the observation of optical modulation of the nonlinearity, phase of **pump 1** (Fig. (5.3)) is precisely varied with respect to that of **pump 2** using a piezoelectrically controlled mirror. The amplitudes of the phase conjugated and negatively refracted beams are recorded on photodetectors as a function of the piezoelectric-mirror position. Background subtraction and normalisation of the data is performed to isolate the nonlinear signals. A periodic modulation in the amplitudes of the nonlinear signals is observed with a close to 100% modulation amplitude

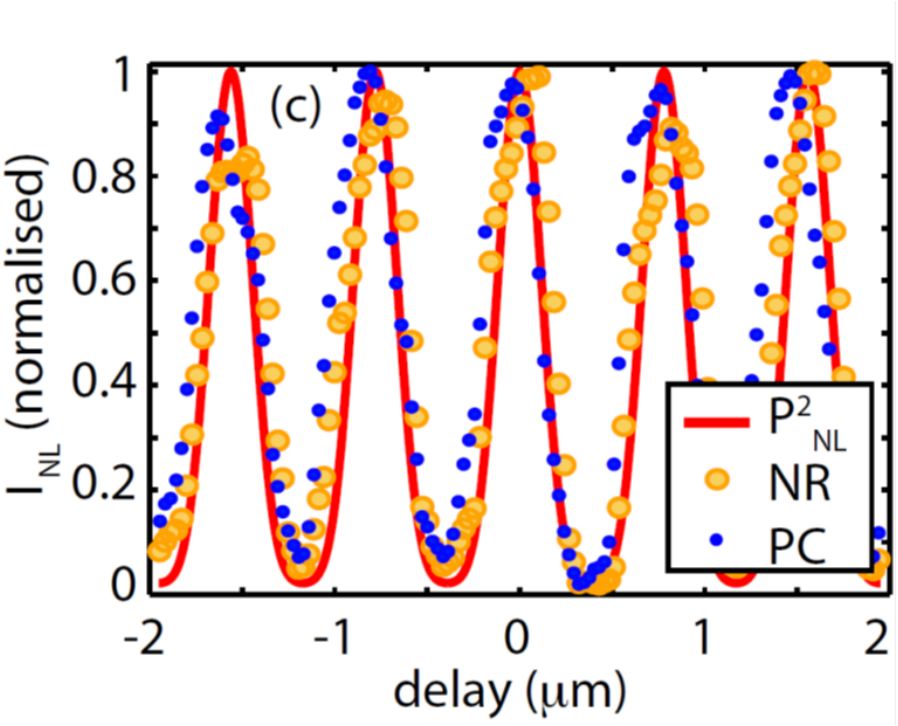

FIGURE 5.7: Generation and modulation of nonlinear signals in the three-beam geometry. The figure shows the phase-conjugated (PC, blue dots) and negatively refracted (NR, yellow circles) beam amplitudes as a function of the relative delay between pump 1 and pump 2. The red curve is the theoretical calculation of time-averaged P_{nl}^2 as described in the text. This figure is adapted from [76].

as shown in Fig. (5.7). The blue and the yellow dots represent the signal amplitudes of the phase conjugate and the optical negative refraction signals, respectively. The red solid line is the normalised plot of the time-averaged P_{nl}^2 without any free parameters (i.e., it was solely calculated from the signal strength measured by the photodetector), other than an overall arbitrary phase that has been adjusted to overlap with the data.

5.3 Imaging with the phase conjugate beam

Imaging of an object using the phase conjugated beam is carried out with the previously discussed DFWM configuration as shown in Fig. (5.8). The figure shows that by placing an object, in this case a microscope slide with the letter "x", in the path of the probe beam the object is re-imaged onto the output phase conjugate beam and the distortions along the

beam path are corrected. These results was presented in *Frontier in Optics/ Laser Science Conference*, Tuscon - 2014 [83].

5.4 Summary

This chapter discussed in detail the various aspects of nonlinear optical interaction in two-dimensional materials, here in particular in subwavelength graphene multilayer. Two-dimensional materials exhibit unique features in the way they interact with light. Linear optical properties such as absorption [13], scattering [71] and reflection [84] can be coherently enhanced or suppressed. These are the examples of the additional control enabled by the reduced dimensionality. They also offer the advantage of being able to be designed to manifest specific optical properties according to certain requirements. Here, we explored the phenomenon of generation of negative refraction as a consequence of time-reversal at a two-dimensional material. We also observe that the third order nonlinearity in a 2D material exhibits another feature, namely it may be coherently controlled by modulating the phase of the input pump beam. By fine tuning the relative phase of the pump beams,

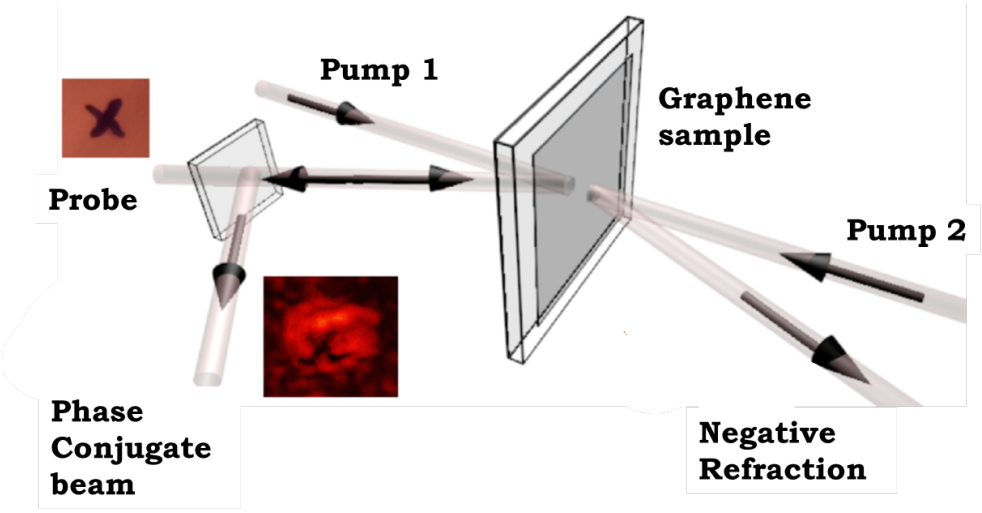

FIGURE 5.8: The experimental layout for imaging with the phase conjugate beam: an input pump and probe beams are overlapped on a graphene sample and generate a phase conjugate and negatively refracted beams. Coherent control (amplitude modulation) of the output beam amplitudes is obtained by finely tuning the relative pump-probe phases with a piezo-controlled mirror (not shown). Experiments were also performed with a second, counterpropagating pump beam (pump 2).

it is possible to control and modulate the DFWM signals, making it an all-optical nonlinear optical switch. We also observe the irrelevance of the matching of perpendicular components of the wavevectors associated with the pump beams for the four-wave mixing process, which hints towards the possibility of simpler geometries for realising this process. We make attempts at new FWM configurations to explore these options which are discussed in the next chapter.

From the observations, it is evident that the generation of the nonlinear signals is purely phase-dependent. Another possibility could be the coherent control of the nonlinearity to perform phase-contrast imaging where the phase of the probe/pump beam is directly mapped onto a corresponding intensity pattern in the phase-conjugated and/or negatively refracted beam. This possibility too is explored and discussed in the next chapter. Similarly, phase coherent control of the polarisation of the phase-conjugated and/or negative refracted beam may be achieved considering the inverse Faraday effect configuration, where the nonlinear medium is excited by a circularly polarised pump [85, 86].

Chapter 6

Negative Refraction in 2D materials and Phase-Contrast Imaging

6.1 Introduction

The phenomenon of coherent perfect absorption in combination with the degenerate four-wave mixing (DFWM) process in an optically two-dimensional graphene sample leads to the generation and coherent control of nonlinear optical interactions. The nonlinearity is observed as a time-reversed signal along with a negatively refracted field. This concept was discussed, explored and demonstrated in the previous chapter. The FWM was achieved by the traditional configuration involving three input optical fields, giving rise to the nonlinear signals. Interestingly, four-wave mixing in an optically two-dimensional material offers advantages unseen in bulk media. The 'phase-dependent' nature of the nonlinearity of graphene in addition to the irrelevance of perpendicular wavevector matching between fields paves the road to simpler FWM geometries, with possibly fewer optical fields. Such new geometries for enabling nonlinear optical interactions in 2D materials would potentially lead to more efficient and simpler configurations in integrated optical circuits. This chapter explores the alternative methods of generating negative refraction in 2D graphene multilayers. It also includes an application of the phase-dependent nature of the nonlinearity in graphene in the form of *phase-contrast imaging*.

Three experimental configurations are explored in the quest for alternative geometries to enable nonlinear optical interactions in graphene: (a) using two optical fields - pump and probe, (b) using only two optical beams in reflection mode and (c) using only one optical beam in reflection mode. The following sections outline these experimental arrangements

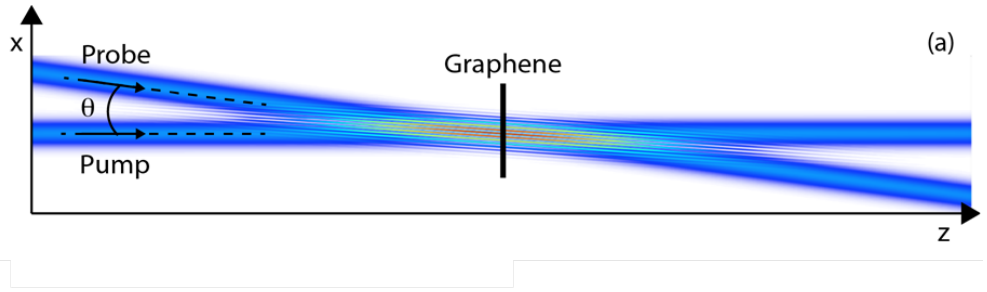

FIGURE 6.1: Two beam interaction: the figure is a schematic representation of the two optical interacting at the graphene sample. It shows the pump and probe beam layout with respect to the graphene film. This figure is adapted from [76].

and discuss the observations. The second part of this chapter is dedicated to investigating the phase-contrast imaging technique. For this, the traditional FWM configuration of three optical fields interacting at the graphene sample is revisited. Phase-contrast imaging (PCI) is an imaging technique, where phase-objects are translated into intensity objects. Since the negative refraction process in the coherent-control geometry involving graphene is highly phase-sensitive, an attempt is made to enable phase-contrast imaging by varying the spatial-phase of one of the pump beams. We observe that the phase-profile picked up by one of the pump beams is translated into an intensity-profile of the negative refraction signal. The experimental methods and the observations are discussed in this chapter.

6.2 Two-beam geometry

The experimental components for this geometry are the same as those used in the experiments discussed in the previous chapter. The laser source (785 nm, 100 fs, Titanium Sapphire laser), energy of the input optical beams, the nonlinear medium - graphene sample (30 layers, 9 nm thickness, 50 % absorption in the visible range) are all the same as discussed previously. In this configuration of the experiment, which we refer to as the single-pump-beam case, the pump and the probe are incident on the graphene sample from the same side. The Sagnac interferometer is not relevant here as one of the pump beams (pump2 as seen in Fig. (5.1)) is blocked and the interaction between pump 1 and the probe beam is enabled. Both the beams are aligned to have the same optical path length and the coherent illumination of the graphene sample is ensured by adjusting the delay-line in the path of the probe beam. *pump1* is now steered onto the graphene sample

by a mirror which is mounted on a piezoelectric stage. The piezoelectric stage, controlled via LabView, is used to scan the delay of the pump pulse with respect to the probe such that the graphene sample is subject to consecutive nodes and antinodes of the resultant field. The two optical beams interact as a function of their relative phase delay, see Fig. (6.1). In this case too we observe both the phase conjugation and optical negative refraction. However, the conditions vary from the bulk case where the longitudinal phase matching constraint suppresses these processes.

This geometry supports the generation of the phase-conjugated and negatively refracted signals. The possibility of coherently modulating these nonlinear signals is also investigated. Figs. (6.2(a-c)) show the calculated spatial distribution of the time-averaged nonlinear polarisation P_{nl}^2 at the graphene film for three different phase delays between the pump and the probe. The spot size of the two beams at the sample is 80 μm, which is a critical parameter in this geometry. For three different relative phase delays, as can be seen, changing the phase only leads to a lateral shift of the spatial interference pattern. Under this condition the DFWM nonlinear signals will be observed because of the presence of the nonlinear polarisation. Changing the relative phase of the beams only accounts for a very weak modulation in their amplitudes, as shown in Fig. (6.2(d)) that shows the calculated time-averaged nonlinear polarisation, P_{nl}^2. Hence, to achieve more efficient modulation of the nonlinear signals, the spatial distribution of the beams needs to be tailored, such that at certain relative phase difference between the beams, the nonlinearity is switched off or *almost* switched off. As shown in Figs. (6.2(e)-(g)), if the spot size of the beams is reduced so that it is equivalent to or smaller than the fringe spacing of the interference pattern, then changing the relative phase leads to longitudinal *and* transverse modulation of the polarisation wave intensity, which in turn allows to coherently control the amplitude of the DFWM signals, similarly to the previous case of the traditional FWM configuration.

The experimental setup is designed to reproduce the condition of the calculations shown in Figs. (6.2(e)-(g)), i.e., one interference fringe at the graphene sample. This was achieved by aligning the input beams with a relative 1.8° angle and by focusing them to a spot-size of 20 μm, in order to match the fringe width and the beams' spot-size. Under this arrangement, the strength of the negative refraction signal is recorded as a function of piezoelectric-mirror delay. A periodic modulation (a maximum to extinction) of the negative refracted beam is observed, as shown in Fig. (6.2(h)). In the plot, the yellow dots represent the negative refraction signal amplitude. The amplitude of the phase conjugated

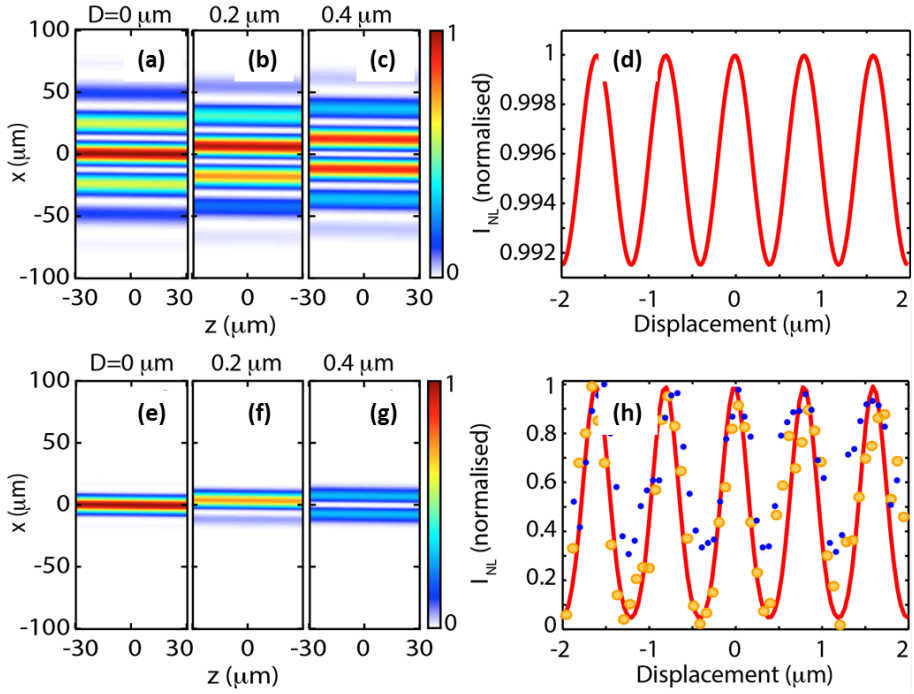

FIGURE 6.2: Two beam interaction: (a), (b), and (c) are zoomed in images of the calculated transverse (x) and longitudinal (z) distribution of the time-averaged nonlinear polarisation P_{nl}^2 for different relative phases, ϕ, of E_{pump} and E_{probe} as indicated in the figure. The two beams have the same diameter of 80 μm and generate several spatial interference fringes. The calculated intensity of the negatively refracted beam is shown in (d) as a function of relative phase delay ϕ: only a very weak modulation is observed. (e), (f) and (g) show the same as in (a)-(c) but with smaller beam diameters of 20 μm. (h) shows the experimental data for the measured negatively refracted (NR yellow circles) and phase conjugated (PC, blue dots) beams as a function of piezoelectric-mirror displacement. A strong $\sim 100\%$ modulation is observed, in agreement with the theoretical calculation of time-averaged P_{nl}^2 (red curve). This figure is adapted from [76].

beam exhibits a similar modulation (blue dots). The modulation, however, occurs with a reduced visibility due to linear back-scattering of the pump signal from the sample surface, which proved difficult to completely eliminate due to focusing lenses in the new experimental conditions.

It is noted that phase conjugation is typically performed with two counterpropagating pump beams in bulk media but may be observed with a single pump beam (along with an input probe beam) when using a surface nonlinearity [87] . In our experiments, the advantage provided by the two-dimensionality of graphene in terms of its phase-dependent nonlinearity is exploited to see similar results. It is also observed that in the previous geometry of FWM, with three input optical fields, the modulation periodicity was given by the standing wave periodicity (i.e. $\lambda/2$). On the other hand, in the two-beam geometry the amplitude of the nonlinear signals is periodically modulated with a periodicity equal to the pump wavelength, i.e., λ = 785 nm. The results shown in Fig. (6.2(h)) demonstrate that this simplified arrangement provides an equally effective method of generating an all-optical modulation of nonlinear signals in 2D films. The same method could also be extended for the case of metamaterials, and in general to looking into alternative imaging applications [27] .

At this point, the focus is on simplifying geometries to achieve negative refraction using thin films. As the next step, FWM geometries with only one optical beam are explored and discussed in the next section.

6.2.1 Nonlinear coherent mirrors and negative reflection

In this third example we perform the experiment with two input beams, but in a reflection-configuration as shown in Fig. (6.3(a)). The pump beam, focused using a lens with f = +50 cm, is at normal incidence to the graphene surface and the transmitted beam is reflected by a mirror placed closely behind and parallel to the film. The mirror distance from the film is reduced to be much smaller than the length of the optical pulse ($\sim$ 30 μm) and is fine-tuned using a piezoelectric stage. The reflected pump beam now acts as a second pump and its relative phase with respect to the input beam is controlled by the

mirror. This allows the same control over the resulting polarisation wave as in the examples discussed earlier, in the way that the nonlinearity is 'phase dependent'.

Figure (6.3(b)) shows the amplitude of the DFWM signal that is back-reflected along the direction of the input probe beam as a function of the mirror position. The signal is clearly modulated with nearly 100% visibility and shows a $\sim$ 4x enhancement with respect to the same measurement performed without the mirror, as indeed the nonlinear medium is now

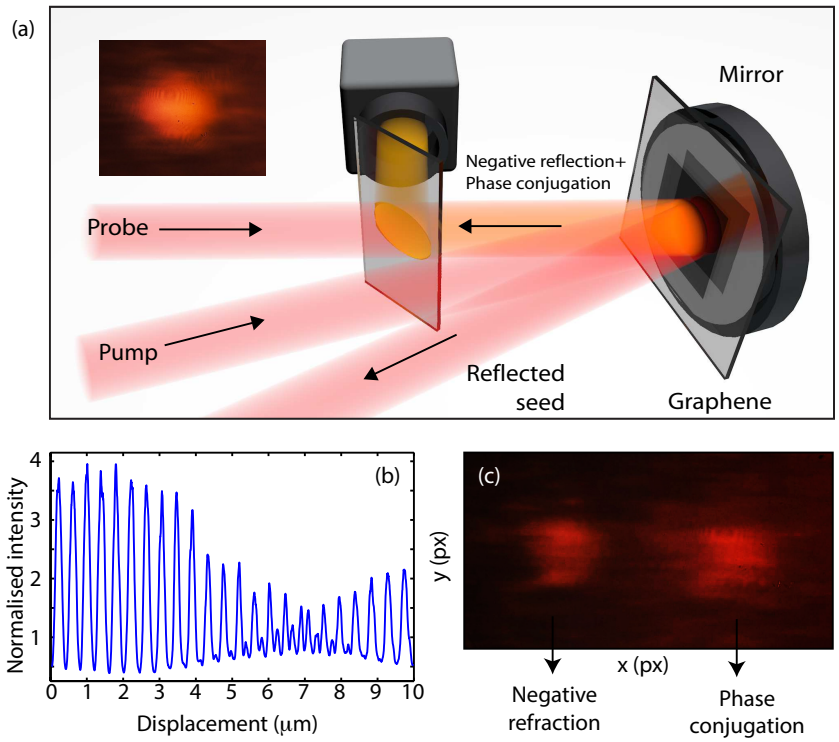

FIGURE 6.3: Nonlinear coherent mirror: (a) Schematic representation of the experimental layout with a single pump beam at normal incidence to the graphene film and the probe beam at a small angle. A mirror is placed parallel to the film and its distance from the graphene film is controlled with a piezoelectric actuator. (b) Shows the recorded back-reflected signal (along the probe direction) as a function of mirror distance. (c) Shows the spatial profile of the back-reflected signal recorded on a CCD camera with the mirror slightly detuned in angle. Two beams are observed: one is the phase-conjugated signal the other is the negatively refracted (and reflected back from the mirror) signal, as indicated in the figure. When the mirror is properly aligned parallel to the film, these two beams add coherently to form a single beam shown in the inset to (a).This figure is adapted from [76].

placed inside a Fabry-Perot cavity composed by the metallic mirror and the partially reflective graphene-air interface. Interestingly, the back-reflected signal is not a pure phase conjugated signal as one may have expected given the backward propagation direction (with respect to the probe). Indeed, a negatively refracted beam is also expected. However, considering the beam arrangement shown in Fig. (6.3(a)), the negatively refracted beam would be reflected from the mirror and overlap, after passing through the graphene film, with the phase conjugated beam. This was verified by slightly detuning the angle of the mirror: in this way the negatively refracted and phase conjugated beams are emitted with slightly different angles and appear as two separate beams on a CCD camera placed at the photodetector position, as shown in Fig. (6.3(c)) (the negatively refracted beam has a $\sim 50\%$ lower intensity due to the absorption in the graphene film). Remarkably, as a result of the fact that they are generated in phase, these two signals sum coherently when they are overlapped, giving an enhanced signal as shown in the CCD image inset in Fig. (6.3(a)).

Lastly, an attempt is made to further simplify this configuration by using only one optical beam. Single beam phase conjugation, where the two pumps and the seed originate from the same beam was reported iby J. Feinberg [88], where a photorefractive crystal - $BaTiO_3$ - is used as the nonlinear medium. It uses a geometry where the single pump beam is internally reflected by the edge of the crystal and trapped within. This last geometry too is a step in that direction, in the sense that we use only one pump beam. The actual experimental configuration is stripped down to a single laser beam, the graphene sample and a mirror. A retro-reflecting mirror is placed at a slight angle of 3° with respect to the graphene sample and only a single pump beam is incident normally on the graphene sample as shown in Fig.6.4(a). The mirror and the graphene film, as in the last case, are very close to each other so that the optical pulse overlaps on itself upon reflection. The angle between the mirror and the graphene sample is kept low enough to ensure spatial overlapping of the reflected pump on itself at graphene. This configuration can be described as the folded version of the first geometry discussed in this chapter, where generation of a negative refracted beam is achieved by using only two input beams incident at an angle, albeit from opposite sides of the graphene film. We therefore expect here too a negatively refracted beam that will appear as a reflected signal as shown schematically in Fig. (6.4(b)).

Conservation of the transverse momentum dictates that the DFWM will cause a nonlinear signal to appear reflected at an angle of -2θ, where θ is the incident pump beam angle

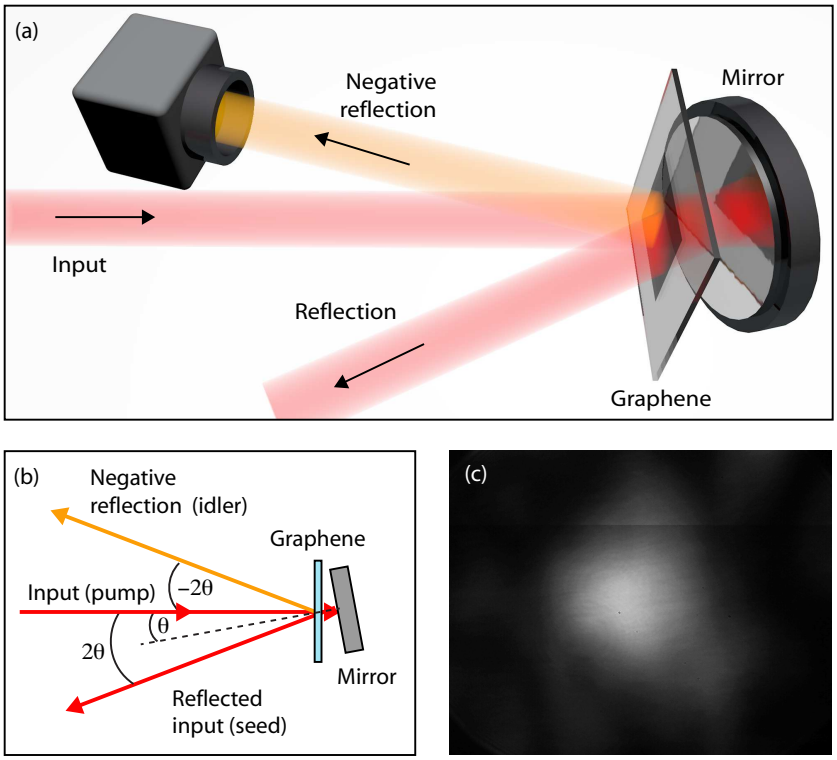

FIGURE 6.4: Negative reflection: (a) and (b) show a schematic representation of the experimental layout and wave-vector diagram with a laser beam incident normal to the graphene sample and with the mirror placed very closely to the film (at a distance shorter than the optical pulse length) but at a slight angle. Conservation of transverse momentum implies that the interacting beams generate a reflected beam at an angle 2θ (as expected from a standard mirror) but also a "negative" reflection at the opposite -2θ angle. (c) Shows an image of the negatively reflected beam measured at angle -2θ on a CCD camera. This figure is adapted from [76].

relative to the mirror normal. In other words, this beam appears as a "negatively reflected" beam and whose image, recorded with a CCD camera, is shown in Fig. (6.4(c)). It is observed at an angle of 3 degrees with respect to the input pump beam, but on the negative side when compared to the normal reflection from the mirror. This configuration of a FWM process using graphene hence leads to the observation of a new kind of signal, i.e., the negative reflection.

All these alternative geometries hence prove that the two dimensional materials with the right optical arrangements lead to interesting observations of nonlinear optical interactions. The coherent control of light interaction in 2D materials not only leads to generation of negative refraction and phase-conjugated fields, but also opens the path for simplifying four-wave mixing geometries.

6.3 Application of Nonlinearity in Graphene: Phase Contrast Imaging

Phase-contrast imaging is a prominent technique which is used in transmission electron microscopy, X-ray tomography and other high-resolution imaging domains. It is a method for differentiating or imaging structures which have similar transparencies or similar reflectivity, but have different refractive indices. Let us suppose an object which has structures of differing refractive indices within it. An amplitude or intensity profile of a light beam reflecting from it or transmitting through it might not be enough to interpret the local phase-differences across the cross-section of the beam. In phase-contrast imaging, the aim is to image these phase-distortions that an optical field might experience on its encounter with an object, hence distinguishing structures of different retardation. A tool to this effect is the Nobel prize winning invention: the phase-contrast microscope, developed by Frits Zernicke in 1953.

The basic working principle of phase-contrast microscopy is to separate the illuminating background light from the scattered light by the specimen (which make up the foreground details) and to manipulate these differently. In traditional phase-contrast microscopes, the image contrast is improved in two steps: the background light is phase-shifted by -90° by passing it through a phase-shift ring. This eliminates the phase difference between the

background and the scattered light, leading to an increased intensity between foreground and background. Secondly, the background is dimmed by a filter ring, which results in some of the scattered light being phase-shifted and dimmed by the rings. However, the background light is affected to a much greater extent, which creates the phase-contrast effect. These configurations involve several optical phase elements and function in the linear regime. A nonlinear imaging system for phase-contrast imaging could simplify this configuration.

The observation of a 'phase-dependent' nonlinearity in graphene, which is responsible for the generation of negative refraction, could potentially be used for phase-contrast microscopy. This section presents a new method of performing phase-contrast imaging using DFWM in graphene multilayer. The traditional FWM geometry with a Sagnac interferometer as discussed in the previous chapter is used to realise this technique. A Spatial Light Modulator (SLM) is introduced into the configuration to create phase distortions to be imaged. The aim is to introduce local phase distortions into one of the pump beams and then image them (in terms of intensity distortions) in the resulting phase-conjugated or negatively refracted beam. The following section discusses the experimental setup and the results of these experiments. Three different kinds of simple phase-contrast profiles are imaged, with sub-micron resolution using near-infrared (wavelength (800 nm). This demonstration of phase-contrast imaging involves the phase objects of illumination (of graphene) being translated to intensity-profiles by the object (graphene under coherent absorption).

6.3.1 Experimental Methods

The experimental layout, as shown in Fig. (6.5), follows almost the same outline as that for FWM with three optical fields, which was discussed in the previous chapter. It involves a Sagnac interferometer, and three laser beams breaking off from the laser output from Ti:Sapphire laser (785 nm, 30 nm, 100 fs). In addition to this, 'structured illumination' is enabled by a spatial light modulator (SLM) which is programmed to add additional phase-components onto one of the pump beams, *pump 2*. The pump beam, *pump 2* and the unaltered pump beam, *pump 1* counter-propagate in the Sagnac interferometer and coherently illuminate the graphene multilayer sample (30 layers, 9 nm thickness on a fused silica substrate). This coherent control geometry *(cite Zheludev)* and an additional probe beam which produces our resultant negative refraction signal form the components

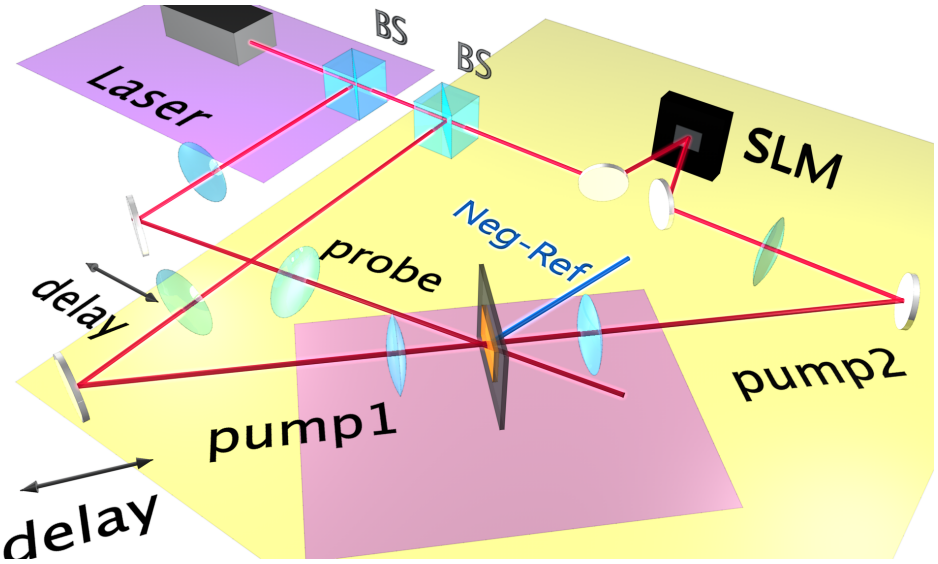

FIGURE 6.5: Schematic representation of the experimental setup for phase-contrast imaging. It is very similar from the experimental layout for the traditional FWM with CPA, discussed in Chapter (5), except for the SLM which is added to the **pump 2** arm of the interferometer.

of the setup. The layout is designed such that it allows the phase matched pump beams to form a standing-wave at the graphene sample. The graphene sample, which is mounted on a translation stage, is aligned to meet the standing wave at an antinode, so as to enable maximum absorption, to increase the strength of negative refraction. At perfect phase-matching conditions, the three optical fields interact at the graphene sample to generate a phase-conjugated beam and a corresponding negative refraction signal, shown in blue (*Neg-Ref*). Owing to convenience of alignment negatively refracted signal is used for imaging the phase-contrast objects. Below is a brief description of the SLM tool that is used for the measurements.

Spatial Light Modulator: A Spatial Light Modulator (SLM) is an electrically programmable device that modulates light according to a fixed spatial (pixel) pattern. It provides light control on a pixel-by-pixel basis. Is is made of liquid crystal arrays and each pixel can be electronically controlled. The SLM that is used for this set of experiments is a an XY Series, 'Phase and Amplitude SLM from *Meadowlark*. It has a chip size of (7.68 x 7.68) mm; (512 x 512) pixel array, with pixel size of (15 x 15) μm and a working wavelength range of 760 - 865 nm. The damage threshold of the SLM chip is 1 mJ and with a pulsed light source, the maximum intensity that could be used is calculated to be 5.4 GW/cm^2.

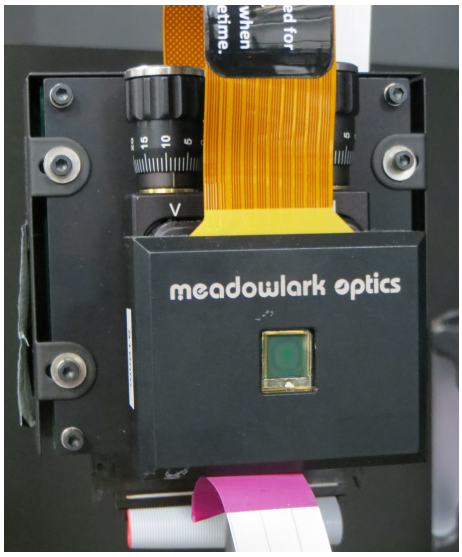

FIGURE 6.6: The Meadowlark Spatial Light Modulator. The active region is a liquid-crystal array chip designed to work specifically around 760 - 865 nm

Incorporating the SLM into one of the interferometer arms needs special attention as a few conditions need to be satisfied: the path length between the SLM and the graphene sample is chosen such that (i) the beam at SLM plane is imaged at the graphene sample, and (ii) it is sufficient to scale down the spot-size at graphene to enable nonlinear optical interactions. This also ensures brevity in the introduction of phase-profiles on to *pump 2*, which is originally of a plane phase-front. Another difference in this setup to be noted is that the laser beams are not focussed at graphene, but instead reduced to beam-spots of $\sim$300 μm by using telescopes on each interacting beam. The pump and the probe beams are collimated at graphene in order to preserve their plane wavefronts, when the spot size of the beam incident on the SLM chip is of the order of a few *mm*. The SLM yields several diffracting orders and a grating mask is applied on the SLM for separating the modes and the first order is used for the experiments. The mode separation is performed by using a pin-hole at the focal length in the telescopic arrangement. The arm lengths of the Sagnac interferometer are designed to be 80 cm, so as to accommodate the conditions of using the SLM into one of them.

6.3.2 Results and Discussion

The phase-masks are generated by a MATLAB program (given in the Appendices (A)) which produces a greyscale image of the phase-profiles which are then digitally applied

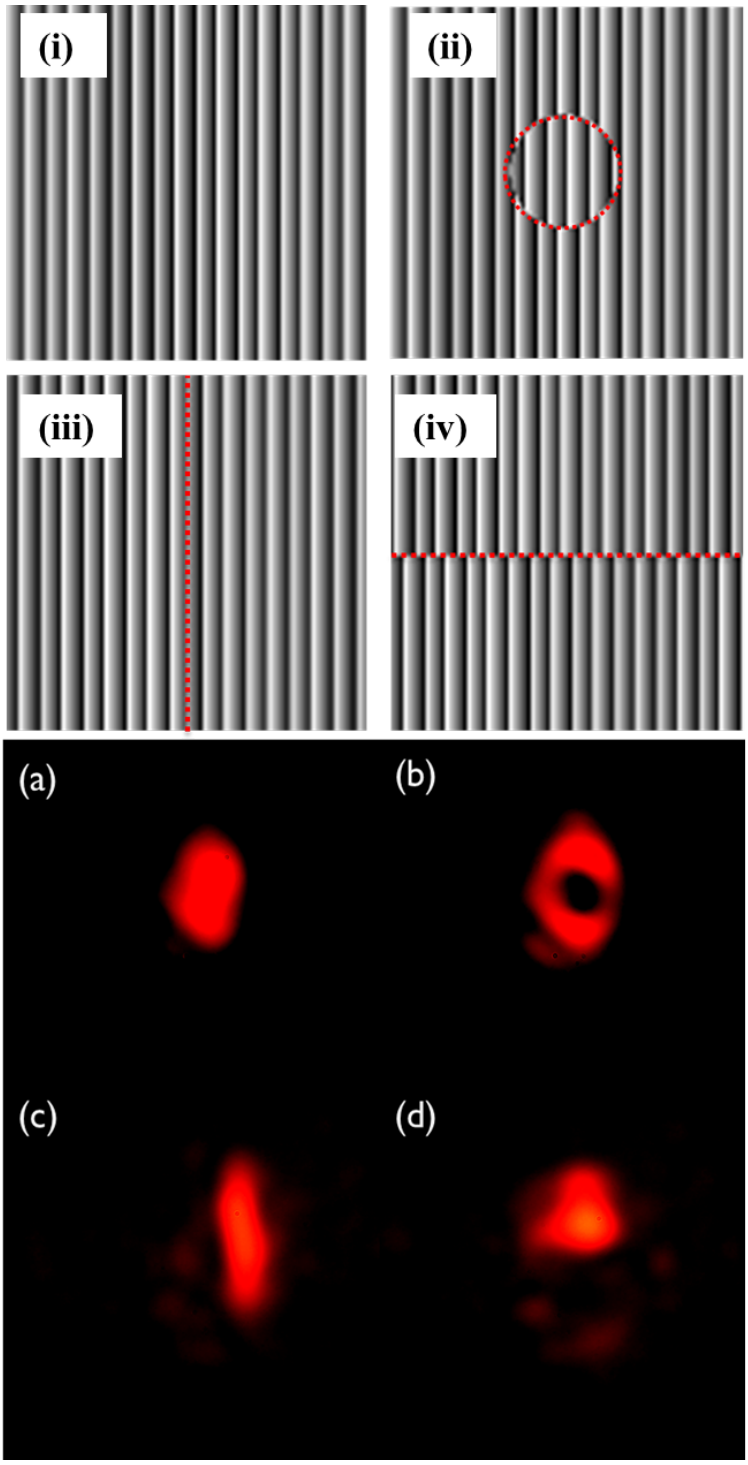

FIGURE 6.7: (i) - (iv): SLM masks generated in Matlab to produce different phase-contrast profiles to be applied to one of the pump beams. The bottom set of figures are negative-refraction signals when (a) no phase profile is applied, (b) with a doughnut phase profile applied to the pump P2. (c) and (d) show the nonlinear signal when a vertical and horizontal phase contrast profile is added to the pump, respectively.

to the SLM using the Meadowlark SLM software. The phase profiles are generated by introducing an additional phase of π to specific regions of the mask to produce contrasting features. For example, in Fig. (6.7 (ii)) the SLM mask introduces a phase contrast in the form of a doughnut, where a circular part of the mask (marked in red) has an additional phase of π. The pump, *pump 2*, when incident on the SLM chip is centered on the doughnut phase-profile using the Matlab program (given in Appendix A) that generates the SLM masks. *pump 2* encounters a phase-contrast profile on the SLM resulting in the modification of its phase-front. This altered pump meets *pump 1* to coherently interact with *probe* at the graphene sample. Now, only the regions of the pump beams which are phase-matched give rise to the negatively refracted signal, as can be seen in Fig. (6.7 (b)). The negative refraction signal when no additional phase-profile is added (SLM mask is Fig. (6.7 (i))) is shown in Fig. (6.7 (a)). Comparing this to the image in (b) shows the phase-contrast being imaged in the negative refraction signal. Two more phase profiles are applied to the SLM, as shown in Fig. (6.7 (iii)) $\&$ (iv), a vertical and horizontal phase-contrast step, respectively. The corresponding intensity profiles of the negative refraction signal are given in Figs. (6.7 (c) $\&$ (d)), respectively.

The smallest phase-object to be imaged on the negative refracted signal is a circle of the dimensions $\sim$200 μm. Phase-contrast images were also created using phase-differences less than π , but the contrast in the negative refraction intensity profile is not 100%. The images seen in Figs. (6.7 (a)-(d)) show the results of phase structured illumination of graphene and the subsequent coherent interaction of optical fields, producing a negative refraction. The phase-dependent generation of the negative refraction due to the four-wave mixing configuration provided the premise for developing a phase-contrast imaging technique as discussed above. The smallest size of phase objects imaged is a few microns. This kind of imaging, which exploits the coherent control of light with graphene (2D material) and its unusual nonlinearity using NIR wavelengths is unique and the first of its kind. Since this method is essentially based on utilising the special consequences of FWM in 2D materials, any wavelength of light could possibly be used for phase-contrast imaging, provided the nonlinear medium has a large $\chi^{(3)}$ value.

6.4 Summary

In conclusion, this chapter offers three alternative geometries to realise nonlinear optical interactions in 2D materials, graphene in particular. The phase-dependent nature of nonlinearity enables a series of optical wave mixing configurations that either optimise previously existing geometries or allow completely new possibilities. The two-dimensional nature of the material also implies that only one pump beam is required to generate a phase-conjugated beam and also a negatively refracted beam. Moreover, by choosing a geometry such that the beam diameters are of the same order or smaller than the transverse interference pattern (controlled by the relative pump-probe angle), it is possible to observe full coherent control/modulation of the DFWM signals even with only two input beams. In the final FWM configuration, it is observed that a reflective surface placed behind the two-dimensional film at a small angle acts as a nonlinear mirror that can generate a "negatively reflected" beam.

Beyond the fundamental implications of the phase-dependence of the nonlinearity in two-dimensional media, these ideas may find applications, for example in the field of imaging. Perfect imaging has been demonstrated using two nonlinear films, e.g. metamaterial films, placed at a close distance and each individually pumped with two counterpropagating beams, i.e. with a total of four beams. The results here show that only one pump for each film is required and in principle, only one pump beam impinging on both films should be necessary to achieve the same perfect imaging results. This could greatly change the scene of miniaturisation of imaging systems, especially nonlinear imaging systems. In the same vein, a 'phase-contrast imaging' concept is explored and demonstrated as discussed in the second section of this chapter. This technique is a result of the marriage of two concepts: the coherent perfect absorption in 2D materials and the 'phase-dependent' nonlinearity observed in graphene multilayers. The 'self conjugate' property of graphene is also an important aspect in this regard, as the nonlinear signal used for phase-contrast imaging is the negative refraction signal. Graphene, belonging to this exclusive club of 'self-conjugate' materials, enables the generation of negative refraction along with a phase-conjugated field, which is typically the result of four-wave mixing.

Chapter 7

Conclusions

This work was primarily focused on achieving coherent control of optical interactions using two-dimensional graphene multilayers. Unstructured graphene films (consisting 30 atomic layers) with a travelling-wave absorption close to 50% in a coherent perfect absorption (CPA) configuration was used to demonstrate an all-optical modulation of linear absorption. This arrangement allowed total absorption to be controlled between 100% (full absorption) and 0% (full transmission). Subsequently, the same arrangement was used to control other light-matter interaction channels. In the specific case discussed in Chapter (4), the scattering efficiency from the graphene sample was modulated with a modulation contrast of $\sim 90\%$. This coherent enhancement or suppression of linear optical properties (absorption [13], scattering [71] and reflection [84]) of graphene multilayers is an example of the additional control enabled by the reduced dimensionality. As graphene is known to exhibit strong nonlinear optical response [89], nonlinear optical interactions in graphene multilayers were consequently examined in similar arrangements.

Optical phase-conjugation and negative refraction were achieved from graphene multilayers, through degenerate four wave mixing. The third order nonlinearity was found to be coherently controllable by modulating the phase of the input pump beam, as a consequence of the two-dimensionality of the graphene sample and a modulation contrast $\sim 100\%$ achieved. Additionally, a 'phase-dependent' nonlinearity was realised as a result of the high third order nonlinearity ($\chi^{(3)}$) and the optical two-dimensionality of graphene multilayers. This advantage of phase-dependent nonlinearity enabled a series of new optical wave mixing configurations. These arrangements allowed for optimising previously existing geometries or provided completely new possibilities for enabling nonlinear optical interactions in 2D materials. Alternative geometries for observing negative refraction and optical phase conjugation were explored. Firstly, a two-beam geometry was devised such that the diameters of the beams interacting at the graphene sample were of the same

order or smaller than their transverse interference pattern (controlled by the relative pump-probe angle), which allowed for the observation of full coherent modulation of the DFWM signals. In the second case, we demonstrated the generation of a phase-conjugated beam along with a negatively refracted beam in a simpler, one beam geometry. The last configuration for nonlinear performing nonlinear optics in graphene multilayers involved a reflective surface placed behind the two-dimensional film at a small angle, which acted as a nonlinear mirror and generated a 'negatively reflected' beam. All these results offer all-optical methods for manipulation of optical linear and nonlinear interactions using 2D materials.

In addition to the fundamental implications of the phase-dependence of the nonlinearity and all the alternative configurations it supports in a 2D material, a possible application in the form of 'phase contrast imaging' was considered and performed. This nonlinear imaging experiment followed the DFWM geometry with three input beams interacting at the graphene sample to produce negative refraction (we chose to use the negatively refracted beam for imaging over the phase conjugate beam, because of the convenience in terms of the experimental arrangement). Here the phase object in one of the interacting beams was directly mapped onto a corresponding intensity object in the negatively refracted beam. Phase objects of the size of 200 μm were introduced in one of the pump beams using a spatial light modulator (SLM), which were imaged as intensity objects in the resulting negative refracted beam. This offers a technique for performing phase-contrast imaging in the visible wavelength range.

In conclusion, this work mapped an evolution of coherent optical interactions in a 2D material - from developing a method for efficient modulation of optical absorption and scattering to redefining conditions for nonlinear interactions in 2D materials. An alternate type of nonlinearity which is specific to two-dimensional nonlinear optical media - a phase-dependent nonlinearity - was observed and examined. It also records a possible application for this nonlinearity in the form of phase-contrast imaging.

7.1 Future scope of work

Two-dimensional materials, like metamaterials, graphene and heterostructure layers [3, 4] exhibit unique features in their interaction with light and are hence driving intensive research towards developing novel optomechanical and photonic devices with improved functionalities. The experiments performed and reported in this thesis can be extended to any two-dimensional material, provided they satisfy some basic absorption conditions. Hence the results observed here are more of a commentary on all-optical techniques in 2D materials, than being graphene-specific.

The flexibility provided by the coherent perfect absorption geometry could be further examined for developing optical modulators and have the potential of being integrated into all-optical chips. The degree of control demonstrated in these results could be extended to other optical effects as well. Also, the various geomteries explored for achieving nonlinear interactions in graphene multilayers bring up the interesting possibility of generating and controlling the nonlinear response of other promising thin film materials [89, 36, 90]. This thesis examined linear and nonlinear optical interactions, but CPA has also been observed in single photon regime, recently demonstrated in plasmonic metamaterials. Measurements with single photon states reveal the familiar oscillation between total transmission and total absorption. The technique can be further extended to quantum state with more than one photon for instance for N = 2 N00N states, where we expect to see different physical phenomena compared to classical CPA [91]. It has been shown that CPA with N00N states creates novel quantum states [48] and can surprisingly exhibit nonlinear absorption [92].

Another avenue that can be considered for further studies is nonlinear imaging. Two nonlinear films - metamaterial films - placed very closely with each individually pumped with two counterpropagating beams, have been used to demonstrate perfect imaging. The alternative geometries for nonlinear interactions in graphene multilayers discussed in this thesis offer the prospect of simplifying the arrangement of perfect imaging, as our results show that only one pump for each film is required and in principle, only one pump beam impinging on both films should be necessary to achieve the same perfect imaging results. Additionally, more experiments could be performed for improving the method of the phase-contrast imaging technique proposed in this work.

Summarising, coherent perfect absorption and optical nonlinear interactions in two-dimensional materials provide for some interesting results and observations and the flexibility of manufacture of new two-dimensional materials adds to this advantage, opening up new geometries for optical interactions.

Appendices

Appendix A

MATLAB Code

The MATLAB code for applying different phase-masks on the Meadowlark Spatial Light Modulator (SLM) for phase-contrast imaging experiment is given here:

```
% SLM Projection File
clear all;
close all;

%% Parameters
% Phase mask for an Axicon 0 off; 1 on
Axicon = 1;

Gaussian = 0;  % 0 off; 1 on

% Phase mask to create circular phase shifted area
Mask1 = 0;
radius = 0.003;
% x-axis and y-axis values to center the phase circle
centre_x = 300;
centre_y = 219;

%Phase mask to create a vertical partition with
%out-of-phase regions
Mask1_b = 0;

% set to ZERO when no additional phase tailoring
%needed
Half_v = 0;
```

```
% to find the horizontal centre of the beam
Half_h = 0;

Grid = 1; % 0 off; 1 on
gs =256;  % Grid size for BNS SLM must be < 512
2*2.54e-2/gs
tic;
modx = 2;
root = 0; % 0 off; 1 on
rfact = 2e-2; % sqrt of R dependence -- rfact*sqrt(R)
Numberoflines = 60;  %no. of grid lines
Numberofrings = 30;  %no. of rings for Axicon
n = 4.3;
rx = -0.21
ry = 0.175


%% Code

% AXICON
N = Numberofrings;  %Number of rings
[x, y] = meshgrid(-1:(1/gs):1-(1/(gs*2)));
r = N*2*pi*sqrt((x-rx).^2 + (y-ry).^2);
A = mod(r,modx*pi);

% GAUSSIAN
N = Numberofrings;  %Number of rings
[x, y] = meshgrid(-1:(1/gs):1-(1/(gs*2)));
r =-N*2*pi*(((x-rx).^2 + (y-ry).^2));
R =mod(r,modx*pi);

% MASK 1(phase_inverted_circle)
[x, y] = meshgrid(-1:(1/gs):1-(1/(gs*2)));
m =(((x-rx).^2 + (y-ry).^2));
for i = 1:length(m)
    for j = 1:length(m)
if m(i,j) <= radius
```

```
    m(i,j) = pi;
else
    m(i,j) = 0;
end
    end
end

 % MASK 1_b(phase_inverted_circle)
 [x, y] = meshgrid(-1:(1/gs):1-(1/(gs*2)));
 m1_b =(((x-rx).^2 + (y-ry).^2));
 for i = 1:length(m)
     for j = 1:length(m)
 if m1_b(i,j) <= radius
     m1_b(i,j) = pi;
 else
     m1_b(i,j) = 0;
 end
     end
 end

% HALF_verticle
v = zeros(512:512);
for i = 1:512
    for j = 1:512
        if j <= centre_y
            v(i,j) = pi;
        else
            v(i,j) = 0;
        end
    end
end

% HALF_horizontal
h = zeros(512:512);
for i = 1:512
    for j = 1:512
        if i <= centre_x
```

```
            h(i,j) = pi;
        else
            h(i,j) = 0;
        end
    end
end


% GRATING
N = Numberoflines;  %Number of lines
x = meshgrid(0:(1/(gs*2)):1-(1/(gs*2)));

X   = -(x-rx)*N*2*pi*Grid + Z*Spiral + Gaussian*R +
Axicon*A + root*rootr + v*Half_v +
   h*Half_h + m*Mask1;

%array1 = 'plot_data.xlsx'
%xlswrite(array1,X,'Sheet',1)

% multiply by 2Pi for phase.
M = mod(X, modx*pi) ;


%Plot Figure

handlefig = figure(1);
set(handlefig,'Position',[50 50 512 512]);

set(handlefig,'Visible','on');
p = pcolor(M), shading interp;
colormap('gray');
axis([0 n 0 n]) ;
axis off;

%For displaying on the SLM as a square
% centered at the center of the screen
%set(gcf, 'Position', [1409 1 1024 1024])
```

```
%For displaying on the primary screen
%set(gcf, 'Position', [128 1 1024 1024])

%For display modification inside
%set(gca, 'Position', [0.62 0.62 0.8 0.8])
%the image window


thedata = get(p,'CData');
% CONTROLS THE DARKNESS OF THE FIGURE
darknessadjust = 2*pi;
thedata = thedata./darknessadjust;
td(:,:,1) = zeros(512, 512);
td(:,:,2) = thedata;
td(:,:,3) = zeros(512, 512);

%ADJUST THE PATH TO WHERE YOU WANT IT
imwrite(td,'PCI./axicon.bmp');

toc;
```

Chapter 8

References

[1] K. S. Novoselov, A. K. Geim, S. V. Morozov, D. Jiang, Y. Zhang, S. V. Dubonos, I. V. Grigorieva, and A. A. Firsov, *Electric field effect in atomically thin carbon films*, Science, **306** (5696), 666-669 (2004).

[2] W. Cai and V. Shalaev, *Optical Metamaterials, Fundamentals and Applications* (Springer, 2010).

[3] A. K. Geim and K. S. Novoselov, *The rise of graphene*, Nature Mater. **6**, 183-191 (2007).

[4] A. K. Geim and I. V. Grigorieva, *Van der Waals heterostructures*, Nature **499**, 419-425 (2013) .

[5] A. E. Siegman, *Excess spontaneous emission in non-Hermitian optical systems. I. Laser amplifiers*, Phys. Rev. A **39**, 1253-1263 (1989).

[6] W. A. Hamel and J. P. Woerdman, *Nonorthogonality of the longitudinal eigenmodes of a laser*, Phys. Rev. A **40**, 2785-2787 (1989).

[7] Y. D. Chong, Li Ge, Hui Cao, and A. D. Stone, *Coherent perfect absorbers: time-reversed lasers*, Phys. Rev. Lett. **105**, 053901 (2010).

[8] W. Wan, Y. Chong, L. Ge, H. Noh, A. D. Stone, and H. Cao, *Time-reversed lasing and interferometric control of absorption*, Science **331**, 889-892 (2011).

[9] S. Dutta-Gupta, O. J. F. Martin, S. Dutta Gupta, and G. S. Agarwal, *Controllable coherent perfect absorption in a composite film*, Opt. Express **20**, 1330-1336 (2012).

[10] G. Pirruccio, L. M. Moreno, G. Lozano, and J. G. Rivas, *Coherent and Broadband Enhanced Optical Absorption in Graphene*, ACS Nano. **7**(6), 4810-4817 (2013).

[11] S. Huang and G. S. Agarwal, *Coherent perfect absorption of path entangled single photons*, Opt. Express **22**(17), 20936-20947 (2014).

[12] S. Longhi, *Time-Reversed Optical Parametric Oscillation*, Phys. Rev. Lett. **107**, 033901 (2011).

[13] J. Zhang, K. F. MacDonald, and N. I. Zheludev, *Controlling light-with-light without nonlinearity*, Light: Science & Applications **1**, e18 (2012).

[14] S. A. Mousavi, E. Plum, J. Shi, and N. I. Zheludev, *Coherent control of birefringence and optical activity*, Appl. Phys. Lett. **105**, 011906 (2014).

[15] X. Fang, M. L. Tseng, J. Ou, K. F. MacDonald, D. P. Tsai and N. I. Zheludev, *Ultrafast all-optical switching via coherent modulation of metamaterial absorption*, Appl. Phys. Lett. **104**, 141102 (2014).

[16] S. Thongrattanasiri, F. H. L. Koppens, and F. J. Garcìa de Abajo, *Complete optical absorption in periodically patterned graphene*, Phys. Rev. Lett. **108**, 047401 (2012).

[17] J. Zhang, C. Guo, K. Liu, Z. Zhu, W. Ye, X. Yuan and S. Qin, *Coherent perfect absorption and transparency in a nanostructured graphene film*, Opt. Express **20**, 12524–12532 (2014).

[18] J. Hao, J. Wang, X. Liu, W. J. Padilla, L. Zhou, and M. Qiu, *High performance optical absorber based on a plasmonic metamaterial*, Appl. Phys. Lett. **96**, 251104 (2010).

[19] T. V. Teperik, F. J. Garcìa de Abajo, A. G. Borisov, M. Abdelsalam, P. N. Bartlett, Y. Sugawara, and J. J. Baumberg, *Omnidirectional absorption in nanostructured metal surfaces*, Nat. Photonics **2**, 299-301(2008).

[20] C. Hägglund, S. P. Apell, and B. Kasemo, *Maximized optical absorption in ultrathin films and its application to plasmon-based two-dimensional photovoltaics*, Nano. Lett. **10**, 3135-3141 (2010).

[21] N. Liu, M. Mensch, T. Weiss, M. Hentschel, and H. Giessen, *Infrared perfect absorber and its application as plasmonic sensor*, Nano. Lett. **10**, 2342-2348 (2010).

[22] M. Liu, X. Yin, E. Ulin-Avila, B. Geng, T. Zentgraf, L. Ju, F. Wang and X. Zhang, *A graphene-based broadband optical modulator*, Nature **474**, 64–67 (2011).

[23] J-L. Xu, X. L. Li, Y.Z. Wu, X.P. Hao, J.L. He, and K.J. Yang, *Graphene saturable absorber mirror for ultra-fast-pulse solid-state laser*, Opt. Lett. **36**, 1948-1950 (2011).

[24] F. Wang, Y. Zhang, C. Tian, C. Girit, A. Zettl, M. Crommie, and Y. R. Shen, *Gate-variable optical transitions in graphene*, Science **320**(5873), 206-209 (2008).

[25] R. R. Nair, P. Blake, A. N. Grigorenko, K. S. Novoselov, T. J. Booth, T. Stauber, N. M. R. Peres and A. K. Geim, *Fine structure constant defines visual transparency of Graphene*, Science **320**, 1308 (2008).

[26] J. B. Pendry, *Time reversal and negative refraction*, Science **322**, 71-73 (2008).

[27] P. Y. Chen, and A. Alù, *Subwavelength imaging using phase-conjugating nonlinear nanoantenna arrays*, Nano Lett. **11**, 5514-5518 (2011).

[28] D. Schurig, J. J. Mock, B. J. Justice, S. A. Cummer, J. B. Pendry, A. F. Starr, and D. R. Smith, *Metamaterial electromagnetic cloak at microwave frequencies*, Science **314**, 977-980 (2006).

[29] A. S. Schwanecke, V. A. Fedotov, V. V. Khardikov, S. L. Prosvirnin, Y. Chen, and N. I. Zheludev, *Optical magnetic mirrors*, J. Opt. A **9**, L1–L2 (2007).

[30] C. M. Soukoulis and M. Wegener, *Past achievements and future challenges in the development of three-dimensional photonic metamaterials*, Nat. Photon. **5**, 523–530 (2011).

[31] Y. Zhang, T-T Tang, C. Girit, Z. Hao, M. C. Martin, A. Zettl, M. F. Crommie, Y. R. Shen, and F. Wang, *Direct observation of a widely tunable bandgap in bilayer graphene*, Nature **459**, 820–823 (2009).

[32] J. Mu, C. Hou, H. Wang, Y. Li, Q. Zhang, and M. Zhu, *Origami-inspired active graphene-based paper for programmable instant self-folding walking devices*, Sci. Adv. **1**, e1500533 (2015).

[33] T. Zhang, H. Chang, Y. Wu, P. Xiao, N. Yi, Y. Lu, Y. Ma, Y. Huang, K. Zhao, Z-B. Liu, J-G. Tian, and Y. Chen, *Macroscopic and direct light propulsion of bulk graphene material*, Nat. Photon. **9**, 471-476 (2015).

[34] D. R. Smith, J. B. Pendry, and M. C. K. Wiltshire, *Metamaterials and negative refractive index*, Science **305**, 788-792 (2004).

[35] Q. Bao, H. Zhang, Y. Wang, Z. Ni, Y. Yan, Z. X. Shen, K. P. Loh, and D. Y. Tang, *Atomic-layer graphene as a saturable absorber for ultrafast pulsed lasers*, Adv. Funct. Mater. **19**, 3077-3083 (2009).

[36] H. Harutyunyan, R. Beams, and L. Novotny, *Controllable optical negative refraction and phase conjugation in graphite thin films*, Nature Physics. **9**, 423-425 (2013).

[37] E. Hendry, P. J. Hale, J. Moger, A. K. Savchenko, and S. A. Mikhailov, *Coherent nonlinear optical response of graphene*, Phys. Rev. Lett. **105**, 097401 (2010).

[38] Q. Yu, L. A. Jauregui, W. Wu, R. Colby, J. Tian, Z. Su, H. Cao, Z. Liu, D. Pandey, D. Wei, T. F. Chung, P. Peng, N. P. Guisinger, E. A. Stach, J. Bao, S-S. Pei and Y. P. Chen, *Control and characterization of individual grains and grain boundaries in graphene grown by chemical vapour deposition*, Nat. Mater. **10**, 443-449 (2011).

[39] K. Kobayashi, *Complementary media of electrons*, J. Phys. Condens. Matter **18**, 3703-3720 (2006).

[40] Z-P. Yang, L. Ci, J. A. Bur, S-Yu. Lin, and P. M. Ajayan, *Experimental Observation of an Extremely Dark Material Made By a Low-Density Nanotube Array*, Nano Lett. **8**, 446-451 (2008).

[41] M. Cai, O. Painter, and K. J. Vahala, *Observation of critical coupling in a fiber taper to a silica-microsphere whispering-gallery mode system*, Phys. Rev. Lett. **85**, 74-77 (2000).

[42] J. Zhang, J-Y. Ou, K. F. MacDonald, and N. I. Zheludev, *Optical response of plasmonic relief meta-surfaces*, J. Opt. **14**, 114002 (2012).

[43] H. Cao, Y. G. Zhao, S. T. Ho, E. W. Seelig, Q. H. Wang, and R. P. H. Chang, *Random laser action in semiconductor powder,* Phys. Rev. Lett. **82**, 2278 (1999).

[44] K. N. Reddy, and S. Dutta Gupta, *Light-controlled perfect absorption of light*, Opt. Lett. **38**, 5252-5255 (2013).

[45] S. Longhi, *PT-symmetric laser absorber*, Phys. Rev. A. **82**, 031801 (2010).

[46] S. Dutta-Gupta, R. Deshmukh, A. V. Gopal, O. J. F. Martin, and S. Dutta Gupta, *Coherent perfect absorption mediated anomalous reflection and refraction*, Opt. Lett. **37**, 4452-4454 (2012).

[47] V. Degiorgio, *Phase shift between the transmitted and reflected optical field of a semireflecting lossless mirror is* $\pi/2$, Am. J. Phys. **48**, 81-82 (1980).

[48] S.M. Barnett, J. Jeffers, A. Gatti, and R. Loudon, *Quantum optics of lossy beam splitters*, Phys. Rev. A. **57**, 2134 (1998).

[49] M. Furchi, A. Urich, A. Pospischil, G. Lilley, K. Unterrainer, H. Detz, P. Klang, A. M. Andrews, W. Schrenk, G. Strasser, and T. Mueller, *Microcavity-integrated graphene photodetector*, Nano Lett. **12**, 2773–7 (2012).

[50] J.-T. Liu, N.-H. Liu, J. Li, X. J. Li, and J.-H. Huang, *Enhanced absorption of graphene with one-dimensional photonic crystal*, Appl. Phys. Lett. **101**, 052104 (2012).

[51] J. Piper and S. Fan, *Total absorption in a graphene monolayer in the optical regime by critical coupling with a photonic crystal guided resonance*, ACS Photonics **1**, 347353 (2014).

[52] R. Alaee, M. Farhat, C. Rockstuhl, and F. Lederer, *A perfect absorber made of a graphene micro-ribbon metamaterial*, Opt. Express **20**, 28017–28024 (2012).

[53] J. Zhang, C. Guo, K. Liu, Z. Zhu, W. Ye, X. Yuan, and S. Qin, *Coherent perfect absorption and transparency in a nanostructured graphene film*, Opt. Exp. **22**(10), 12524-32 (2014).

[54] A. C. Ferrari, J. C. Meyer, V. Scardaci, C. Casiraghi, M. Lazzeri, F. Mauri, S. Piscanec, D. Jiang, K. S. Novoselov, S. Roth, and A. K. Geim, *Raman Spectrum of Graphene and Graphene Layers*, Phys. Rev. Lett. **97**, 187401 (2006).

[55] H. Noh, Y. Chong, A. D. Stone, and H. Cao, *Perfect coupling of light to surface plasmons by coherent absorption,* Phys. Rev. Lett. **108**, 186805 (2012).

[56] P. Franken, A. Hill, C. Peters and G. Weinreich, *Generation of Optical Harmonies*, Phys. Rev. Lett. **7**, 118 (1961).

[57] R. L. Byer, *Nonlinear optical phenomena and materials*, Ann. Rev. Mater. Sci. **4**, 147-190 (1974).

[58] R. W. Boyd and G. L. Fischer. 2001. *Encyclopedia of Materials: Science and Technology*. Elsevier Science Ltd. 6237-6244 p.

[59] G. S. He, *Optical phase conjugation: principles, techniques, and applications*, Progress in Quantum Electronics **26**, 131-191 (2002).

[60] J. B. Pendry, *Negative refraction makes a perfect lens*, Phys. Rev. Lett. **85**, 3966-3969 (2000).

[61] B. Y. Zelȍdovich, V. I. Popovichev, V. V. Ragulśkii, and F. S. Faisullov, *Connection between the wavefronts of the reflected and exciting light in stimulated Mandel'stam-Brillouin scattering*, Sov. Phys. JETP Lett. **15**, 109-113 (1972).

[62] R. W. Hellwarth, *Generation of time-reversed wave fronts by nonlinear refraction*, J. Opt. Soc. Am. **67**, 1–3 (1977).

[63] G. S. He, Y. Cui, M. Yoshida and P. N. Prasad, *Phase-conjugate backward stimulated emission from a two-photon-pumped lasing medium*, Opt. Lett. **22**, 10-12 (1997).

[64] R. W. Boyd, *Nonlinear Optics: Third Edition*, (Elsevier, 2008) p. 523-539.

[65] B. Y. Zelȍdovich, N. F. Pilipetskii, A. N. Sudarkin, and V. V. Shkunov, *Wave-front reversal by an interface*, Sov. Phys. Dokl. **25**, 377 (1980).

[66] J. J. Maki, W. V. Davis, R. W. Boyd, and J. E. Sipe, *Phase conjugation using the surface nonlinearity of a dense potassium vapor*, Phys. Rev. A **46**, 7155–7161 (1992).

[67] V. G. Veselago, *The electrodynamics of substances with simultaneously negative values of ϵ and μ,* Sov. Phys. Usp. **10**, 509 (1968).

[68] D. R. Smith, W. J. Padilla, D. C. Vier, S. C. Nemat-Nasser, and S. Schultz, *Composite medium with simultaneously negative permeability and permittivity*, Phys. Rev. Lett. **84**, 4184-4187, (2000).

[69] W. J. Padilla, D. N. Basov, and D. R. Smith, *Negative refractive index metamaterials*, Mater. Today **9**, 28-35 (2006).

[70] K. S. Novoselov, A. K. Geim, S. V. Morozov, D. Jiang, M. I. Katsnelson, I. V. Grigorieva, S. V. Dubonos, and A. A. Firsov, *Two-dimensional gas of massless Dirac fermions in graphene*, Nature **438**, 197-200 (2005).

[71] S. M. Rao, J. J. F. Heitz, T. Roger, N. Westerberg and D. Faccio, *Coherent control of light interaction with graphene*, Opt. Lett. **39**, 5345–5347 (2014).

[72] R. Bruck, O. L. Muskens, *Plasmonic nanoantennas as integrated coherent perfect absorbers on SOI waveguides for modulators and all-optical switches*, Opt. Express **21**, 27652 (2013)

[73] B. Sensale-Rodriguez, R. Yan, S. Rafique, M. Zhu, W. Li, X. Liang, D. Gundlach, V. Protasenko, M. Kelly, D. Jena, L. Liu, and H. Grace Xing, *Extraordinary Control of Terahertz Beam Reflectance in Graphene Electro-absorption Modulators*, Nano Lett. **12**, 4518-4522 (2012).

[74] R. Yan, B. Sensale-Rodriguez, L. Liu, D. Jena, and H. Grace Xing, *A new class of electrically tunable metamaterial terahertz modulators*, Opt. Express **20**, 28664-28671 (2012).

[75] A. Taflove, S. C. Hagness, *Computational Electrodynamics: The Finite-Difference Time-Domain Method*, Artech House, 3rd ed. (2005)

[76] S. M. Rao, A. Lyons, T. Roger, M. Clerici, N. I. Zheludev and D. Faccio, *Geometries for the coherent control of four-wave mixing in graphene multilayers*, Sci. Rep. **5**, 15399 (2015).

[77] N. Bloembergen, and P. S. Pershan, *Light waves at the boundary of nonlinear media*, Phys. Rev. **128**, 606-622 (1962).

[78] Y. R. Shen, *Basic theory of surface sum-frequency generation*, J. Phys. Chem. C **116**, 15505-15509 (2012).

[79] R.K. Jain, *Degenerate four-wave mixing in semiconductors: application to phase conjugation and to picosecond-resolved studies of transient carrier dynamics*, Opt. Eng. **21**, 212199 (1982).

[80] A. J. Fischer, D. S. Kim, J. Hays, W. Shan, J. J. Song, D. B. Eason, J. Ren, J. F. Schetzina, H. Luo, J. K. Furdyna, Z. Q. Zhu, T. Yao, J. F. Klem, and W. Schäfer, *Femtosecond coherent spectroscopy of bulk ZnSe and ZnCdSe/ZnSe quantum wells*, Phys. Rev. Lett. **73**, 2368-2371 (1994).

[81] S. Palomba, S. Zhang, Y. Park, G. Bartal, X. Yin, and X. Zhang, *Optical negative refraction by four-wave mixing in thin metallic nanostructures*, Nat. Mater. **11**, 34-38 (2012).

[82] C. Fiorini, F. Charra, J. M. Nunzi, and P. Raimond, *Quasi-permanent all-optical encoding of noncentrosymmetry in azo-dye polymers*, J. Opt. Soc. Am. B **14**, 1984-2003 (1997).

[83] S. M. Rao, A. Lyons, T. Roger, M. Clerici ,and D. Faccio, *Coherent control of optical negative refraction in graphene*, Frontiers in Optics, FTh2A. **4** (2014).

[84] J. Shi, X. Fang, E. T. F. Rogers, E. Plum, K. F. MacDonald, and N. I. Zheludev, *Coherent control of Snell's Law at metasurfaces*, Opt. Express **22**, 21051-21060 (2014).

[85] Yu. P. Svirko and N. I. Zheludev, *Coherent and incoherent pump-probe specular inverse Faraday effect in media with instantaneous nonlinearity*. J. Opt. Soc. Am. B **11**, 1388-1393 (1994).

[86] S. V. Popov, N. I. Zheludev, and Y. P. Svirko, *Coherent and incoherent specular inverse Faraday effect: $\chi^{(3)}$ measurements in opaque materials*, Opt. Lett. **19**, 13-15 (1994).

[87] J. J. Maki, W. V. Davis, R. W. Boyd, and J. E. Sipe, *Phase conjugation using the surface nonlinearity of a dense potassium vapor*, Phys. Rev. A **46**, 7155-7161 (1992).

[88] J. Feinberg, *Self-pumped, continuous-wave phase conjugator using internal reflection*, Opt. Lett. **7**, 486-488 (1982).

[89] E. Hendry, P. J. Hale, J. Moger, A. K. Savchenko and S. A. Mikhailov, *Coherent nonlinear optical response of graphene*, Phys. Rev. Lett. **105**, 097401 (2010).

[90] L. M. Malard, T. V. Alencar, A. P. M. Barboza, K. F. Mak, and A. M. de Paula, *Observation of intense second harmonic generation from MoS2 atomic crystals*, Phys. Rev. B **87**, 201401(R) (2013).

[91] T. Roger, S. Restuccia, A. Lyons, D. Giovannini, J. Romero, J. Jeffers, M. Padgett, and D. Faccio, *Coherent absorption in N00N states,* arXiv:1603.04363v1 (2016).

[92] J. Jeffers, *Interference and the lossless lossy beam splitter*, Journal of Modern Optics **47**, 1819-1824 (2000).